Accurate Temperature Measurements on Semiconductor Devices

Richard Henry Hopper

A thesis submitted to
De Montfort University
for the degree of
DOCTOR OF PHILOSOPHY

Electronic Engineering
Faculty of Technology
De Montfort University
Leicester
January 2010

ABSTRACT

Self-heating can have a detrimental effect on the performance and reliability of high power microwave devices. In this work, the thermal performance of the gallium arsenide (GaAs) Gunn diode was studied. Infrared (IR) thermal microscopy was used to measure the peak operating temperature of the graded-gap structured device. Temperature measurements were experimentally validated using micro-thermocouple probing and compared to values obtained from a standard 1D thermal resistance model. Thermal analysis of the conventionally structured Gunn diode was also undertaken using high resolution micro-Raman temperature profiling, IR thermal microscopy and electro/thermal finite element modelling.

The accuracy of conventional IR temperature measurements, made on semiconductor devices, was investigated in detail. Significant temperature errors were shown to occur in IR temperature measurements made on IR transparent semiconductors layers and low emissivity/highly reflective metals. A new technique, employing spherical carbon microparticles, was developed to improve the measurement accuracy on such surfaces. The new ‘IR microparticle’ technique can be used with existing IR microscopes and potentially removes the need to coat a device with a high emissivity layer, which causes damage and heat spreading.

DEDICATION

This work is dedicated to my parents, Miles and Elizabeth Hopper, who provided much needed love and support. Sadly, my father passed away before this work was completed.

ACKNOWLEDGEMENTS

This project would not have been possible without the help and support of others. I must start by thanking my supervisors Dr. Chris Oxley and Dr. Gwynne Evans for their encouragement, wise advice and constructive criticism during the work.

I would also like to thank e2v (Lincoln) Ltd. for supporting the work on the Gunn diode, especially Mike Carr, Bob Foulger and Nigel Priestley**.** Sheffield and Aachen Universities also kindly assisted with device fabrication.

Finally, I would like to thank the Engineering and Physical Sciences Research Council (EPSRC) for their financial contribution to the project.

KEY ACRONYMS

ACC	adaptive cruise control
AFM	atomic force microscopy
AlGaAs	aluminium gallium arsenide
AlGaN	aluminium gallium nitride
Au	gold
CCD	charge-coupled device
FET	field effect transistor
GaAs	gallium arsenide
GaN	gallium nitride
HEMT	high electron mobility transistor
IR	infrared
MBE	molecular beam epitaxy
MMIC	monolithic microwave integrated circuit
MOVPE	metalorganic vapour phase epitaxy
NDR	negative differential resistance
RF	radio frequency
SEM	scanning electron microscope
Si	silicon
TLM	transmission line method
TSP	temperature sensitive parameter
VPE	vapour phase epitaxy

CONTENTS

CHAPTER 1. INTRODUCTION

1.1 Motivation

Increasing levels of miniaturisation and integration result in ever higher power density demands being placed on RF devices. One of these devices is the gallium arsenide (GaAs) Gunn diode - extensively used as a high frequency microwave source in high reliability applications, for example, adaptive cruise control (AAC) and millimetric radar systems. Under normal operating conditions, power densities exceeding 50 kW/cm^2 exist in the active transit layer of the device, leading to significant self-heating [1]. Self-heating can adversely affect the RF performance and under certain conditions can result in complete failure of operation. Thermal analysis, including the accurate measurement of operating temperature, is required to ensure reliable operation.

A large number of techniques exist for making experimental temperature measurements on semiconductor devices. Infrared (IR) thermal microscopy is an established technique for rapidly obtaining large area, two-dimensional, surface temperature maps and has been extensively used in this work. Although capable of giving accurate temperature measurements on high emissivity surfaces, the technique is known to be affected by temperature errors which occur, for example, when low emissivity/highly reflective metal surfaces are studied [2]. A high emissivity coating can be applied to try and improve measurement accuracy, however, coating causes heat spreading and may damage the device. The development of a new technique to improve the accuracy of IR temperature measurements made on uncoated semiconductor devices is, therefore, desirable.

1.2 Outline of the Work

A review was undertaken to consider the techniques that exist for making temperature measurements on semiconductor devices. The advantages and disadvantages of each technique are discussed. Infrared thermal microscopy was identified as being a potentially useful tool for making temperature measurements on the GaAs Gunn diode.

The thermal performance of the GaAs graded-gap Gunn diode was studied. Infrared temperature measurements were made on the metal top contact of the device and used to extract its peak operating temperature. Infrared temperature measurements were also made on the substrate layer of the device. However, a temperature comparison with thermal modelling work suggested errors in these IR measurements. Infrared transmission through the transparent GaAs semiconductor was thought to be a possible source of error.

The thermal performance of the conventional GaAs Gunn diode was also studied. A micro-Raman spectroscopy system, at Bristol University, was used to obtain a high resolution (~ 1 μm) temperature profile along the semiconductor layers of the device, including on the active transit layer. As well as these experimental measurements, electro/thermal modelling of the conventional Gunn diode was also undertaken to enable the thermal resistances of its structural elements to be assessed in more detail. The modelled temperature results were experimentally validated using IR thermal microscopy.

Work was undertaken to assess the accuracy of IR surface temperature measurements made on electrically powered semiconductor devices. An AlGaN/GaN TLM structure and a metallised heated test structure, fabricated on GaAs, were studied. The work highlighted the difficulty in obtaining accurate IR surface temperature measurements, especially on low emissivity/highly reflective metals and optically transparent semiconductor layers.

A new measurement technique was developed to significantly improve the accuracy of IR temperature measurements made on semiconductor devices. The new technique

employs radiative, carbon microparticles, which are placed in isothermal contact with the surface under study. The ‘IR microparticle’ technique was found to significantly increase the accuracy of IR temperature measurements made on transparent semiconductor layers and low emissivity metals; it can remove the need to coat surfaces with a high emissivity layer.

1.3 Structure of the Thesis

Chapter 1 describes the motivation and outlines the work.
Chapter 2 contains a review of the published techniques which exist for making temperature measurements on semiconductor devices.
Chapter 3 describes the work undertaken to assess the thermal performance of the GaAs graded-gap Gunn diode, including the IR temperature measurements and thermal modelling.
Chapter 4 describes the work undertaken to assess the thermal performance of the conventional GaAs Gunn diode. Thermal measurement of the device using micro-Raman spectroscopy, IR thermal microscopy and electro/thermal modelling is described.
Chapter 5 considers the temperature errors which can occur when conventional IR measurements are made on semiconductor devices, especially when studying optically transparent semiconductor layers and low emissivity/ reflective metal surfaces.
Chapter 6 describes a new technique, employing spherical carbon microparticles, which can be used to improve the accuracy of IR temperature measurements made on uncoated semiconductor devices.
Chapter 7 concludes the main body of the thesis. It contains a summary of the findings and suggestions for future work.

1.4 List of Published Papers with Abstracts

Six publications have arisen from this work.

1. Oxley, C.H.; Hopper, R.H., "Effect of transparency within a semiconductor on emissivity mapping for thermal profile measurements of a semiconductor device," IET Science, Measurement & Technology, vol.1, no.2, pp.79-81, March 2007

   Abstract -The paper reports on infra-red (IR) measurements made on silicon (Si) and Gallium Arsenide (GaAs) substrates which are transparent to IR radiation. The work showed that the measured emissivity is dependent on the wafer back-face technology, for example a gold heat-sink or epoxy attach. The work also indicated that the measured emissivity for thermal mapping of a device is a function of emitted radiation from the front, back face, layer interfaces as well as internally reflected radiation and will be dependent on the thickness of the semiconductor wafer. Experimental work has shown that the two temperature emissivity correction method will give a very close value of the total surface emissivity received from the sample.

2. Oxley, C.H.; R.H. Hopper, “Infrared microscopy a tool for the manufacturing environment,” Proceedings 5th International conference on Manufacturing Research, De Montfort University, Leicester, Sept. 2007

   Abstract - Infrared (IR) thermography is a powerful technology for performing non-invasive measurement of material emissivity and temperature. The technology has significantly improved over the last decade resulting in a state-of-the-art spatial resolution of approximately 2.6 microns. The paper will describe IR microscopy measuring technologies including emissivity correction procedures to obtain accurate material emissivity and 2-D thermal profiles across the surface of a sample. Examples will be presented showing how the technique can be used to measure the junction temperature (Tj) of active semiconductor devices and the thermal distribution between the active device, heat-sink and package. The measurement enables improved thermal

design management, resulting in increased reliability, leading to reduced development and manufacturing costs.

3. Hopper, R.H.; Oxley, C.H.; Seddon, R.; Foulger, R.; Priestley, N., "Infrared radiance and temperature measurements on the mesa side of Gunn diodes," IET Science, Measurement & Technology, vol.2, no.1, pp.39-41, Jan. 2008

Abstract - Radiance and temperature profiles for the first time have been measured along the mesa side of Gunn diode samples, using an infrared microscope with a spatial resolution of 2.5 μm. Bulk heat generation occurs in the transit region, but measurements have shown a small amount of additional ohmic heating in the substrate layer, which will influence the maximum temperature of the device. The presented thermal measurements have been used to improve the existing thermal finite-element model of the diode. The measurements also represent an alternative method to obtain a more accurate temperature of the diode top contact without coating the sample with a high emissivity layer.

4. Hopper, R.H.; Oxley, C.H.; Pomeroy, J.W.; Kuball, M., "Micro-Raman/Infrared Temperature Monitoring of Gunn Diodes," IEEE Transactions on Electron Devices, vol.55, no.4, pp.1090-1093, April 2008

Abstract - Temperature measurements have been made on Gunn diode samples, using both infrared (IR) and micro-Raman spectroscopy. Micro-Raman spectroscopy was used to give high resolution temperature measurements on the active transit region of the Gunn diode. These were directly compared with IR thermal measurements made across the mesa region and also on the metallized top contact of the diode.

5. Oxley, C.H.; Hopper, R.H., “Thermal Measurement a Requirement for Monolithic Microwave Integrated Circuit Design,” Proceedings ARMMS RF and Microwave society, Steventon, Oxfordshire, April 2008

Abstract - The thermal management of structures such as Monolithic Microwave Integrated Circuits (MMICs) is important, given increased circuit packing densities and RF output powers. The paper will describe the IR measurement technology necessary to obtain accurate temperature profiles on the surface of semiconductor devices. The measurement procedure will be explained, including the device mounting arrangement and emissivity correction technique. The paper will show how the measurement technique has been applied to study the thermal performance of gallium arsenide (GaAs) MMIC configurations and also to GaAs Gunn diodes.

6. Oxley, C.H.; Hopper, R.H.; Evans, G.A., "Improved infrared (IR) microscope measurements for the micro-electronics industry," Proceedings 2nd Electronics System-Integration Technology Conference, Greenwich, London, Sept. 2008

Abstract - Infrared (IR) measurements of the surface temperature of electronic devices have improved over the last decade. However, to obtain more accurate surface temperatures the devices are often coated with a high emissivity coating leading to temperature averaging across the device surface and damage to the device. This paper will look at the problems of making accurate surface temperature measurements particularly on areas of transparent semiconductor and will address the surface emissivity and surface temperature correction problems using novel measurement approaches based on a mathematical model.

CHAPTER 2. REVIEW OF THERMAL MEASUREMENT TECHNIQUES

2.1 Introduction

Self-heating can adversely affect the performance and reliability of semiconductor devices. For example, both the transconductance g_m and current gain cut-off frequency f_t of the GaAs HEMT decrease as operating temperature increases [3]. With high temperatures, the risk of failure from factors such as thermal breakdown [4] and the electromigration of ohmic contacts [5] is increased. These risks must be assessed, especially if the device is to be used in a safety critical application. Although thermal models [6 - 10] can be used to predict the device operating temperature, they are not always accurate, as thermal parameters, such as thermal conductivities and/or thermal boundary resistances are often unknown [11]. Additionally, thermal models can take significant time to develop and sometimes require the input of detailed electrical simulations. The ability to make accurate experimental temperature measurements on semiconductor devices is, therefore, highly desirable.

A large number of temperature measurement techniques exist. They can be grouped into three main categories: electrical, optical and physical contacting. In the first two categories, either an optical or electrical property of a device is monitored and related to temperature. In the third category, a contacting physical sensor is used. In this review, temperature measurement techniques from each of these categories are discussed. Judgements have been made as to their respective merits and weaknesses, for example, their spatial resolution and accuracy. A table summarising these points is given in the conclusion.

2.2 Introduction to Electrical Techniques

Electrical techniques exploit an electrical temperature sensitive parameter (TSP) of the device under study. For example, the forward voltage of a PN junction is known to be temperature dependent. In order to make electrical temperature measurements, the

TSP of the device has to be initially calibrated against temperature. For calibration purposes, a temperature controlled oven or stage is used to heat the device to known temperatures whilst the TSP is monitored. To make a temperature measurement under power (self-heated) conditions, the device is normally switched back into the electrical state used during the calibration stage and the TSP momentarily measured. The switching time must be short enough to limit any reduction in device operating temperature. In some cases, the TSP of the device can be accurately measured when the device is conventionally powered, if the applied electrical bias does not distort the measurement.

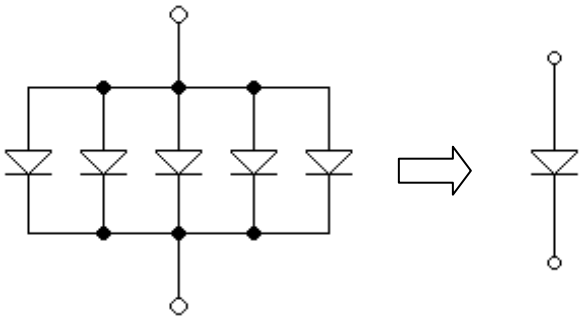

Figure 2.1: Distributed and lumped electrical treatment of a multi-junction bipolar transistor structure.

Electrical techniques have the advantage that they can be used to make temperature measurements on fully packaged devices, using normal electrical connections. A limitation is that they are only able to give an average junction temperature. For example, electrical measurements made on a multi-finger bipolar transistor structure will result in the multiple junctions looking like a single lumped element, see Figure 2.1. This is not a problem if the junction temperatures are uniform. If an inhomogeneous temperature distribution exists, however, an averaging of the peak junction temperature will occur.

2.2.1 Junction voltage

A widely used electrical technique is to measure the temperature dependent forward voltage across a semiconductor junction, for example, a PN junction [12]. The current flow through a PN junction I_{pn} is given by the 'ideal' diode equation

$$I_{pn} = I_s\left[\exp(\frac{qV_{pn}}{kT}) - 1\right] \tag{2-1}$$

where I_s is the reverse saturation voltage, k is Boltzmann's constant, q is the elementary charge and T is the junction temperature in Kelvin.

In a bipolar transistor, the temperature dependent forward base emitter junction voltage V_{be} is often used to make temperature measurements [13 - 17]. To calibrate V_{be} with temperature, the transistor is externally heated and V_{be} monitored under a small and constant collector current. The transistor is then actively biased: a large collect current will flow, causing self-heating. The junction temperature can be determined by transiently switching the collector current back to the level used during the calibration stage and measuring V_{be}. A similar electrical technique, exploiting the temperature dependent forward Shockley junction voltage, has also been used to make measurements on GaN LEDs [18], GaAs FETs [19] and GaN HEMTs [20].

2.2.2 Resistivity

The resistivity of a semiconductor can be related to temperature. Semiconductor resistivity ρ is given by

$$\rho = \frac{1}{nq\mu} \tag{2-2}$$

where q is the elementary charge, n is the carrier density and μ is the carrier mobility. The mobility of a semiconductor is a measure of the ease at which carriers can travel through it under an applied electric field. As temperature increases, the average mobility of carriers will decrease due to phonon scattering. Although the carrier density will also change with temperature, the change in mobility will dominate. The temperature dependent mobility of carriers in GaN has been used to measure the temperature of the AlGaN/GaN HEMT [21].

2.3 Introduction to Optical Techniques

Optical techniques make use of a temperature dependent optical property. They can utilise either emitted or reflected radiation. For example, the level of infrared radiation emitted by the surface of a semiconductor device can be monitored to determine its operating temperature. Optical techniques can be regarded as being non-contacting, as they do not require physical contact with the surface under study. Clearly, non-contacting techniques are advantageous, as unlike thermocouple measurements, they do not cause conducted heat loss from a surface. One disadvantage is that some optical techniques cause interference to the electrical performance of the device under study. An example is when an active optical source, such as a laser, is focussed onto a semiconductor. In this case, some heating and free carrier generation will occur. This effect can be minimised by careful choice of the incident wavelength and power of the laser.

Optical techniques, such as passive IR thermal microscopy, can be used to obtain a matrix of temperature measurements across the surface of a device. This type of 2D imaging is useful for the detection of hotspots (high temperature areas). The spatial resolution is limited by the wavelength of radiation detected. For a typical IR measurement system operating in the 2 - 5 μm waveband, a maximum spatial resolution of ~ 3 μm is achievable [22]. For higher resolution spot temperature measurements (~ 1 μm), techniques employing shorter wavelengths of radiation, such as micro-Raman spectroscopy, can be used.

Optical techniques can have a very high temporal resolution. Rapid fluctuations in device operating temperature can, therefore, be measured, for example, when a transistor is electrically pulsed - this is called ‘thermal transient detection’.

2.3.1 Infrared thermal microscopy

Infrared thermal microscopy is a widely used tool for microelectronic failure analysis and temperature measurement [23]. It is a non-contact technique, utilising naturally emitted infrared radiation from a surface. The technique is useful for the detection of hotspots, as a matrix of temperature measurements can be rapidly made over a wide area (> 200 μm square) [24]. Commercial IR microscopes are readily available,

offering a maximum spatial resolution of ~ 2.5μm[1] (in the 2 - 5 μm waveband) and a range of analysis options, including real time thermal mapping and thermal transient detection [25]. Published thermal analysis using IR includes work on GaAs FETs [26], MMICs [27], RF power amplifiers [28 - 29] and device packaging [30].

To understand the principle behind IR temperature measurements, it is necessary to consider the relationship between temperature and infrared emittance from an ideal black body. The power emitted by a black body W (per unit area) can be defined as a function of wavelength λ at a known temperature T by Planck's radiation law

$$W(\lambda) = \frac{2hc^2}{\lambda^5 \left\{ \exp\left(\frac{hc}{\lambda kT} \right) - 1 \right\}} \tag{2-3}$$

where h is Planck's constant, c is the speed of light and k is Boltzmann's constant.

Figure 2.2 shows the spectral distribution of emitted radiation from a black body at a number of different temperatures. The plot shows that as temperature increases, the total power radiated by the black body increases. A spectral shift also occurs, with the radiation peak decreasing in wavelength. At low temperatures (300 - 500 K), the highest level of emitted radiation occurs in the 2 – 10 μm wavelength band. This band is where most passive IR detectors, for example, indium antimony (InSb) detectors, are designed to operate.

[1] Spatial resolution can be defined by the Sparrow criteria $D = 0.47 \lambda / NA$. Where λ is wavelength, NA is numerical aperture and D is the separation distance.

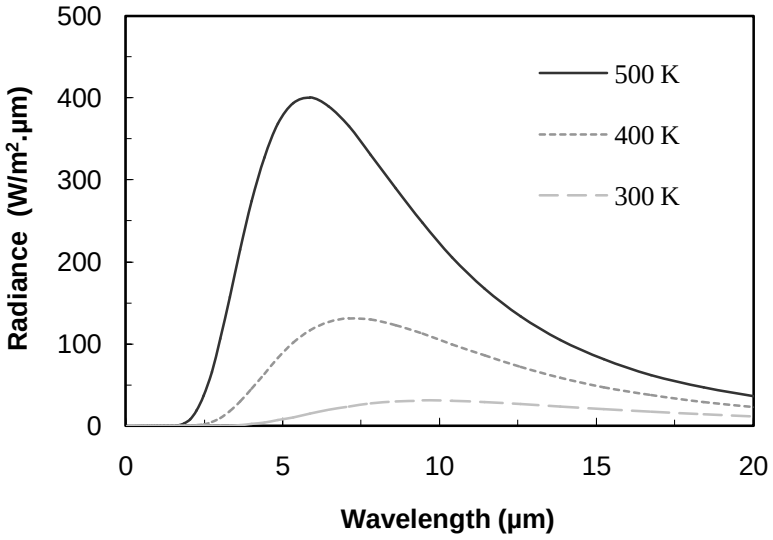

Figure 2.2: Blackbody spectral radiance plotted as a function of wavelength. Results are shown at three different temperatures.

At a specific temperature, most surfaces will emit IR radiation at a fraction of the black body level. A parameter known as 'emissivity' is used to characterise the efficiency of a surface to emit infrared radiation. Emissivity e is defined as the ratio of emitted radiation level from a surface to that of a black body at the same temperature and wavelength

$$e = \frac{R_s}{R_b} \tag{2-4}$$

where R_s and R_b are the radiation levels emitted by the surface and blackbody, respectively. The total radiated power from a surface can be related to its temperature and emissivity by integration of Planck's radiation law over all wavelengths to give the Stefan-Boltzmann equation

$$W = e\sigma T^4 \tag{2-5}$$

where σ is the Stefan-Boltzmann constant. Temperature can, therefore, be found by measuring the emitted radiation level from a surface of known emissivity.

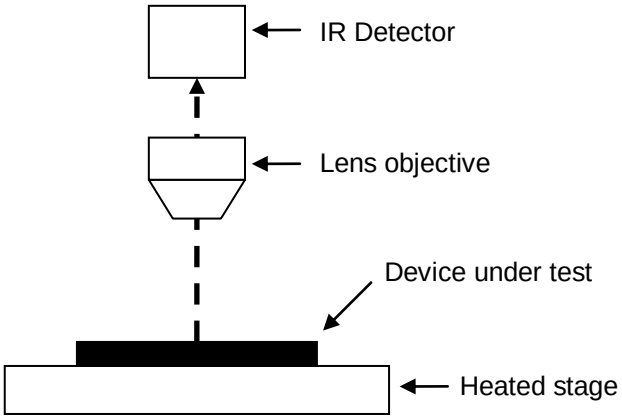

Figure 2.3: Infrared measurement arrangement.

Surface emissivity is a quantity that usually has to be measured, as its value is dependent on a number of factors, including material type and surface finish. Emissivity values on a typical semiconductor device vary widely, with values of less than 0.1 on metals and greater than 0.5 on semiconductor areas, respectively. The surface emissivity can be found by making radiance measurements using the arrangement shown in Figure 2.3. The sample under study is placed on a heated stage which enables its ambient temperature to be controlled. Infrared radiation from the surface is focussed onto the detector of the IR microscope. The level R of IR radiation detected is given by

$$R = R_b e + R_o (1 - e) \tag{2-6}$$

where R_b is the level of radiation emitted by a black body source at an identical temperature to that of the device, e is the surface emissivity and R_o is the level of external background radiation incident on the surface. Some background radiation will be reflected from the surface, given the reflectivity coefficient $r = (1 - e)$. If the level of reflected background radiation is unknown, errors will occur in the emissivity measurement. Provided the surface emissivity is relatively high, the level of reflected

background radiation will normally be insignificant. However, on low emissivity surfaces (< 0.1), such as metals, it can become significant.

Two-temperature emissivity measurements

An improved emissivity measurement technique to eliminate errors caused by constant environmental background radiation was developed by Webb [2]. This approach involves measuring the change in emitted radiation level from a surface due to a known change in temperature. The emissivity is then given by

$$e = \frac{(R_{s2} - R_{s1})}{(R_{b2} - R_{b1})} \tag{2-7}$$

where $(R_{s2} - R_{s1})$ is the change in emitted radiation level from a surface measured between two temperatures (T_1 and T_2) and $(R_{b2} - R_{b1})$ represents the equivalent blackbody change between the same temperatures. The technique improves the accuracy of emissivity measurements provided the external background radiation level (R_o) remains constant during the measurement. Some error will still occur if the level of background radiation changes when the ambient temperature of the sample is changed. This could be the case if interfering background radiation is generated by the heated stage or surrounding fixtures. Additional error can also occur due to thermal expansion or contraction of the stage holding the sample. If movement occurs during the measurement procedure, the surface areas studied will become misaligned, corrupting the calculated emissivity values. Mechanical realignment or data correction can be used to correct for any unwanted movement.

Emissivity determination using reflectivity data

For opaque surfaces, Kirchhoff's radiation law states that the sum of the emissivity and reflectivity coefficients must be equal to unity $e + r = 1$. Thus, by measuring the reflectivity of a surface, its emissivity can be determined [31]. The reflectivity technique has a number of advantages. The measurements do not require the device under study to be heated, therefore, problems caused by thermal expansion and contraction are avoided. Higher signal to noise ratios can generally be obtained, as there is no need to measure the emitted radiation level, which may be weak [32].

Additionally, by modulating the emitted and reflected radiation components, it is possible to simultaneously obtain both emissivity and temperature maps of a surface [33].

2.3.2 Micro-Raman spectroscopy

Micro-Raman spectroscopy can be used to make temperature measurements on semiconductor materials. The technique is based on the measurement of phonon frequency. The measurement system uses a excitation source (normally a laser), which is focused onto the semiconductor. A tiny fraction of the scattered laser light is shifted in frequency and is detectable using a spectrometer. If the phonon shift temperature dependence is known, the measured frequency shift can be used to find the semiconductor's temperature. Micro-Raman measurements have been made on GaN [34] and GaAs [35] HEMTs.

By using short optical wavelengths (< 500 nm), micro-Raman spectroscopy can be used to obtain high spatial resolution temperature measurements on features less than 1 μm in size [34]. Another advantage of the technique is that temperatures can be measured on areas below the surface of a semiconductor, in confocal mode [36]. Such subsurface temperature measurements are useful for studying the temperature distribution through semiconductor layers [11]. Sub-microsecond transient temperature measurements can also be made using micro-Raman [37].

Unlike IR thermal microscopy, micro-Raman temperature measurements are difficult to make over large surface areas, as mechanical scanning and data integration is required. Also, the technique cannot be used on metals, as metal phonons are too low in energy for detection. Another slight disadvantage with the technique is that some temperature error can be caused by laser induced heating and carrier generation within the semiconductor. This error can be minimised by limiting the power of the excitation laser and/or by using a laser wavelength below the band-gap of the semiconductor being measured. On GaN devices, micro-Raman temperature measurements have been made with an accuracy of better than ± 10 ºC [38].

2.3.3 Band-gap techniques

The band-gap energy of semiconductor materials is known to vary with temperature. Variations in the band-gap energy correspond to the spectral position of the absorption edge which can be monitored by measuring emission or reflectivity spectra from a sample. A reflectivity approach has been used to make absorption edge temperature measurements on GaAs [39] and also on SiC [40], with an accuracy of ± 2 °C. Recently, photocurrent measurements have been used to make absorption edge temperature measurements on the GaN HEMT [41]. With the photocurrent approach, a monochromatic light source is focused onto the semiconductor. The wavelength of the monochromatic light source is changed and the photocurrent through the semiconductor monitored. Changes in photocurrent are used to determine the position of the absorption edge and hence the semiconductor's temperature.

2.3.4 Multi-spectral techniques

Planck's radiation law states that the spectral distribution of infrared radiation emitted by a surface will change according to its temperature. This temperature dependence can be used to establish the temperature of a surface without knowledge of its emissivity. A multi-spectral technique using a bicolour infrared CCD sensor has been demonstrated [42]. Infrared sensors were constructed using two different types of diode with low and high barrier heights to give different responses over separate portions of the IR spectrum. The signal ratio from the diodes was used to determine the surface temperature. Methods using a higher number of spectral measurement points have also been developed [43]. A seven-colour technique was shown to give a temperature accuracy of around 10 % at 600 K [44]. Multi-spectral techniques appear to be more suitable for use at high temperatures (> 500 K), as a high level of IR radiance is required to achieve an adequate detector signal to noise ratio. Future improvements in detector technology may make a lower temperature system feasible.

2.3.5 Thermoreflectance

The reflectivity of some materials is dependent on temperature. Although this temperature dependency is small, of the order of 10^{-5} K^{-1} [45], temperature induced changes are possible to detect using a sensitive measurement system. A typical thermoreflectance system is shown in Figure 2.4. The semiconductor device under test

is thermally cycled by a temperature-controlled stage. Light from a high stability source, such as a quartz bulb, is focused onto the surface of the device through a lens arrangement. Reflected light is fed back through a beam splitter onto a photoelectric sensor. The sensor can be a single detector i.e. a photodiode [46] or a photosensitive array [47 - 48]. The recovered signal is amplified by a high gain stage and digitised to a resolution of at least 12 bits. To achieve a sufficiently high signal to noise ration (SNR), a Fast Fourier Transform (FFT) based algorithm or a lock in amplifier is used to recover the thermally modulated reflectance signal. The recovered signal is monitored to establish the thermal reflectance coefficient ($\delta R / \delta T$). To give an indication of its operating temperature, the change in optical reflectance is recorded when the device under test is electrically powered.

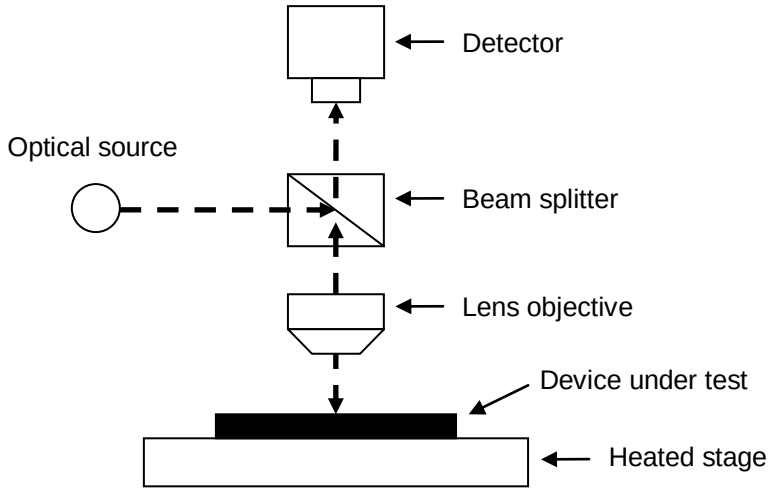

Figure 2.4: Thermoreflectance measurement arrangement.

Thermoreflectance measurements have the advantage that they can be easily optimised for use on a variety of materials. The accuracy of the technique is ultimately dependent on the level of noise contribution from the detector, electronics and quantisation process. Tests using a conventional CCD detector have given poor results due to the low SNR obtained [49], although better results have been obtained using a higher specification CCD camera [50]. More specialised sensors have enabled a temperature resolution of 50 mK [51]. The spectral resolution is limited by the wavelength of light used. Based on the diffraction limit, a resolution of ~ 400 nm

appears achievable using visible light. Thermoreflectance systems can be used to study thermal transients [52].

2.4 Introduction to Physical Contacting Techniques

Physical contacting techniques rely on the transfer of thermal energy from the surface under study to a sensor and include thermocouple probes and temperature sensitive liquid crystals. Physical contacting techniques can be used to make a single point or a matrix of temperature measurements on a surface. For example, atomic force microscopy (AFM) can be used to scan a thermal probe across a surface to create a 2D temperature map. The spatial resolution of a physical contacting technique is only limited by the size of the probe used. Measurements made using AFM have achieved sub-micrometer resolutions [53]. Although capable of high resolution measurements, physical contacting techniques can be slow to respond to thermal transients. A second disadvantage is that temperature errors can occur due to heat loss or poor thermal contact with the probe used. In the case of liquid crystals, their application can cause heat spreading, distorting the surface temperature profile.

2.4.1 Thermocouples

A thermocouple uses two dissimilar metal wires to form a junction. When the junction is heated, a temperature dependent voltage will be generated due to the thermoelectric effect [12]. This voltage is relatively small, of the order 2 - 70 μV/°C (dependent on metal types). A junction can be made from a number of different metal combinations. A common type is the K-type (chromel–alumel) thermocouple junction.

Thermocouple techniques are relatively simple to implement. A disadvantage is that they require a transfer of thermal energy from the surface under study to the thermocouple, which has to be in good contact. Heat transfer can introduce a localised temperature distortion [54]. The maximum accuracy of thermocouple measurements is limited to around 1 °C. The spatial resolution of the technique is determined by the size of the thermocouple probe. Commercially available probes are generally greater than 20 μm in diameter; they are, therefore, mainly suitable for making temperature measurements on larger sized electronic devices, for example, high power MOSFETs [55].

2.4.2 AFM

Atomic force microscopy (AFM) can be used to scan thermal probes over the surface of a device using a cantilever system. Probes can be manufactured using a number of methods [56 - 57]. Unlike optical techniques, the spatial resolution is not diffraction limited, the main limiting factor being the size of the thermal probe used. Temperature probes, manufactured using nanotubes, have enabled temperature resolutions of 5 nm [58]. A disadvantage with the technique is that some temperature errors can occur due to heat transfer between the surface and probe, which has a thermal capacity [59]. Recently, AFM temperature measurements have been made on GaAs PHEMTs [60], AlGaN/GaN HEMTs [61] and nMOSFETs [62].

2.4.3 Liquid crystals

Temperature sensitive light inhibiting liquid crystals can be applied to the surface of a semiconductor device. The choice of liquid crystal is based on the temperature at which the crystals change from an aligned state to a random state, called the 'transition temperature'. The crystal transition is visible through a microscope using polarised light. Although the technique offers high accuracy, a disadvantage is that only a single transition temperature point can be established with each type of liquid crystal. To determine the transition temperature requires subjective analysis, although laser illumination can be used to make the technique less subjective [63]. Liquid crystals are commercially available to study temperatures in the range of -30 ºC to 120 ºC [64]. A spatial resolution of 0.5 μm is claimed to be possible [65], although the liquid crystal layer will tend to spread heat. Recently, liquid crystals have been used to make temperature measurements on AlGaN/GaN HEMTs [66] and LEDs [67].

2.4.4 Fluorescence

The surface temperature of a semiconductor device can be measured using a fluorescent material. Materials, such as fluorochrome europium tenoyltrifluoroacetonate (EuTTA), will emit optical radiation when externally excited by a high energy optical source. To make a temperature measurement, the florescent material is usually coated onto the surface of the device, in either liquid [68] or powder form [69], and excited by a laser or LED. A microscope and CCD sensor can be used to measure the level of emitted radiation from the florescent material to give

an indication of its surface temperature. Relatively high spatial resolutions (~ 1 μm) can be obtained, as short optical wavelengths can be used. A disadvantage with the technique is that the coating will cause a small amount of heat spreading and may damage the device. To remove the need for coating, a florescent particle can be attached to a probe tip and scanned across a surface using AFM [70]. However, heat loss through the probe means that only qualitative temperature measurements can be obtained with this approach.

2.5 Conclusions

A wide variety of techniques exist for measuring the operating temperature of semiconductor devices. Electrical techniques have the advantage that they can be used to make temperature measurements on packaged devices, using standard electrical connections. A disadvantage is that they are only able to give an average junction temperature. Temperature measurements can be made with a high spatial resolution over areas using scanning thermal probes (AFM). However, physical contacting techniques require the transfer of thermal energy from the feature under study to the sensing element, which can distort the temperature measurement.

Optical techniques, such as IR thermal microscopy, can be used to obtain real time two-dimensional surface temperature maps over large areas of a semiconductor device; allowing the easy identification of hot spots. It is one of the few techniques which can be used to make temperature measurements on the metal contacts of devices, such as the GaAs Gunn diode studied in this work. Currently, the spatial resolution of IR is limited to ~ 2.5 μm. This resolution is not as high as some other optical techniques, such as micro-Raman spectroscopy, which can be used to make high resolution spot temperature measurements on semiconductors (< 1 μm) (but not on metals). The temperature accuracy of IR is also dependent on the surface emissivity.

Ultimately, the choice of temperature measurement technique depends on a number of factors, including the type of device to be studied and the required temperature accuracy and spatial resolution. Table 2-1 summarises the main advantages and disadvantages of each of the techniques discussed.

Technique	**Advantages**	**Disadvantages**
Electrical Section 2.2	- Can be used on packaged devices	- Only gives an average junction temperatures
IR Section 2.3.1	- Real time 2D imaging - Large area temperature maps	- Temperature accuracy is emissivity dependent - Resolution limited (~ 2.5 um)
Micro-Raman Section 2.3.2	- Spatial resolution < 1 µm	- Slow acquisition time - Cannot be used on metals
Band gap Section 2.3.3	- Good accuracy	- No commercial systems - Cannot be used on metals
Multi-spectral Section 2.3.4	- Emissivity independent	- Only suitable for high temperature measurements
Thermo-reflectance Section 2.3.5	- Spatial resolution < 1 µm	- No commercial systems
Thermocouple Section 2.4.1	- Readily available	- Only gives single point measurements - Limited resolution (20 µm)
AFM Section 2.4.2	- Spatial resolution < 1 µm	- Heat loss due to probe - Small area measurements
Liquid crystal Section 2.4.3	- Easy to apply	- Subjective analysis required - Thermal spreading occurs
Fluorescence Section 2.4.4	- Relatively high spatial resolution ~ 1 µm	- Requires coating, which is destructive to device and causes heat spreading

Table 2-1: Summary of the temperature measurement techniques.

CHAPTER 3. THERMAL ANALYSIS OF THE GALLIUM ARSENIDE GRADED GAP GUNN DIODE

3.1 Introduction

3.1.1 Background

Gallium arsenide Gunn diodes are widely accepted high frequency microwave sources. In recent years, the graded-gap Gunn diode has been used as a 77 GHz signal source for adaptive cruise control (ACC) [71]. Adaptive cruise control systems are fitted in cars to enable the position and velocity of vehicles travelling ahead to be determined. The system is commonly marketed as a safety feature; as it can be used to automatically apply the brakes of a vehicle if an obstacle is detected. The Gunn diode is a critical component to the system and must have a high reliability. The reliability and performance of the device are known to be adversely affected by high temperature operation, which can be caused by both self-heating and high ambient temperatures [72]. Thermal characterisation, especially to obtain the peak device operating temperature, is required to ensure longevity of performance over a wide ambient temperature range (- 40 to 115 °C).

Thermal models can be used to predict the operating temperature of the Gunn diode [73 - 74]. The accuracy of any thermal model is ultimately dependent on having a good understanding of the device parameters. Some parameters, for example, the nature and number of air gaps (voids) between the mounting chip and package header, are not always known. Experimental temperature measurements are, therefore, needed to confirm the actual device operating temperature. An electrical technique can be used to make temperature measurements on the Gunn diode [75]. However, the electrical technique has some limitations. It can only be used to obtain the average operating temperature within the active transit layer of the device and cannot be used to make 2D temperature maps, for example, on the metallised and semiconductor areas. As the technique requires pulse operation of the device, electrical instabilities can occur which may distort the measurement.

3.2 Current Work

In this work, IR thermal microscopy was used to make temperature measurements on the GaAs graded-gap Gunn diode. Until recently, the spatial resolution of passive IR thermal microscopy was limited to ~ 25 μm, insufficient to make detailed temperature maps on the structure. However, with improvements in detector technology, surface temperature mapping with a spatial resolution of ~ 3 μm is now possible. Infrared thermal microscopy was used to obtain the peak operating temperature of the Gunn diode. Temperature results were compared to those obtained from a conventional thermal resistance model. Further work was also undertaken to try and thermally image the semiconductor substrate layer. A paper has been published regarding this work in the IET Proceedings on Science, Measurement & Technology (see Section 1.4, Publication no. 3).

3.3 Device Description

3.3.1 Conventional Gunn diode

The Gunn effect was first observed by J. B. Gunn in 1963-64 [76]. He found that microwave oscillations could be produced if a DC current was passed through a lightly doped GaAs sample. It was noted that the voltage across the sample had to exceed a certain critical voltage before any oscillations were produced. The Gunn effect arises from the energy band structure of GaAs, see Figure 3.1. If high mobility electrons (μ_1 = 8000 $cm^2.V^{-1}.s^{-1}$) propagating in the material acquire sufficient energy, they can transfer into a lower mobility state (μ_2 = 100 $cm^2.V^{-1}.s^{-1}$) in the satellite L-valley of the conduction band. The electron transfer is exploited within the Gunn diode to generate electrical oscillations.

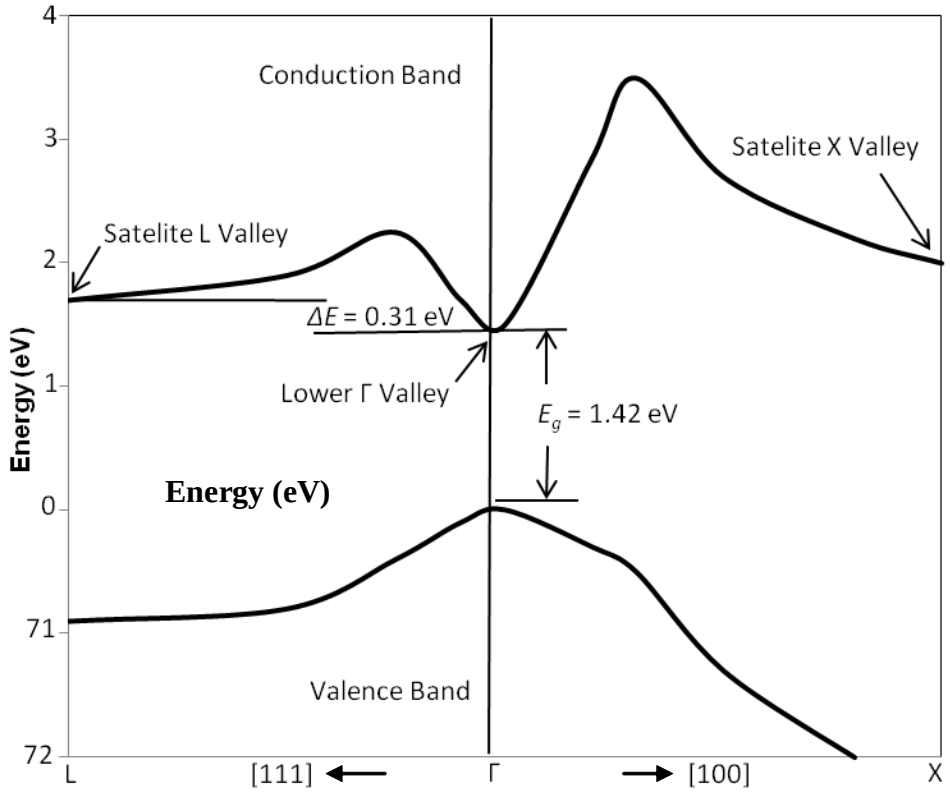

Figure 3.1: Conduction band structure of GaAs at 300 K (reproduced from [77]).

Conventional Gunn diode structures consist of a single lightly doped GaAs layer, called the 'transit layer', contacted top and bottom by two highly doped contact layers, see Figure 3.2. Within the active device, electrons propagating through the transit layer will be accelerated by the applied electric field. Some of the higher energy 'hot electrons' will transfer into the lower mobility state in the conduction band, creating a build-up of slowly moving charge called a 'domain'. The domain will travel across the GaAs layer and will be nucleated at the anode. Given a high enough electric field strength, the process of domain creation and nucleation is repeated many times, leading to electrical oscillation.

The fundamental operating frequency f_t of the Gunn diode is related to the average transit layer electron velocity v_{av} and transit layer length l by

$$f_t = \frac{v_{av}}{l} \tag{3-1}$$

In use, the diode can be operated in ‘transit time mode’, when the operating frequency is independent of the external circuit. However, in most applications a resonant circuit is used to reduce the voltage across the transit layer during part of the oscillation cycle, delaying domain growth [78]. In this so-called ‘delayed domain mode’, the device can be used over a much broader bandwidth.

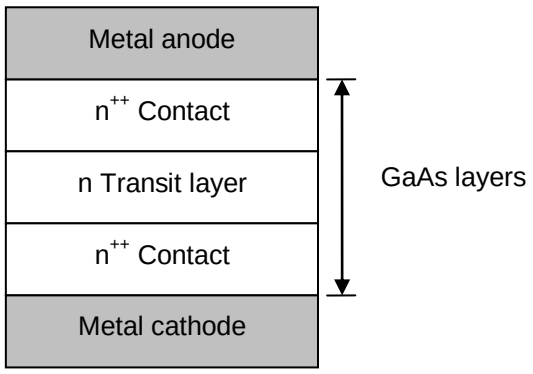

Figure 3.2: Conventional Gunn diode structure.

The forward DC IV characteristics of a typical conventional Gunn diode are shown in Figure 3.3. At low voltages, there is a rapid increase in current flow through the device as the bias voltage is increased. However, when a critical threshold voltage V_{th} (3.8 V) is reached, the current level peaks and then decreases. At voltages above V_{th}, a significant number of electrons travelling in the GaAs transit layer will reside in the lower mobility state, having transferred into the satellite valley of the conduction band. The average reduction in electron mobility gives rise to a region of negative differential resistance (NDR), shown by the current slump in the non-linear IV characteristics.

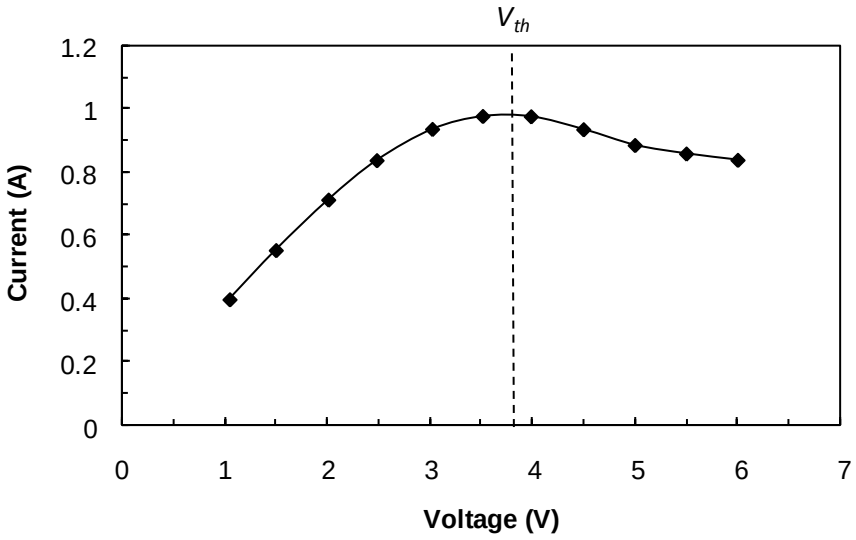

Figure 3.3: IV characteristics of the conventional Gunn diode.

3.3.2 Improved graded-gap structure

In recent years, the RF efficiency of the Gunn diode has been improved by use of an AlGaAs/GaAs heterostructure. To understand how the heterostructure offers increased efficiency, it is necessary to consider the limitations with domain growth in the conventional device. In the conventional Gunn diode, a critical electric threshold field E_{th} (approximately 0.32 V/μm) has to be present across the transit layer before a domain is formed. A finite time is required to accelerate electrons to sufficient energy to transfer them into the upper satellite valley of the conduction band. The propagation distance required to generate these hot electrons creates a dead zone in the transit layer, adding a lossy parasitic resistance which limits the device efficiency. In a conventional Gunn diode, the dead zone can be 10 - 20 % of the total transit layer length [79].

The efficiency of the conventional Gunn diode can be enhanced by injecting high energy, hot electrons, directly into the transit layer. These diodes are often referred to as ‘graded-gap’ devices [80]. The basic structure of the graded-gap Gunn diode is shown in Figure 3.4. A graded AlGaAs layer is used to act as a hot electron injector. The AlGaAs layer creates a region of high electric field strength in which electrons

are heated. These hot electrons are injected via an n^+ contact layer into the transit layer where domain formation happens almost instantly, significantly reducing the length of the dead zone. Compared to the conventional device, losses due to the parasitic transit layer resistance are reduced. The graded-gap Gunn diode, therefore, has an increased electrical efficiency. It also has superior frequency stability, as the high electron injection temperature (~ 2000 K) means that small changes in operating temperature have a less significant effect on the average electron velocity.

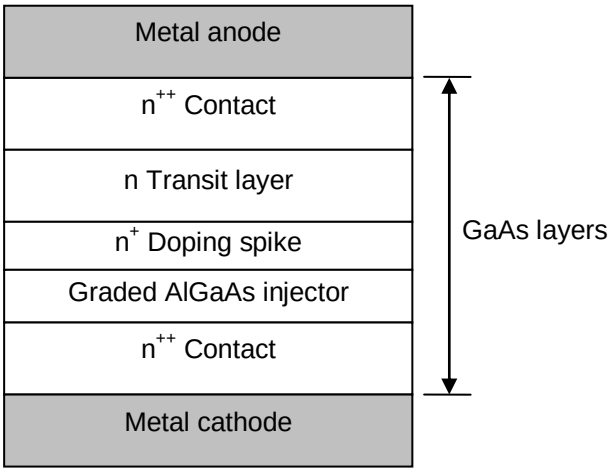

Figure 3.4: Grade-gap Gunn diode structure.

The forward DC IV electrical characteristics of a typical graded-gap Gunn diode are shown in Figure 3.5. The peak current level at the critical threshold voltage V_{th} is now less well defined than in the case of the conventional device. At voltages above V_{th}, a higher proportion of electrons entering the transit layer will immediately transfer into the lower mobility state, limiting the drop in current level.

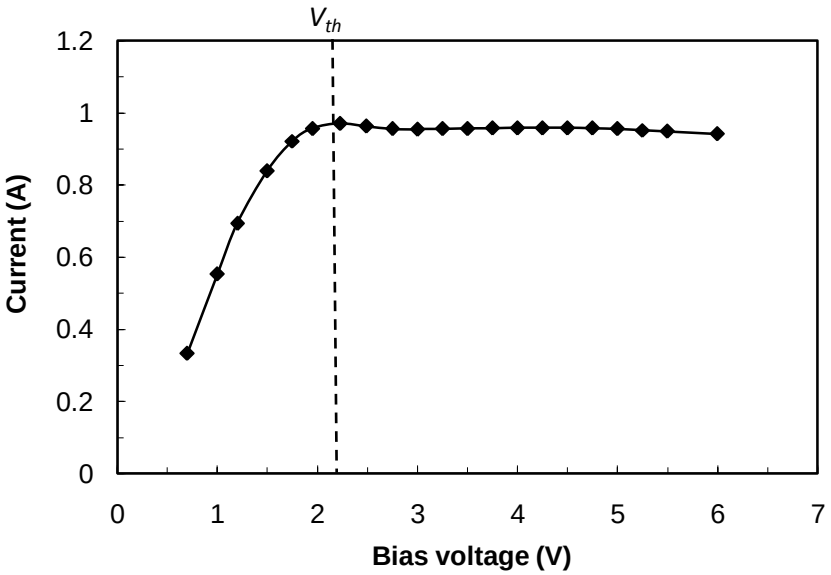

Figure 3.5: Forward IV characteristics of a typical GaAs graded-gap Gunn diode.

To extract microwave energy from the Gunn diode, it is placed in a resonant cavity and coupled to a waveguide [81]. Planar devices have also been developed to enable direct integration with microstrip transmission lines and ultimately in MMICs [82].

3.4 Device Fabrication

The graded-gap Gunn diode samples used in this study were fabricated by e2v (Lincoln) Ltd. A schematic diagram showing a cross-sectional view of the device is shown in Figure 3.6. An Au bond wire is used to make contact with an Au top contact, beneath which are the semiconductor layers forming the mesa. The mesa is cylindrical in shape and has a diameter between 60 – 80 μm and a total thickness of 12.7 μm.

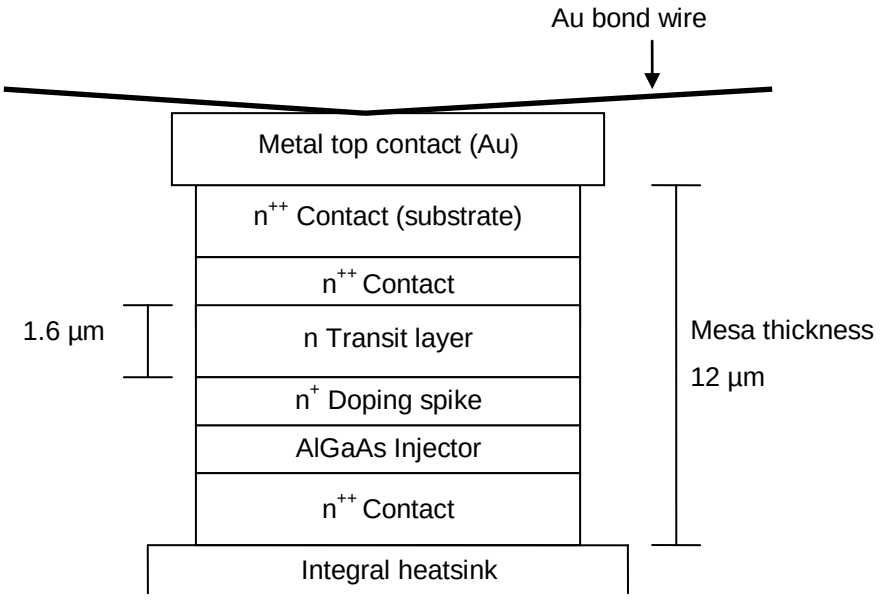

Figure 3.6: Construction of the graded-gap Gunn diode.

The semiconductor layers forming the mesa were grown on a GaAs substrate using molecular beam epitaxy (MBE). A thin (100 nm) layer of AlGaAs is used as a hot electron injector, having a linearly graded Al concentration, increasing from 10 % at the cathode to 30 % near the transit layer. A GaAs n^+ doping spike (10 nm) is used to prevent the depletion region in the forward biased injector from extending into the transit layer [83]. The GaAs transit layer is 1.6 µm in length and is lightly doped (1×10^{16} electrons/cm³). Two highly doped (4×10^{18} electrons/cm³) GaAs n^{++} layers, either side, are used to form ohmic contacts. To efficiently remove heat from the device, the substrate is electroplated to an Au integral heatsink.

The mesa structure of the Gunn diode is ultrasonically bonded onto a cylindrical copper package, which has overall dimensions 4 mm depth and 3 mm diameter, see Figure 3.7. A metallised ceramic ring surrounds the mounted diode and provides an anode contact to the external circuit. A metal bond wire is electrically connected between the metallised ring and the metal top contact. To extract RF energy, the packaged device is normally mounted in a resonant cavity. In this study, a resonant cavity was not used, as we were not interested in extracting RF energy. In any case,

the CW electrical RF efficiency of the Gunn diode is low (~ 4 %), so the extracted power loss in a cavity would be minimal.

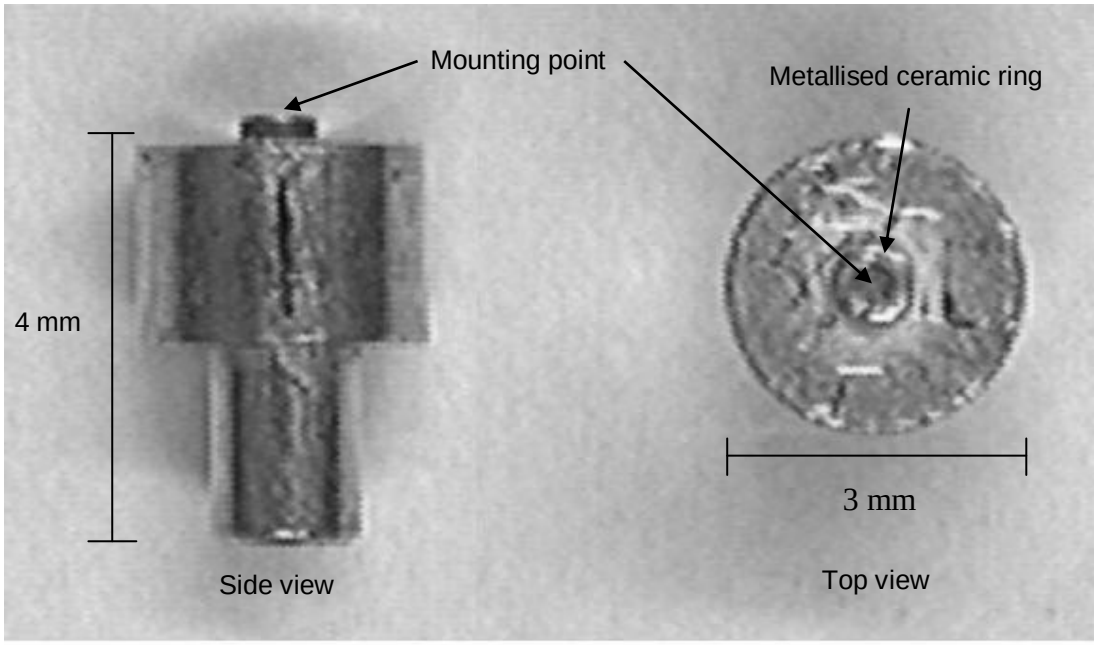

Figure 3.7: Optical image showing the copper package of the GaAs graded-gap Gunn diode.

3.4.1 Heat generation

Under active operational conditions, bulk heat generation occurs within the transit layer of the Gunn diode, where high electric field strengths and current densities exist due to domain formation. A schematic diagram showing the expected temperature profile within the structure is shown in Figure 3.8. Heat flux generated in the transit layer will flow towards the cooler integral metal heatsink. A thermal gradient will be created, with temperatures diminishing from the transit layer towards the package header. The package is normally thermally bonded to an external heatsink, which is held at ambient temperature.

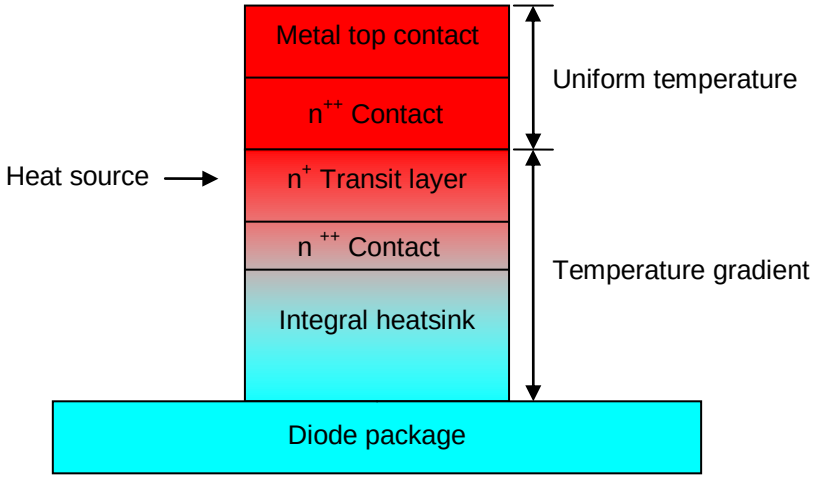

Figure 3.8: Simplified diagram showing the expected temperature profile within the Gunn diode structure. The thin injector layers are omitted for simplicity.

Conventional thermal models of the Gunn diode assume that no heat generation occurs in the highly doped contact layers. Another assumption is that heat loss through the top contact and the thin Au bond wire will be negligible. No temperature gradient should exist between the transit layer and the metal top contact. Temperature measurements made on the metal top contact will, therefore, give a good estimate of the peak device operating temperature.

3.5 Top Contact IR Temperature Measurements

To determine the peak operating temperature of the GaAs grade gap Gunn diode, temperature measurements were made on its top metal top contact using a Quantum Focus (QFI Infrascope II) IR microscope. The dimensions of the sample imaged (Sample 1) are given in Appendix A.

3.5.1 Device mounting arrangement

To make the IR temperature measurements, the Gunn diode was held in a purpose built aluminium jig, designed and constructed in collaboration with e2v (Lincoln) Ltd. An image showing a top view of the jig is shown in Figure 3.9. The jig was designed to allow the packaged Gunn diode to be held in place using a detachable clamping arrangement. A pair of drop down, Au plated, electrical contacts provide an anode connection to the metallised ceramic ring (the earth connection was made through the

body of the jig). A recessed K-type thermocouple was embedded into the jig and used to monitor the ambient package temperature during the emissivity correction procedure and when the device was DC powered. The jig assembly was securely attached to the Peltier heat exchanger of the IR microscope using mounting screws.

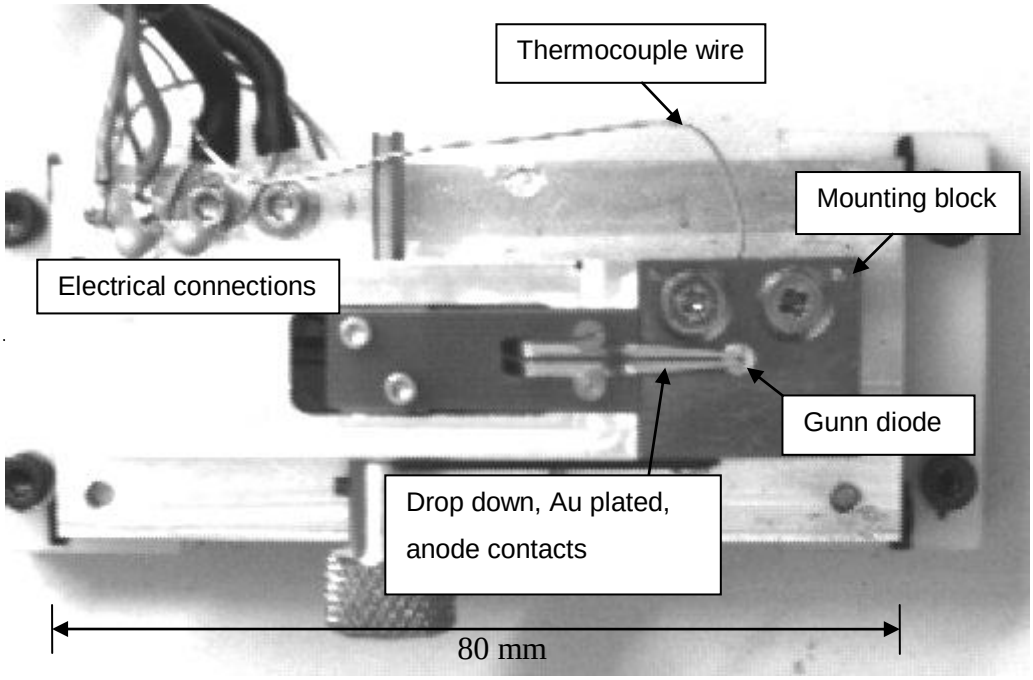

Figure 3.9: Optical image showing the jig used to hold the graded-gap Gunn diode sample for the IR temperature measurements on the top contact of the device.

3.5.2 Temperature measurement procedure

Infrared radiation was collected from the top contact of the Gunn diode using the IR microscope's 5 × lens objective. This gave a field of view of 1180 × 1180 µm and a spatial resolution of 5 µm. The accuracy of IR temperature measurements made directly on metal surfaces is poor due to their high reflectivity/low emissivity [2]. In order to increase the emitted radiation level from the top contact, a high emissivity, non-conductive, paint coating was applied to the metal surface using a fine artists brush. A comparison between the uncoated and coated areas showed that the average emissivity increased from < 0.1 to ~ 0.7 after coating.

Emissivity measurements were made on the coated top contact of the Gunn diode using the two-temperature measurement technique (described in Section 2.3.1 of

Chapter 2). Two radiance measurements were captured with the device heated to ambient temperatures of 50 and 80 °C, respectively. The radiance data was used by the IR system to calculate the emissivity map of the surface. During the emissivity measurement procedure, some sample movement was observed due to thermal expansion of the metal jig. This movement was easily corrected for by mechanical realignment of the IR lens objective of the microscope. After emissivity mapping, IR temperature measurements were made on the top contact with the device biased under DC operating conditions and with the ambient jig temperature stabilised at 80 °C.

3.5.3 Temperature results

An unpowered IR radiance image, showing the area around the top contact of the Gunn diode is shown in Figure 3.10. The circular surface of the metal top contact is clearly visible in the centre of the image. Its overall diameter is 80 μm. An Au bond wire (25 μm in diameter) can be seen to form an electrical connection between the top contact and the metallised ceramic ring surrounding the structure. Underneath the top contact are the semiconductor layers which form the mesa. The mesa is electroplated to the Au integral heatsink, which is partially visible in the image.

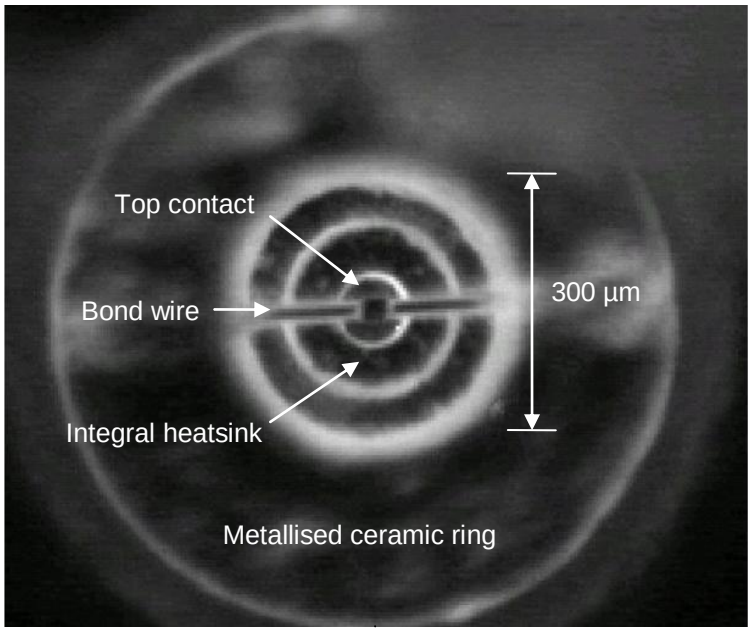

Figure 3.10: Unpowered IR radiance image, showing the area around the top contact of the GaAs graded-gap Gunn diode.

A typical IR temperature image of the top contact of the electrically powered Gunn diode is shown in Figure 3.11. The device was DC powered at 6 W and the ambient baseplate temperature stabilised at 80 °C. Areas of high temperature have been superimposed onto an unpowered radiance image. The measured temperature profile looks realistic, with peak temperature areas (~ 290 ºC) on the metal top contact, which is above the mesa. Temperatures can be seen to decrease away from the top contact along the attached metal bond wire. Infrared thermal microscopy provides a convenient tool for rapidly obtaining the temperature profile on the coated metallised structure, enabling the extraction of the peak device operating temperature.

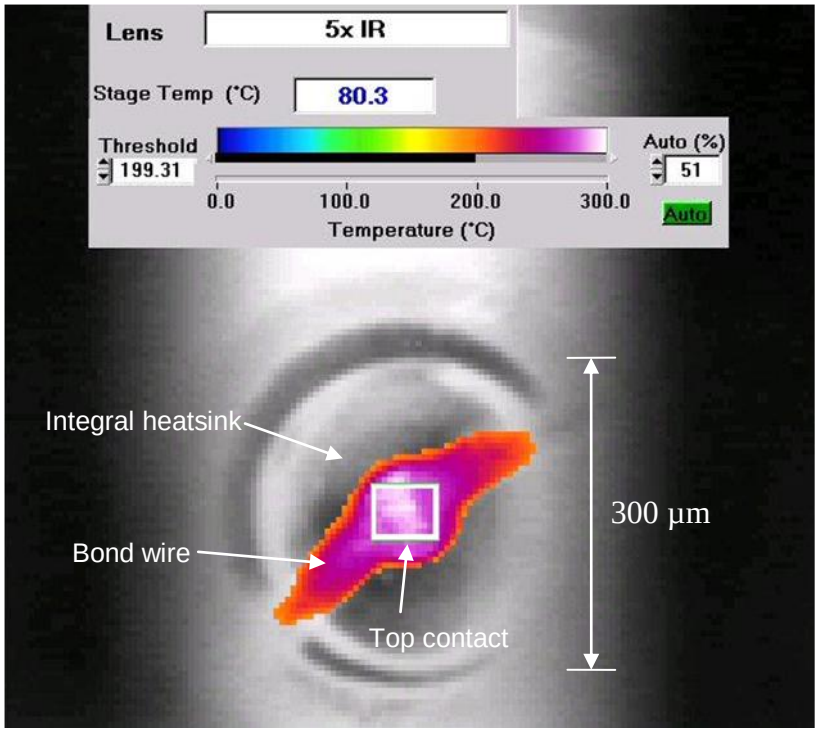

Figure 3.11: Infrared temperature image measured on the top contact of the electrically powered graded-gap Gunn diode. P_{dis} = 6 W, T_{amb} = 80 ºC.

Infrared temperature measurements were made on the top contact with the device biased over a range of DC power levels (0.1 - 5.7 W). The measured peak temperature rise is plotted as a function of power in Figure 3.12. As expected, the temperature increases with increased power dissipation, rising to 190 °C at 5.7 W.

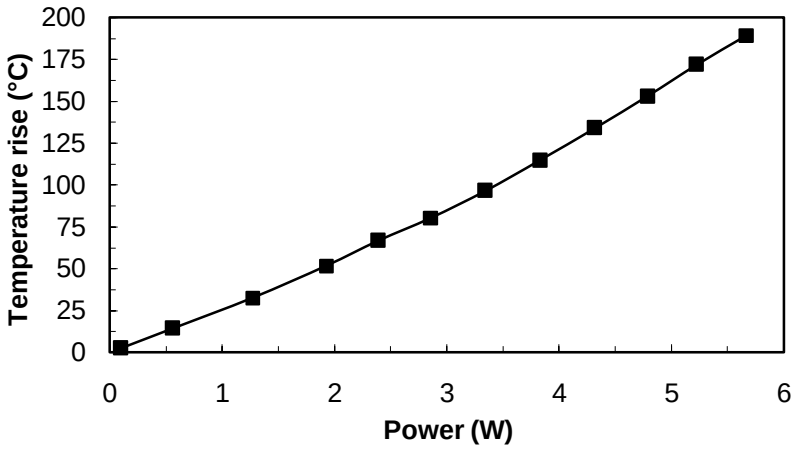

Figure 3.12: Measured temperature rise on the top contact of the graded-gap Gunn diode plotted as a function of dissipate power. T_{amb} = 80 ºC.

The thermal performance of the Gunn diode is traditionally characterised by its thermal resistance R_{th} which is given by

$$R_{th} = \frac{\Delta T_{rise}}{P_{dis}} \tag{3-2}$$

where ΔT_{rise} is the peak temperature rise generated by the device for a given dissipated power P_{dis}. The thermal resistance of the Gunn diode was calculated from the results of the IR temperature measurements and is plotted as a function of dissipated power in Figure 3.13. The thermal resistance of the Gunn diode increases with increasing power from approximately 25 °C/W at a low power level of 0.1 W, to 33.4 °C/W at 5.7 W. Some of the increase in thermal resistance may be attributable to the temperature dependent thermal conductivity of GaAs [77]. The thermal conductivity of the material will decrease at higher power levels due to increased heating in the semiconductor. As temperature rises, heat flow from the hot transit layer towards the cooler integral heatsink and package will be impeded.

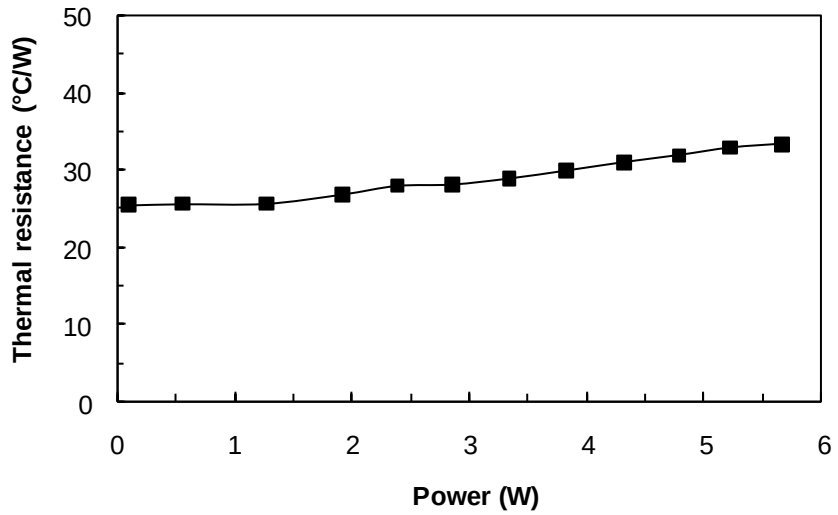

Figure 3.13: Thermal resistance of the graded-gap Gunn diode plotted as a function of dissipated power. T_{amb} = 80 °C.

3.6 Comparisons with a 1D Thermal Resistance Model

To provide a comparison with the results of the IR temperature measurements, a conventional 1D thermal resistance model of the graded-gap Gunn diode was developed to predict its peak operating temperature. Thermal resistance models are routinely used to predict the operating temperature of devices such as transistor structures [84]. They have the advantage of being easier to implement, compared to models developed using differential heat flow analysis. In this case, the thermal resistance model represents an ideal graded-gap Gunn diode for which the following assumptions were made:-

- All power is uniformly dissipated within the transit layer.
- No thermal boundary resistance occurs at material interfaces, for example, due to poor thermal contact.
- No heat loss occurs due to convection and emitted radiation.
- No heat loss occurs through the top contact and bond wire.
- During powering, the ambient package temperature is constant (80 °C).

3.6.1 Thermal model construction

The thermal resistance model takes into account the geometry and thermal conductivity of the semiconductor and metal layers through which heat flux flows, from the transit layer to the integral heatsink and package. The flow of heat flux can be thought of as being analogous to electrical current flow through a series of resistors. Instead of a voltage potential, a temperature drop is created across each element. The thermal resistance model is shown in Figure 3.14.

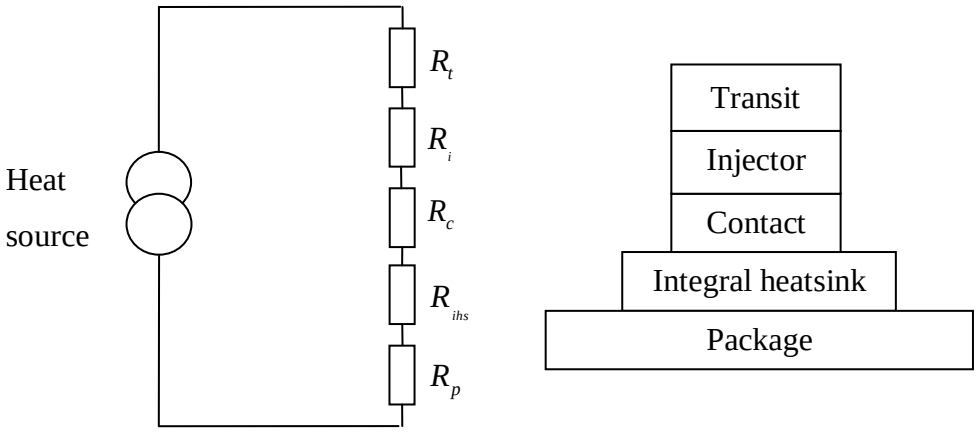

Figure 3.14: Thermal resistance model of the graded-gap Gunn diode.

The total thermal resistance of the Gunn diode R_{tot} is a sum of the individual thermal resistances of the structural elements shown in Figure 3.14 and is given by

$$R_{tot} = R_t + R_i + R_c + R_{ihs} + R_p \tag{3-3}$$

where R_t, R_i, R_c, R_{ihs} and R_p are the thermal resistances of the transit layer, injector layer, contact layer, integral heatsink and package, respectively.

The thermal resistance of each of the cylindrical semiconductor layers forming the mesa can be considered to be analogous to the electrical resistance of a circular wire of known dimensions and cross-sectional area. In this case, the non-geometric parameter controlling the thermal resistance being thermal conductivity k. The

thermal resistance R_{th} of the individual semiconductor layers can, therefore, be approximated by

$$R_{th} = \frac{t}{Ak} \tag{3-4}$$

where A is the cross sectional area of the mesa and t is the thickness of each semiconductor layer. The thermal conductivity of GaAs is known to vary with temperature and doping density. From published data [77], the thermal conductivity of the GaAs transit layer k_t in W/m.K can be approximated by

$$k_t = 62000\, T^{-1.25} \tag{3-5}$$

where T is the temperature of the material in Kelvin. Likewise, the thermal conductivity of the highly doped GaAs contact layer k_c can be approximated by

$$k_c = 44550\, T^{-1.25} \tag{3-6}$$

The thermal conductivity of AlGaAs, having a known Al composition, is given by [85]. Given an average Al composition in the injector layer of 0.2 and assuming a similar temperature dependence to the GaAs layers, k_i was approximated by

$$k_i = 28120\, T^{-1.25} \tag{3-7}$$

The thermal conductivities of the transit, injector and contact layers were substituted into expression (3-4) to give their respective thermal resistances. The total thermal resistance of the Gunn diode R_{tot} is, therefore, given by the sum of the individual thermal resistances of its structural elements

$$R_{tot} = \frac{1}{A}\left[\frac{t_t}{62000\ T_t^{-1.25}} + \frac{t_i}{28120\ T_i^{-1.25}} + \frac{t_c}{44550\ T_c^{-1.25}}\right] + R_{ihs} + R_p \qquad (3\text{-}8)$$

where A is the mesa cross-sectional area. t_t, t_i and t_c are the thicknesses of the respective semiconductor layers and T_t, T_i and T_c were taken as their average temperatures. As the thermal resistance of the integral heatsink and package constitutes a spreading thermal resistance, which cannot be calculated using this simple approach, values obtained from an ANSYS© thermal model, developed by the manufacturer, were used. The model is described in Section 3.8.4 of this chapter.

The peak operating temperature rise T_{rise} generated by the Gunn diode can be calculated as a product of R_{tot} and P_{dis} by

$$T_{rise} = P_{dis} R_{tot} \qquad (3\text{-}9)$$

3.6.2 Implementation

To find the peak device operating temperature at a particular power level, the expressions given in Section 3.6.1 were solved using an iterative routine, which was implemented in MATLAB© software. Figure 3.15 shows a flow chart of the model. The model initially calculates the thermal conductivities and then thermal resistances of the structural elements of the Gunn diode at ambient temperature (unpowered conditions). The thermal resistance values are used to calculate the device operating temperature at low power. At this operating temperature, new thermal conductivity and thermal resistance values are then calculated. The iterative process is repeated, with the power level increased incrementally until it matches the level required P_{dis}; at this point the peak device operating temperature is given. The MATLAB© code developed for the thermal model is given in Appendix B.

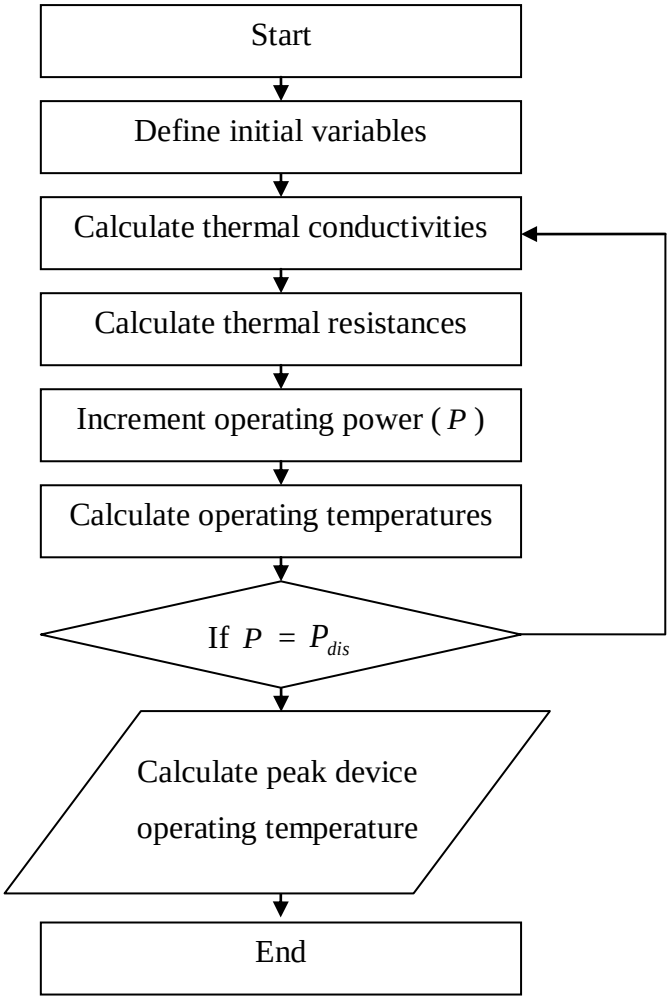

Figure 3.15: Flow chart showing the 1D thermal resistance model of the Gunn diode.

3.6.3 Temperature comparison with IR results

Modelled thermal conductivity and thermal resistance values obtained for the Gunn diode's semiconductor mesa layers are shown in Table 3-1. The thermal resistance of the transit layer constitutes the most significant thermal resistance of these semiconductor layers (6.4 °C/W). This thermal resistance is, however, dwarfed by the thermal resistance of the integral heatsink and package, which is estimated by the ANSYS model to have a combined thermal resistance of 21.7 °C/W.

Layer	k (W/m.K)	R_{th} (°C/W)
Transit	20.4	6.4
Injector	36.3	0.36
Contact	32.5	3.2

Table 3-1: Modelled thermal conductivity k and thermal resistance R_{th} values of the semiconductor layers of the graded-gap Gunn diode at an operating power of 6 W.

A comparison was made between the peak device operating temperatures obtained from the thermal model and those obtained from the IR temperature measurements made on the Gunn diode's top contact. The temperature comparison is shown over a range of power levels (0.1 – 6.0 W) in Figure 3.16. There is reasonable agreement between both sets of results to within ± 10 °C, however, there is some small discrepancy. At high power levels (> 4 W), the measured IR results show a more rapid temperature rise with increasing power.

A number of factors could lead to the small discrepancies between the measured and modelled temperature rise: (1) other sources of thermal resistance could exist which are not included in the conventional thermal model, for example, thermal voids between the chip and integral heatsink (2) The power dissipation profile within the device may differ from the uniform nature assumed. This could be because of temperature induced mobility changes [86] and heating in the injector layer [87] (3) Errors in the IR temperature measurements may have caused some discrepancy, for example, due to reflected background radiation from surrounding parts of the structure. Nevertheless, the comparison shows that the measured IR temperatures are of a similar order to those expected from the thermal model.

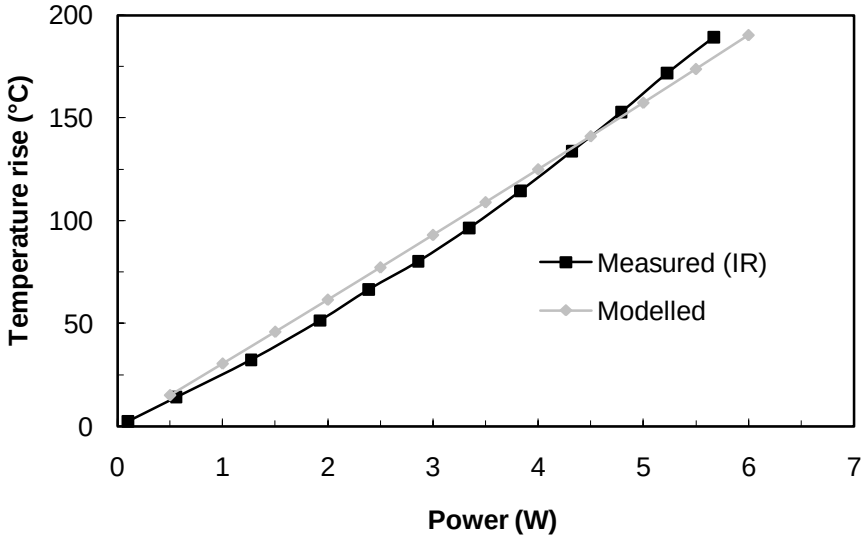

Figure 3.16: Comparison between modelled and measured peak operating temperature rise for the Gunn diode. The temperature rise is plotted against dissipated power. T_{amb} = 80 ºC.

3.7 Experimental Validation

Micro-thermocouple probing was used to validate the accuracy of the IR temperature measurements made on the top contact of the graded-gap Gunn diode. Thermocouples have been routinely used as a low cost way of obtaining temperature measurements on electronic devices, for example, on packages [88].

3.7.1 Micro-thermocouple measurement procedure

A precision fine wire K-type thermocouple probe, with a 25 µm diameter probe tip (Omega), was used to monitor the operating temperature on the metal top contact of a second Gunn diode sample. The device dimensions are given in Appendix A (Sample 2).

A diagram showing the experimental arrangement used for the micro-thermocouple measurements is shown in Figure 3.17. The thermocouple probe was mechanical supported by soldering its leads to a metallised ceramic pad adjacent to the sample. Fine tweezers were used to position the probe tip onto the top contact. Good physical contact was made with the surface to facilitate the transfer of thermal energy. Some

underestimation of the actual surface temperature may occur if the contact is poor [88]. Temperatures were monitored using a calibrated Kane May digital thermometer (KM330).

The micro-thermocouple technique is time consuming to implement because of the manual skill required to accurately mount the probe tip. The technique is, therefore, only suitable for a one-off measurement and is not a procedure which can be routinely implemented, for example, to test batch samples in a manufacturing process.

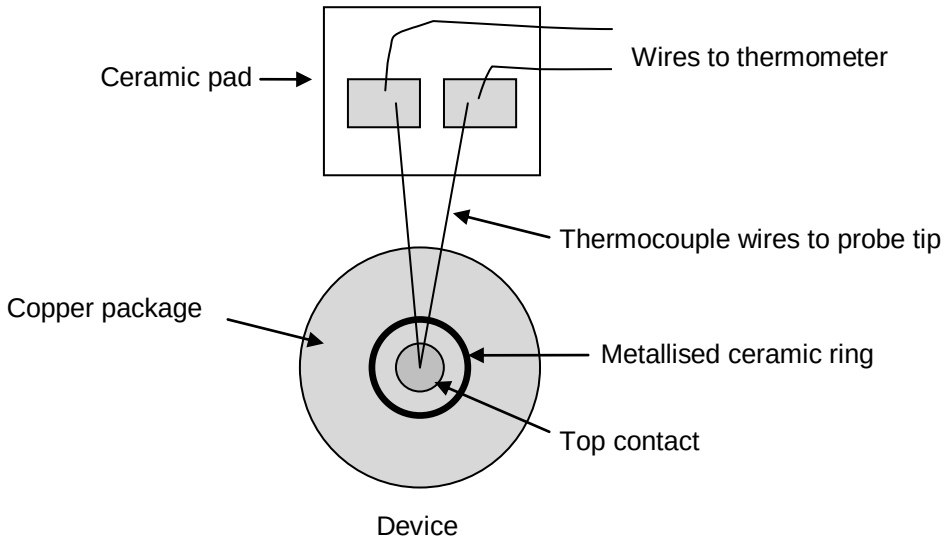

Figure 3.17: Experimental arrangement used for the micro-thermocouple measurements.

3.7.2 Comparison with IR results

A graph showing a comparison between the micro-thermocouple and IR temperature measurements is shown in Figure 3.18. The Gunn diode was biased over a range of DC power levels (2.4 – 5.7 W). A good correlation occurs between both sets of results, with a measured temperature difference of less than ± 5 °C, at all power levels. For example, at an operating power of 6 W, the IR and micro-thermocouple measurements show increases in temperature of 150 °C and 151 °C, respectively. This close agreement improves confidence in the accuracy of the IR temperature measurements and rules out the possibility that there are significant sources of experimental error.

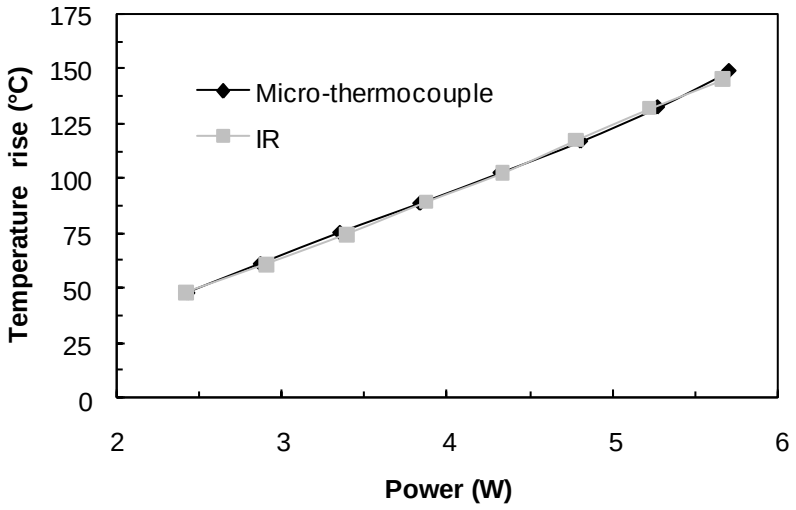

Figure 3.18: Comparison between the operating temperature rise measured on the Gunn diode using micro-thermocouple probing and IR thermal microscopy. T_{amb} = 80 ºC.

3.8 Infrared Temperature Profiling on the Substrate Layer

As discussed, it has conventionally been assumed that temperatures are uniform within the substrate layer of the Gunn diode and match the peak device operating temperature. In this work, IR thermal microscopy was used to image the substrate layer, in an attempt to confirm this assumption.

3.8.1 Infrared measurements on the substrate layer

A packaged graded-gap Gunn diode sample was modified to image the substrate layer. Normally the packaged device has a metallised ceramic ring which surrounds the mesa and acts as an electrical contact. For this work, half of the ceramic ring was removed by e2v (Lincoln) Ltd. to expose the mesa side for imaging. A SEM image showing the exposed mesa side is shown in Figure 3.19. The image depicts the top overhanging metal contact, above the cylindrical mesa layers. The mesa is clearly visible underneath. The substrate layer forms the bulk of the mesa and is 10 μm in thickness and has a diameter of 60 μm. The device dimensions are given in Appendix A (Sample 3).

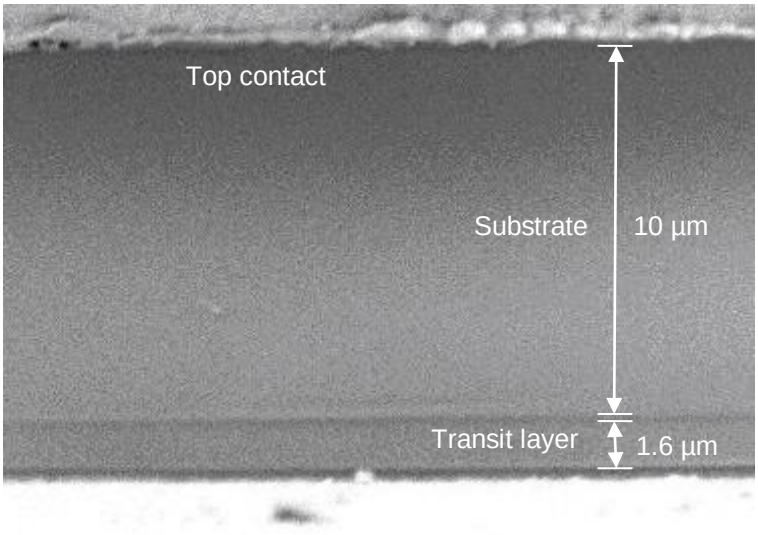

Figure 3.19: Scanning electron microscope image showing the semiconductor layers forming the mesa of the graded-gap Gunn diode.

The modified Gunn diode sample was mounted into an aluminium jig for imaging of the substrate layer by the IR microscope. Figure 3.20 shows a diagram of the jig. The jig has a hinged front end with a recessed circular cavity to accommodate the push fit pico package. The hinged section of the jig can be rotated to facilitate optimum viewing of the mesa side. In practice, it was found that the optimum viewing angle was when the diode was rotated on its side by approximately 90 ° to its vertical position (see Figure 3.20).

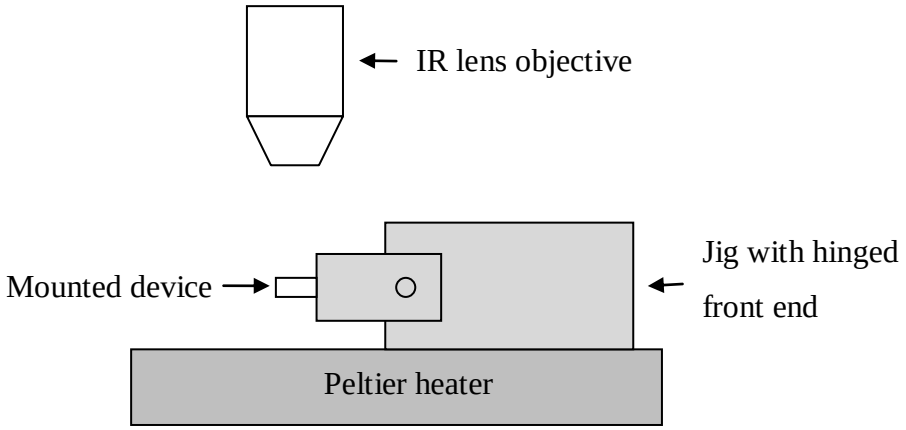

Figure 3.20: Experimental arrangement used to mount the Gunn diode sample for the IR measurements on the substrate layer.

A visible image showing the Gunn diode electrically connected in the jig is shown in Figure 3.21. A sliding metal contact was used to make an electrical anode connection with the metallised ceramic ring (the earth connection was made via the body of the jig). The whole jig assembly was mounted onto the Peltier heated stage of the IR microscope to enable its temperature to be controlled during the emissivity correction procedure and subsequent device powering. A recessed thermocouple was embedded 3 mm away from the mounting point to give an estimate of the ambient temperature.

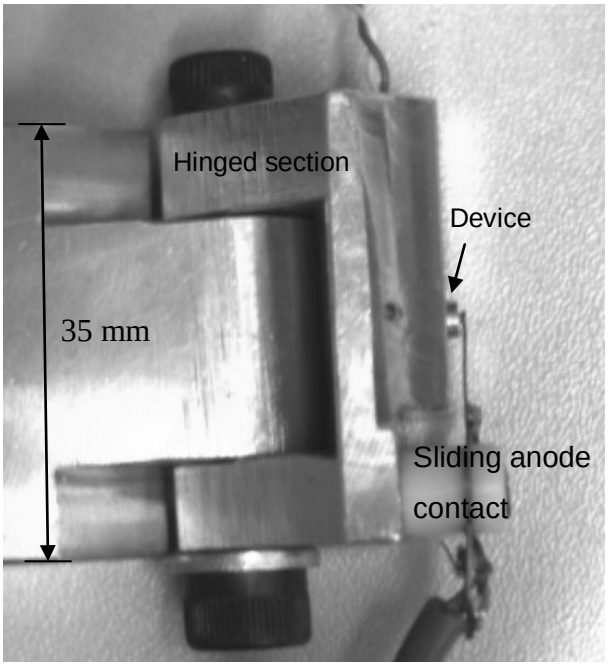

Figure 3.21: Optical image showing the Gunn diode electrically connected in the jig.

Infrared temperature measurements were made along the substrate layer using the QFI Infrascope II IR microscope. A 25 × lens objective was used for imaging, giving a total field of view of 232 × 232 μm and a spatial resolution of 2.5 μm. Emissivity measurements were made using the two-temperature technique described in Section 2.3.1 of Chapter 2. The average emissivity measured on the semiconductor area was found to be 0.4, sufficiently high to give low noise radiance images.

3.8.2 Temperature results

Infrared temperature measurements were made on the mesa side of the graded-gap Gunn diode over a range of DC power levels. A typical IR temperature image of the mesa side, at a bias level of 2.8 W, is shown in Figure 3.22. The image shows areas of high temperature superimposed onto an un-powered black and white radiance image of the structure. The mesa (12.7 µm in height) is visible in the lower portion of the image (marked), above which is the top overlapping Au metal contact, which has an attached Au bond wire (25 µm in diameter). Areas of peak temperature occur along the surface of the mesa. Temperatures are highest in the substrate layer, in a region closest to the top contact. The measured peak temperature on the substrate layer is 227 °C, a rise above the ambient jig temperature of 147 °C.

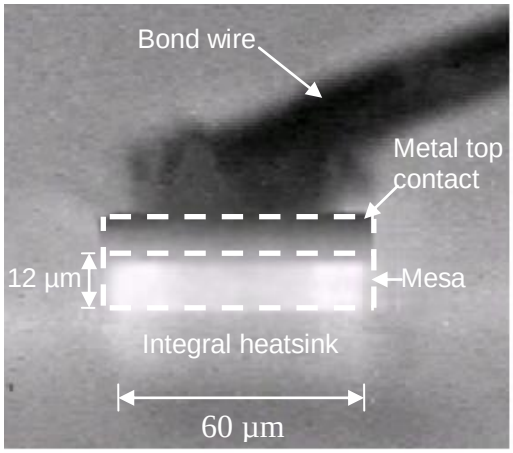

Unpowered IR radiance image (for reference).

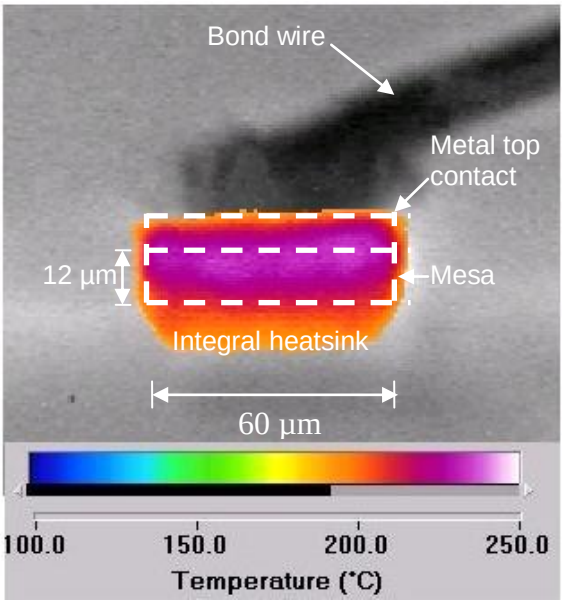

Figure 3.22: Infrared radiance and temperature images of the mesa side of the graded-gap Gunn diode. Temperature hotspots have been superimposed onto a black and white radiance image of the structure. P_{dis}= 2.8 W, T_{amb} = 80 °C.

A graph showing the measured IR temperature profile along the length of the substrate layer is shown in Figure 3.23. Measurements were made with the device biased at a number of power levels (1.8, 2.5 and 2.8 W, respectively). As expected, the operating temperature increased with increased power dissipation, rising from a peak of 86 °C at 1.8 W, to 150 °C at 2.8 W. Interestingly, a small temperature

gradient occurred along the length of the substrate layer, with temperature rising towards the top contact. At 2.8 W, a temperature rise of ~ 17 °C was measured. As discussed, previous authors have assumed that no power dissipation occurs in the substrate layer and a uniform temperature distribution exists along its length [73]. It was initially thought that the IR measurements indicated that a small amount of power was, in fact, being dissipated as heat within this layer, which would affect the device operating temperature. The flow of heat flux from the substrate layer towards the cooler integral heatsink was thought to cause the measured temperature rise shown in Figure 3.23.

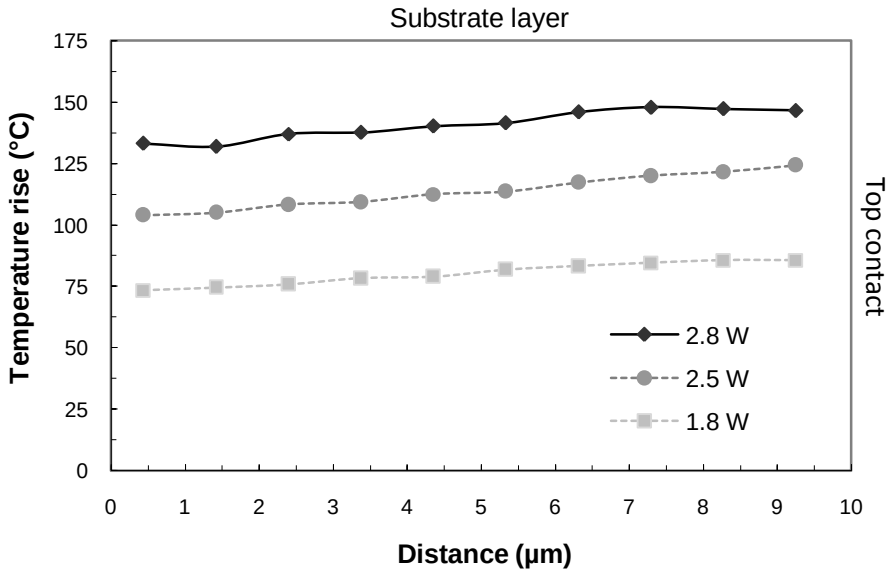

Figure 3.23: Infrared temperatures profile measured along the length of the substrate layer of the graded-gap Gunn diode at a number of power levels. T_{amb} = 80 °C.

3.8.3 Expected power loss

The expected power loss in the substrate layer was estimated mathematically. Semiconductor resistivity ρ is given by

$$\rho = \frac{1}{q(n\mu_n + p\mu_p)} \tag{3-10}$$

where q is the electron charge (1.602×10^{-19} C), n and p are the density of electrons and holes with mobility μ_n and μ_p, respectively. Assuming a negligible density of minority carriers (holes), ρ can be approximated by

$$\rho \cong \frac{1}{qn\mu_n} \tag{3-11}$$

where n is essentially equal to the donor density of electrons within the material (N_d = 2×10^{18} electrons/cm^3). Taking the mobility of the GaAs substrate layer to be μ_n = 2800 cm^2/V.s at the measured operating temperature [12], the resistivity of the substrate was calculated to be 1.1 mΩ.cm. Given the resistivity and the physical dimensions of the substrate, its DC electrical resistance can be estimated using

$$R = \frac{\rho t}{A} \tag{3-12}$$

where t is the thickness of the substrate layer (10 μm) and A is its cross sectional area. The DC resistance of the substrate layer was calculated to be 15 mΩ. When the device is biased, a small proportional of the total power will be dissipated in the substrate layer. This power loss can be calculate using the standard expression

$$P = I^2 R \tag{3-13}$$

where R is the resistance of the substrate and I is current flow. Given a typical power dissipation of 5 W, calculations show that 8 mW will be dissipated in the substrate layer, which results in an estimated power loss of 0.16 %.

3.8.4 Finite element thermal model construction

Thermal modelling was used to test the hypothesis that ohmic heating in the graded-gap Gunn diode may account for the measured temperature rise along the length of the substrate layer. An ANSYS finite element thermal model of the device was developed in collaboration with e2v (Lincoln) Ltd. The finite element model

represents an improvement on the 1D thermal resistance model discussed in Section 3.6, as it can be used to give a detailed 3D simulation of the steady state temperature distribution throughout the structure.

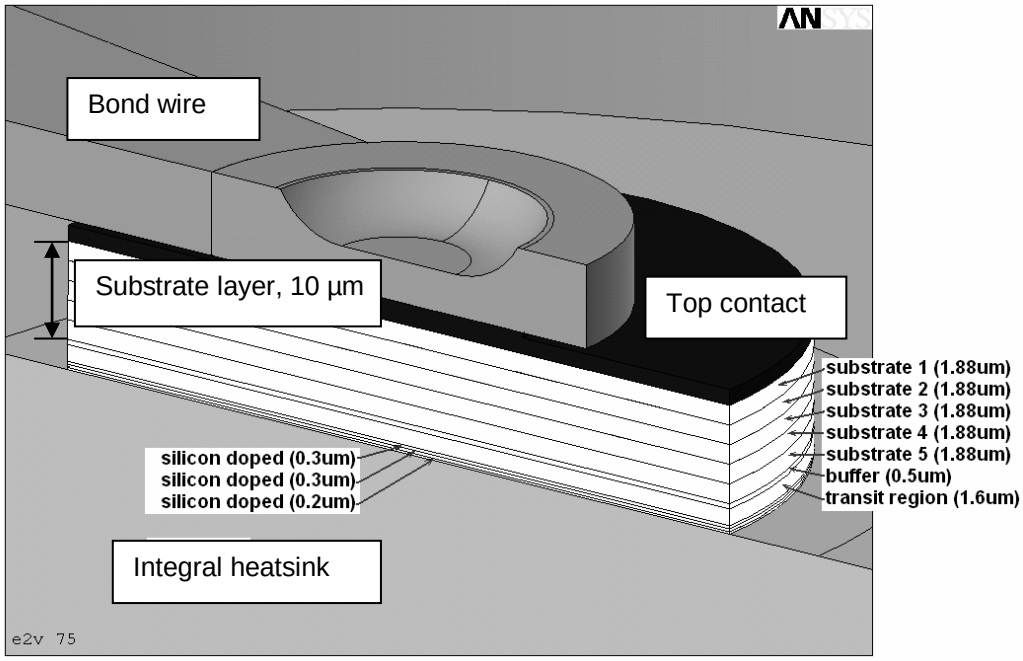

Figure 3.24: Construction of the ANSYS thermal model of the graded-gap Gunn diode.

A cross sectional view of the modelled structure developed by e2v (Lincoln) Ltd. is shown in Figure 3.24. The structure shows the bond wire attached to the metal top contact of the device (shaded black). Beneath the top contact are the cylindrical GaAs layers forming the mesa. All dimensions were set to match those of the measured device. In the model, 0.16 % of the total power was uniformly dissipated in the substrate layer to simulate the calculated power loss due to ohmic heating (the remaining power was uniformly dissipated in the transit layer).

3.8.5 Comparison with IR temperature profile

A comparison between the modelled and measured (IR) temperature profiles along the length of the Gunn diode's substrate layer is shown in Figure 3.25. At a bias level of 2.8 W, the thermal model shows a virtually uniform temperature rise (125 °C) along the entire length of the substrate layer. In contrast, the IR temperature measurements

show an elevated temperature rise towards the top contact. The work strongly suggests that errors occur in the IR temperature measurements made on the substrate layer.

Errors in the IR temperature measurements were thought to be a consequence of the optical transparency of the GaAs to IR radiation [89]. It is thought that some interfering IR radiation will be transmitted through the semiconductor, for example, from the metallised areas, distorting the measured surface temperature profile. Errors due to optical transparency are considered in Chapter 5.

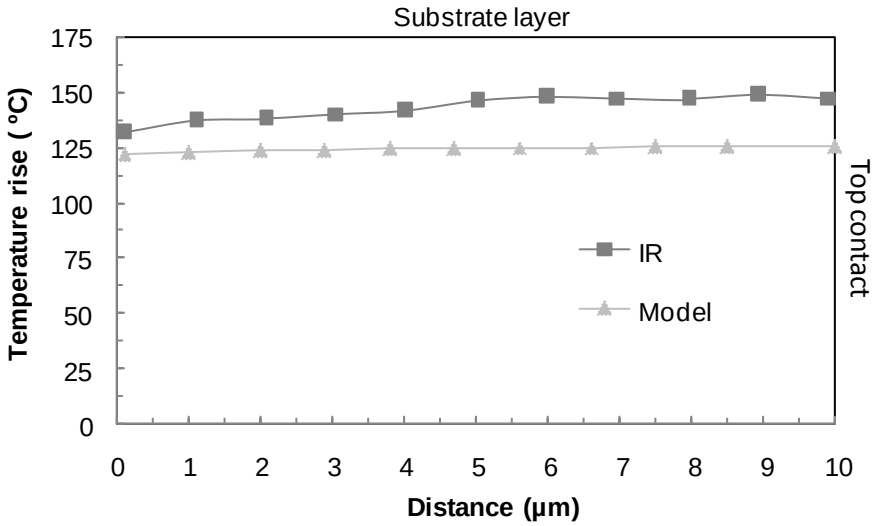

Figure 3.25: Modelled and measured IR temperature profiles longitudinally along the substrate layer of the graded-gap Gunn diode. P_{dis} = 2.8 W, T_{amb} = 80 °C.

3.9 Conclusions

The work has shown how IR thermal microscopy can be used to make rapid 2D temperature measurements on the metal top contact of the Gunn diode, enabling the extraction of its peak operating temperature. With the graded-gap device studied, large increases in operating temperature were measured. A peak temperature rise of 160 °C was recorded at an operating power of 5 W. Measured operating temperatures were found to be of a similar order to those predicted by a conventional 1D thermal resistance model and were in good agreement with micro-thermocouple

measurements. One disadvantage with making IR temperature measurements on the metal top contact is the need to coat the device with a destructive high emissivity layer. An improved IR measurement technique, which removes the need for coating, is discussed in Chapter 6.

Infrared temperature measurements were also made on the substrate layer of the graded-gap Gunn diode. However, temperature errors were thought to occur with these measurements. It is possible that some interfering background IR radiation is transmitted through the optically transparent GaAs, distorting the measured temperature profile. Temperature errors related to optical transparency are considered in Chapter 5.

CHAPTER 4. THERMAL ANALYSIS OF THE CONVENTIONAL GALLIUM ARSENIDE GUNN DIODE

4.1 Introduction

Work was undertaken to study the thermal performance of the conventional GaAs Gunn diode through a combination of experimental temperature measurements and thermal modeling. Temperature measurements made on the mesa side of the device can be used to study the temperature profile along the semiconductor layers and also obtain the peak device operating temperature. Although IR thermal microscopy can be used to make temperature measurements on the mesa side (see Section 3.8 of Chapter 3), its spatial resolution is limited to ~ 2.5 μm, a disadvantage, particularly as future development work will lead to the physical dimensions of the device being reduced in size to increase the operating frequency [90]. Another drawback with IR is the difficulty in making accurate measurements on semiconductor layers due to their optical transparency (see Chapter 5).

Micro-Raman spectroscopy is an established technique for making accurate high resolution temperature measurements on semiconductor devices, for example, GaAs and GaN transistors [37], [91]. In this work, micro-Raman spectroscopy was used to make high resolution temperature measurements on the GaAs mesa side of the conventional Gunn diode. A paper has been published regarding this work in the IET Journal of Science, Measurement & Technology (see Section 1.4, Publication no. 4). As well as the experimental measurements, further work was also undertaken to develop an electro/thermal model of the conventional Gunn diode using Sentaurus TCAD finite element software. The model was used to assess the thermal resistance of the structural elements which make up the device; including the integral heatsink and package which cannot be fully optically accessed for thermal measurement.

4.2 Device Details

The conventional X-band Gunn diode samples used in this study were epitaxially grown on a GaAs substrate using vapour phase epitaxy (VPE) by e2v (Lincoln) Ltd. A

diagram showing the layered structure of the Gunn diode is shown in Figure 4.1. The mesa layers consist of a lightly doped GaAs transit layer, sandwiched between two GaAs n^{++} layers (termed contact and substrate layers). The electron doping concentration in the transit layer was 1.5×10^{15} electrons/cm^{-3} and in the contact and substrate layers $0.5 - 2.0 \times 10^{18}$ electrons/cm^3, respectively. In the first sample studied, the contact layer thickness was 10 µm, the transit layer thickness was 10 µm and the substrate layer had a thickness of 80 µm. Overall, the total thickness of the mesa was 100 µm and it had a nominal diameter of 160 µm. Unlike the graded-gap diode described in Chapter 3, the conventional device does not incorporate a hot electron injector. The device dimensions are given in Appendix C (Sample 1).

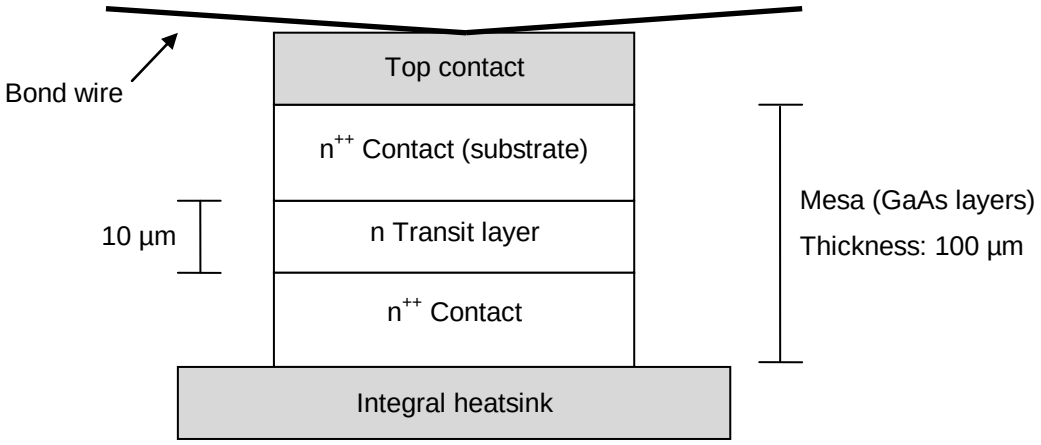

Figure 4.1: Simplified diagram showing the construction of the conventional X-band Gunn diode.

Figure 4.2 shows an optical image of the conventional X-band Gunn diode. An Au bond wire is visible in the upper portion of the image which forms an electrical anode connection between a surrounding metallised ceramic ring (partially removed for inspection) and the square metal top contact. Beneath the metal top contact are the GaAs semiconductor layers forming the mesa. Within the mesa, the bulk of electrical power supplied to the device will be dissipated as heat in the transit layer. To improve the removal of heat from the diode, the mesa is Au electroplated and ultrasonically bonded to a cylindrical Au integral heatsink. The integral heatsink has a thickness of

80 μm and a diameter of 300 μm. The integral heatsink is, in turn, ultrasonically bonded onto a push fit copper pico package (of identical dimensions to that used to package the graded-gap device discussed in Chapter 3).

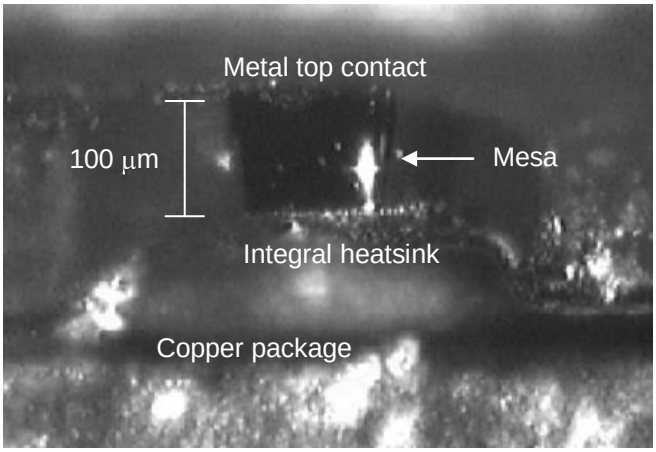

Figure 4.2: Optical image (5 × magnification) showing a side profile of the conventional X-band Gunn diode. The image is slightly distorted due to the narrow optical field of view.

A higher magnification optical image was also taken of the mesa side (see Figure 4.3). The edges of the transit layer (10 μm in length) can be identified in the image. The transit layer is sufficiently long to allow multiple point temperature measurements to be made along its length using high resolution (~ 1 μm) micro-Raman spectroscopy.

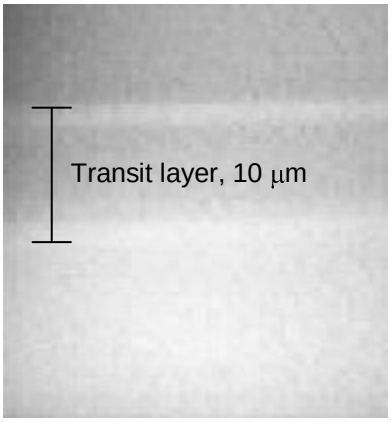

Figure 4.3: Optical image (25 × magnification) of the mesa side of the conventional X-band Gunn diode showing the transit layer.

4.3 Micro-Raman Temperature Measurements

Micro-Raman spectroscopy was used to study the temperature profile along the mesa side of the conventional X-band Gunn diode. Micro-Raman spectroscopy is an active technique which uses laser excitation of the semiconductor. Temperature induced shifts in phonon frequency are measurable using a spectrometer (see Section 2.3.2 of Chapter 2). For this study, a Renishaw micro-Raman spectrometer, integrated into a Leica microscope, was used. The facility is housed in the Physics Department at Bristol University.

4.3.1 Measurement procedure

For temperature measurement purposes, an aluminium jig was used to mount the conventional X-band Gunn diode sample. Figure 4.4 shows the measurement arrangement (more details regarding jig construction are given in Section 3.8.1 of Chapter 3). The jig enabled the device to be mechanically tilted, facilitating direct optical probing of the mesa side by the laser beam of the micro-Raman system. To control its temperature, the jig was thermally mounted onto a Peltier heat exchanger. The whole arrangement could be moved using a motorised XY stage to enable device positioning.

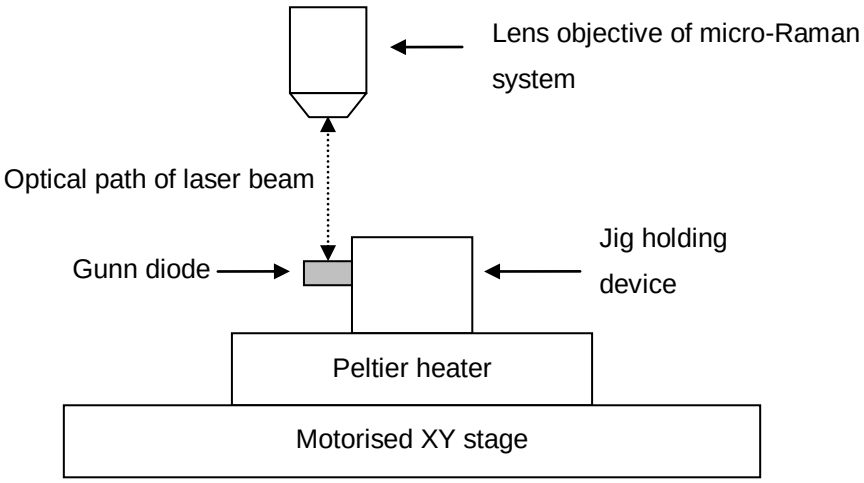

Figure 4.4: Experimental arrangement used to make the temperature measurements along on the mesa side of the conventional X-band Gunn diode using micro-Raman spectroscopy.

The micro-Raman system at Bristol University used an $Argon^{+}$ ion laser with a wavelength of 488 nm for optical excitation of the GaAs. High resolution, sub-micrometer, temperature measurements are achievable by using short wavelengths. The laser excitation energy was higher than the bandgap energy of GaAs. Normally, sub-bandgap lasers are used to prevent localised heating, however, the use of a sub-bandgap laser is not easy to implement for GaAs. Consequently, some of the laser energy will be absorbed by the semiconductor. To try and minimise possible interference with the device performance (due to localised heating and electron-hole/pair generation), the power density of the laser beam was limited to below 20 kW/cm^2. With this power level, no significant change in the DC IV characteristics of the Gunn diode was observed with or without laser illumination.

To make the micro-Raman measurements, the laser beam was focused onto the mesa side using a 50 × lens objective, giving a spot size of slightly less than 1 μm in diameter.[2] It is estimated that the laser beam depth penetration will be limited to the top 100 nm of the GaAs [35], therefore, measurements are effectively on the surface. The temperature dependence of the GaAs longitudinal optical (LO) phonon frequency was initially established by heating the device to a number of different ambient temperatures (25, 35, 50 and 115 °C) and monitoring the phonon frequency shift. The LO-phonon frequency varied linearly with material temperature, with a coefficient of $-0.0173\ cm^{-1}/°C$, agreeing well with published data [92]. The spectrometer has a spectral shift sensitivity of ± 0.1 cm^{-1}, giving a temperature resolution of ± 6 °C. To measure its operating temperature, micro-Raman measurements were made on the device under electrically unbiased and biased conditions. The change in phonon frequency between these conditions, together with its temperature dependence, was used to calculate temperature.

To obtain a temperature profile along the length of the mesa, a mechanical scanning mode was used. In this mode, the probing laser beam acquires a temperature

[2]The spot size is equal to the maximum spatial temperature resolution of the instrument.

measurement at a single spot and is then moved to the next position by mechanical movement of the stage holding the sample. A motorised XY stage, with a lateral resolution of 0.1 μm, was used to move the sample. Long integration times make the mechanical scanning mode unsuitable for fast temperature monitoring, as the system dwells on each spot for a considerable period (~ 120 s). The temperature scan along a 25 μm length of the Gunn diode mesa, with 1 μm step size, took around one hour to complete.

4.3.2 Temperature results

Figure 4.5 shows the location of the measured micro-Raman temperature profile. Temperature measurements were made on the electrically biased device in 1 μm steps, longitudinally, across the semiconductor contact, transit and substrate layers. During measurement, the ambient jig temperature was held at 80 °C.

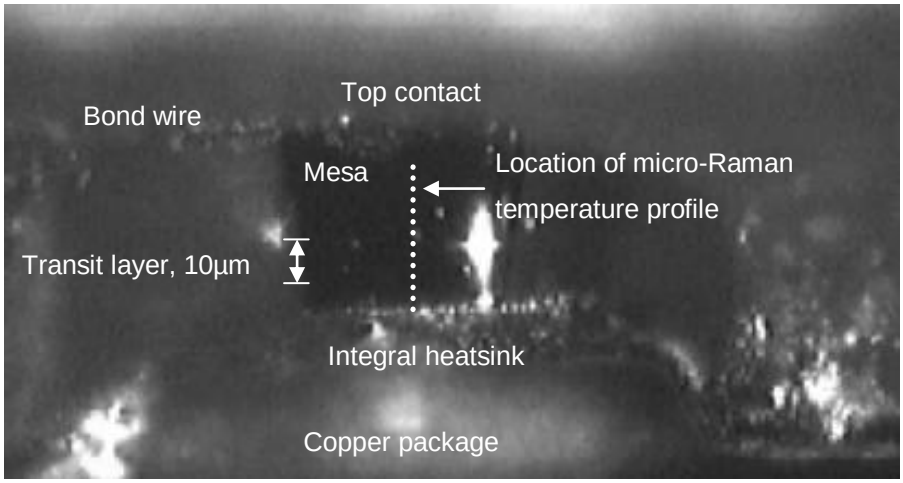

Figure 4.5: Optical image showing the mesa side of the conventional GaAs X-band Gunn diode and the location of the micro-Raman temperature profile.

A graph showing the micro-Raman mesa side temperature profile is shown in Figure 4.6. The contact, transit and substrate layers are marked on the graph. At a power level of 4.6 W, a peak temperature rise of ~ 200 °C was measured on the transit layer, giving a thermal resistance of 45 °C/W. As expected, the device operating temperature decreases along the length of the mesa, from the transit layer (where bulk

heat is dissipated) towards the integral heatsink, where the temperature is lower (~ 135 °C). The measurements suggest some local variation in temperature along the length of the transit layer itself, with a few adjacent measurement points varying in temperature by ± 10 °C. These variations are likely to be due to artefacts in the measurement procedure caused by random system noise. Longer integration of the recovered micro-Raman signal could have been used to reduce noise but at the expense of increased recording time.

Due to the length of the micro-Raman serial recording procedure, only a few temperature measurements were made along the length of the substrate layer. The temperature rise measured on the substrate layer is, however, within 5 °C of the peak device operating temperature. This suggests that ohmic heating in the substrate layer has a negligible effect on the device operating temperature.

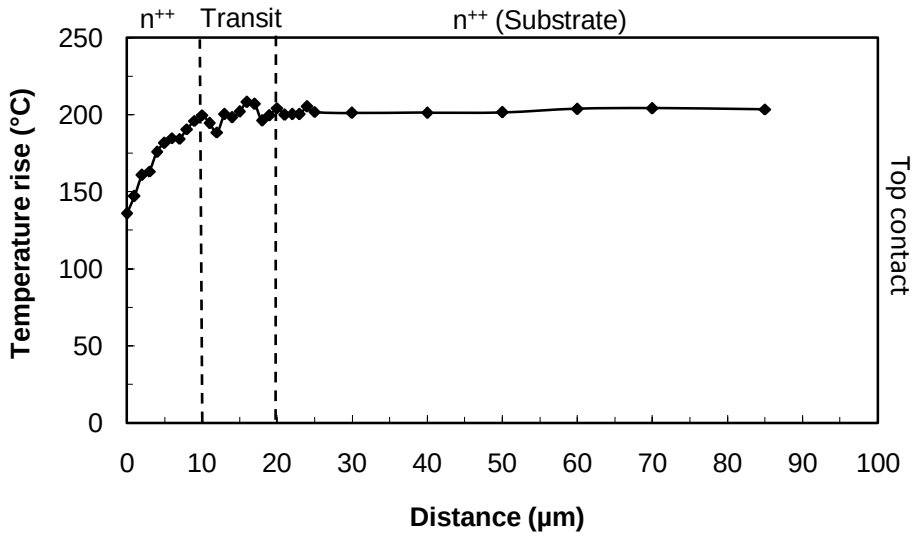

Figure 4.6: Micro-Raman temperature profile measured along the length of the mesa side of the conventional X-band Gunn diode. The number of temperature measurements made in the substrate layer was limited to ensure reasonable recording time. P_{dis} = 4.6 W, T_{amb} = 80 °C.

4.4 Comparison with IR Temperature Measurements

Infrared temperature measurements were also made on the mesa side and top contact of the conventional X-band Gunn diode using the QFI Infrascope II IR microscope. To image the mesa side, a high magnification 25 × lens objective was used, giving a spatial resolution of 2.5 μm. To increase the surface emissivity and reduce possible errors due to optical transparency, the mesa side was coated with a layer of black paint. Emissivity measurements were made on the coated mesa side using the two temperature emissivity measurement procedure described in Section 2.3.1 of Chapter 2. During temperature measurements, the device was powered at 4.6 W and the jig temperature held at 80 °C (identical conditions to the micro-Raman spectroscopy measurements).

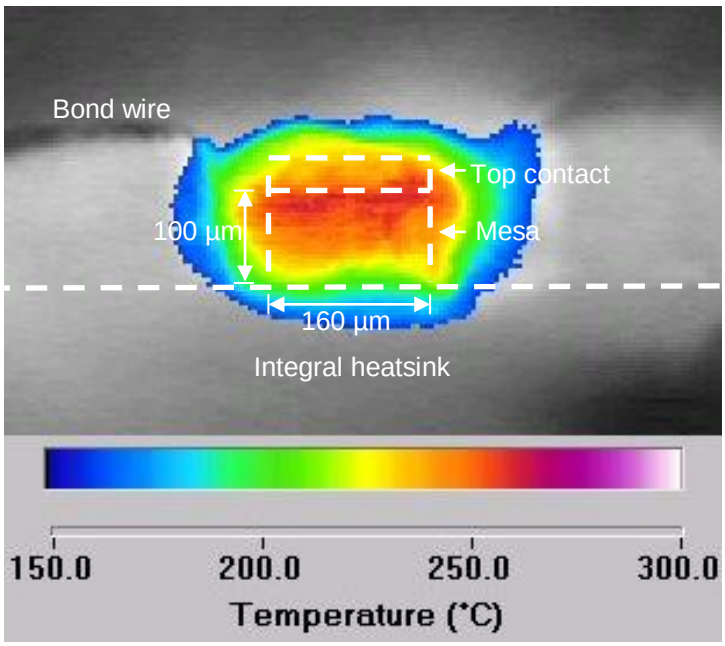

Figure 4.7: Infrared temperature image of the mesa side of the electrically powered conventional X-band Gunn diode. P_{dis} = 4.6 W, T_{amb} = 80 °C.

Figure 4.7 shows a 2D IR temperature map of the mesa side. Temperatures have been superimposed onto a black and white radiance image of the structure. The coated IR results were directly compared to those obtained from micro-Raman spectroscopy. A graph showing the mesa side temperature profile obtained from both sets of measurements is shown in Figure 4.8. The IR measurements show a general

temperature rise along the length of the mesa, from its interface with the integral heatsink (~ 110 °C), towards the top contact (~ 180 °C). The temperature rise appears more pronounced along the contact and transit layers, where heat flux flows towards the integral heatsink. Overall, the IR temperatures are depressed, compared to those measured using micro-Raman, particularly on areas towards the integral heatsink. For example, the IR temperatures are around 80 °C lower on the transit layer. The temperatures measured using IR are likely to be distorted due to the thick high emissivity paint coating. The coating forms a secondary path for heat flux to flow towards the integral heatsink and will cause some reduction in surface temperature. Additionally, there could be some air gaps between the coating and surface. In this case, the comparison clearly shows the advantage of using micro-Raman spectroscopy to obtain high resolution temperature measurements directly on the semiconductor, without the need for coating.

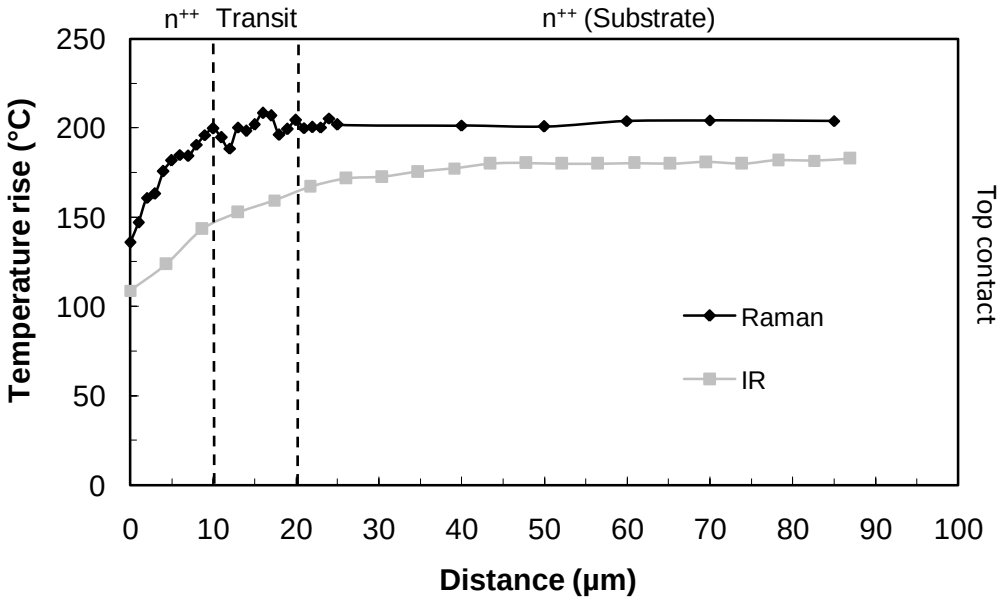

Figure 4.8: Comparison between the IR and micro-Raman temperature profiles measured along the mesa side of the conventional X-band Gunn diode. P_{dis} = 4.6 W, T_{amb} = 80 °C.

The IR microscope was used to thermally image the top contact of the conventional Gunn diode. A 5 × lens objective was used for imaging, giving a field of view of 1180 × 1180 µm square. For measurement purposes, the Gunn diode was held in a purpose built aluminium jig (described in Section 3.5.1 of Chapter 3). Emissivity measurements were made using the standard two temperature procedure. To improve the emissivity of the metal surface, a high emissivity paint coating was applied.

An IR temperature image of the square top contact of the Gunn diode is shown in Figure 4.9. The device was DC biased at 4.6 W. The image shows areas of high temperature, which have been superimposed onto a black and white radiance image of the surrounding structure. A peak temperature of 284 °C was measured on the top contact at an operating power of 4.6 W, a rise above ambient jig temperature (80 °C) of 204 °C. This is in close agreement with the peak temperature rise recorded on the transit layer (heat source) of the device using micro-Raman (~ 200 °C), at the same power level. The experimental comparison confirms the assumption that IR temperature measurements made on the top contact give a good indication of the peak device operating temperature.

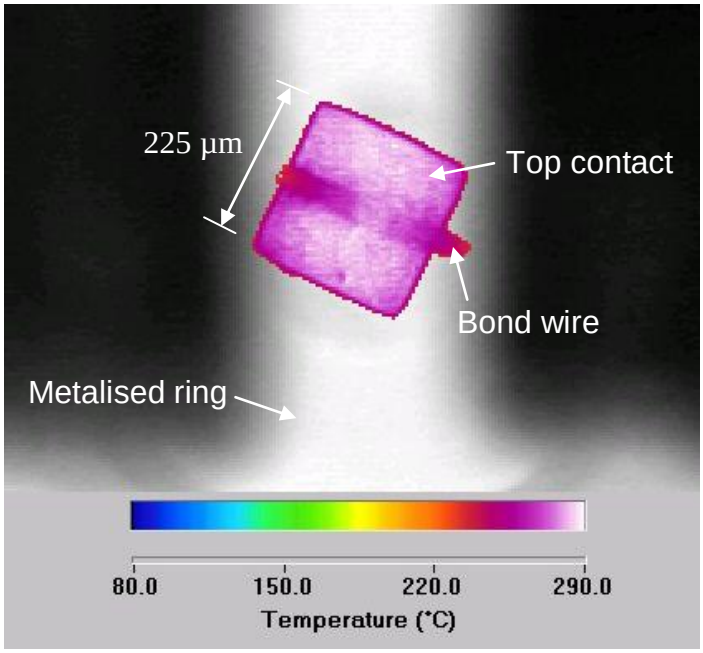

Figure 4.9: Infrared temperature image of the top contact of the electrically powered conventional X-band Gunn diode. P_{dis} = 4.6 W, T_{amb} = 80 °C.

4.5 Electro/Thermal Modelling

In recent years, increased computing power has made finite element modeling of semiconductor devices more feasible. A Sentaurus TCAD finite-element model of the conventional X-band Gunn diode was developed in cooperation with Konstantin Vershinin of the Emerging Technologies Research Centre (EMTERC), De Montfort University, Leicester. A key feature of the model is its use of electron transport modelling, added to its ability to calculate the two-dimensional (2D) operational temperature profile throughout the structure.

4.5.1 Model construction

A diagram showing the modelled conventional Gunn diode structure is shown in Figure 4.10. The diagram shows the transit layer (13 µm in length), sandwiched between the highly doped n^{++} layers (shown in red). The modelled device had a total mesa height of 100 µm and a diameter of 200 µm. The Au integral heatsink, on which the mesa was mounted, was represented as a cylindrical structure with sloping sides (to approximate the actual structure). The package was represented as a cylindrical copper block (dimensions: 2×3 mm length/width). The dimensions of the sample are given in Appendix C (Sample 2).

A number of assumptions were made in the model. Thermal convection and radiation were not considered to play any role in heat loss. The sides of the copper block, representing the package, were kept at a constant ambient temperature to represent the effect of an external heatsink. The whole of the device was thermally simulated, while the 2D electron transport model was only applied to the transit and contact layers.

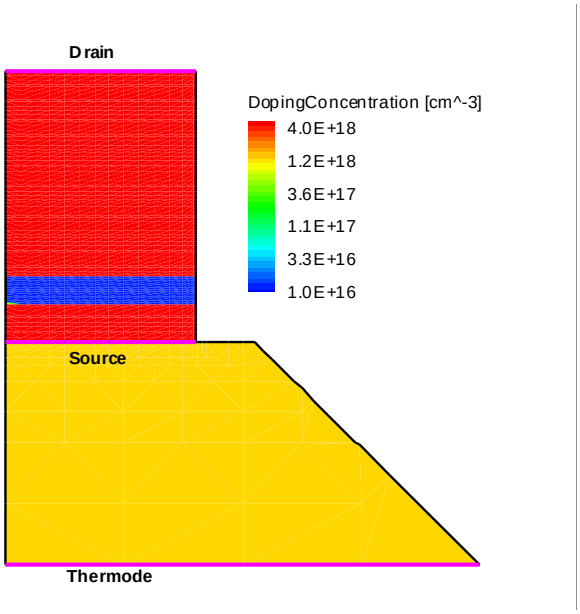

Figure 4.10: Construction of the Sentaurus TCAD finite-element model of the conventional Gunn diode.

4.5.2 Modelled electrical characteristics

A comparison between the modelled and measured DC IV characteristics of the conventional Gunn diode is shown in Figure 4.11. The agreement between the measured and modelled results is good. The critical threshold voltages V_{th} are nearly identical (4 V) and both results show a peak current level of ~ 0.95 A. A region of negative differential resistance (NDR) is also exhibited. The model accurately simulates the electrical characteristics of the device, which are in good agreement with the measured characteristics.

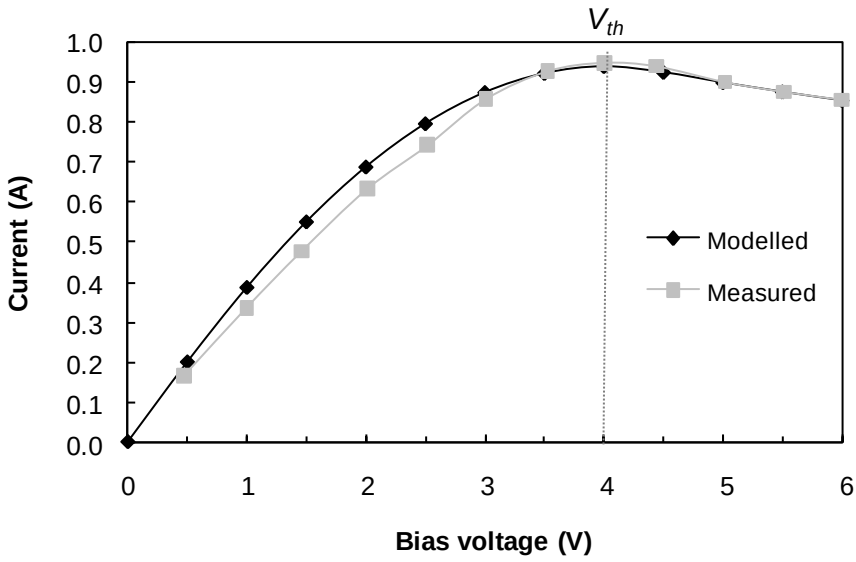

Figure 4.11: Comparison between the modelled and measured IV characteristic of the conventional X-band Gunn diode. The DC current level is shown as a function of bias voltage.

The electric field profile along the length of the transit layer was also extracted from the model and is shown at two bias voltages (1 V and 5 V) in Figure 4.12. At the lower bias voltage (1 V), the average electric field strength is below the critical threshold field E_{th} (~ 3.3 kV/cm) needed to establish domain growth. Under these low field conditions, the majority of electrons propagating across the transit layer will reside in the lower L-valley of the conduction band, in the higher mobility state (μ_1 = 8000 $cm^2.V^{-1}.s^{-1}$). The transit layer will, therefore, act as a passive electrical resistor. At the higher bias voltage (5 V), the electric field strength across the transit layer exceeds the critical threshold field E_{th} and domain growth will occur. Under these conditions, Figure 4.12 shows the electric field strength increasing along the length of the transit layer towards the anode side, where domain growth is strongest. At the interface with the anode, the electric field strength reaches a peak magnitude of 12 kV/cm.

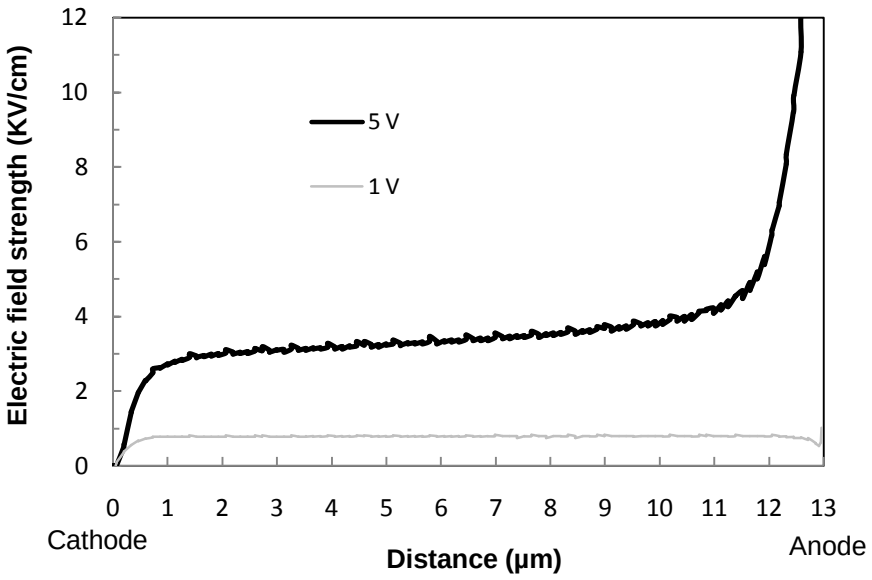

Figure 4.12: Electric field profile modelled along the length of the transit layer of the conventional Gunn diode biased at 1 V, 0.39 A (0.39 W) and 5 V, 0.9 A (4.5 W).

The time averaged power dissipation density along the length of the transit layer was also extracted from the model and is shown in Figure 4.13. The power dissipation density grows along the length of the transit layer towards the anode n^{++} contact. Close to the anode n^{++} contact, the power dissipation density rises sharply, as both the electric field strength and charge density increase strongly in this region, peaking at 48 kW/mm^3.

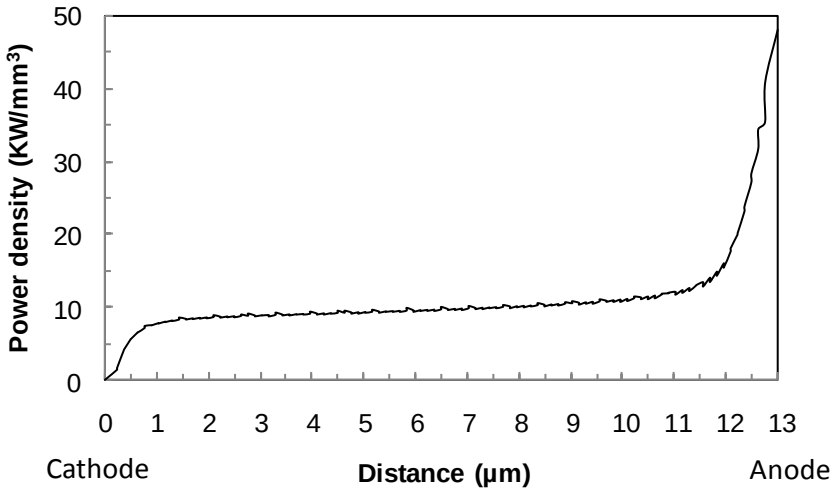

Figure 4.13: Modelled power dissipation density along the length of the transit layer of the conventional Gunn diode biased at 5 V, 0.9 A (4.5 W).

4.5.3 Modelled temperature profile

The modelled temperature profile along the length of the mesa of the conventional Gunn diode is shown in Figure 4.14. The graph shows the temperature rise above ambient package temperature (80 °C), with the device DC biased at 5 V (4.5 W) and 6 V (5.1 W). At both bias voltages, a temperature rise occurs along the mesa, from the cooler integral heatsink towards the hotter transit layer where the majority of power is dissipated. At the lower bias voltage (5 V), the temperature peaks at 113 °C in the transit layer. At the higher bias voltage (6 V), temperatures are elevated, as expected, and peak at 130 °C. Along the length of the substrate layer, the temperature is uniform; suggesting that ohmic heating has a negligible effect on device operating temperature. The shape of the temperature profile agrees well with the micro-Raman measurements made on the sample described in Section 4.3.2 of this chapter.

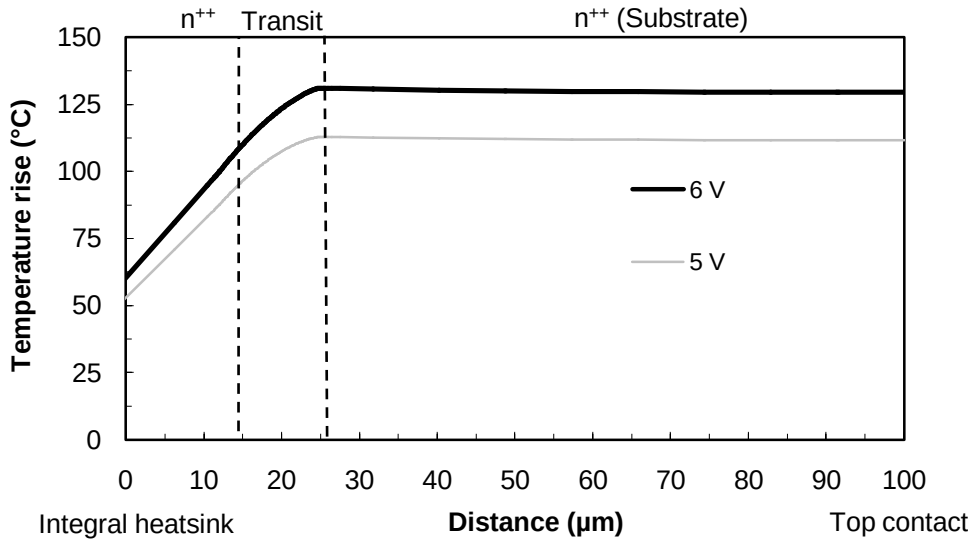

Figure 4.14: Modelled temperature rise along the length of the mesa side of the conventional Gunn diode biased at 5 V, 0.9 A (4.5 W) and 6 V, 0.85 A (5.1 W).

A modelled temperature profile was also extracted over a wider area of the Gunn diode. A graph showing the temperature profile along the entire length of the package, integral heatsink and mesa side, at 6 V (4.8 W), is shown in Figure 4.15. Temperatures increase exponentially from the edge of the package towards the hotter transit layer. The temperature gradient is significantly less pronounced along the metallised layers compared to along the mesa. This can be explained by considering that the metal will have a significantly higher thermal conductivity (k_{Cu} = 4.01 W.cm^{-1}.K^{-1}) compared to that of the semiconductor (k_{GaAs} = 0.5 W.cm^{-1}.K^{-1}). Additionally, increased heat spreading will occur within the metal, as heat flux from the semiconductor will diffuse into a larger area.

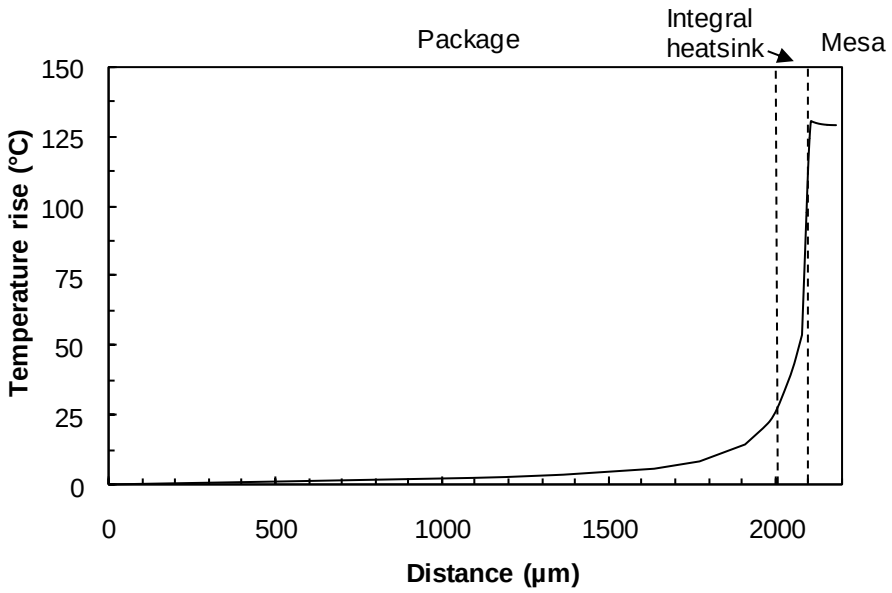

Figure 4.15: Modelled temperature distribution along the length of the package, integral heatsink and mesa of the conventional Gunn diode biased at 6 V, 0.85 A (4.8 W).

The thermal resistance of each structural element through which heat flows was calculated from the modelled temperature results and are shown in Table 4-1. The thermal resistance of the contact layer R_c is shown to constitute the most significant parameter (38 %) making up the total thermal resistance of the conventional Gunn diode. Design modifications to reduce the thermal resistance of the contact layer are feasible. For example, its thickness may be reduced to increase the rate of heat flow towards the integral heatsink. Interestingly, Table 4-1 shows that the thermal resistance of the package and integral heatsink are also significant parameters, even though these structures are made from a high thermal conductivity metals. A possibility is that the Au integral heatsink could be replaced with an even higher thermal conductivity synthetic diamond structure. Commercially available synthetic diamond has a thermal conductivity of up to 2000 W /cm².K, over five times higher than Au [93]. The advantages of this change in terms of thermal performance would, however, have to be weighed against the increased production costs.

Parameter	Value (°C/W)
R_t	4.2
R_c	10.2
R_{ihs}	5.4
R_p	7.1
Total (R_{th})	**26.9**

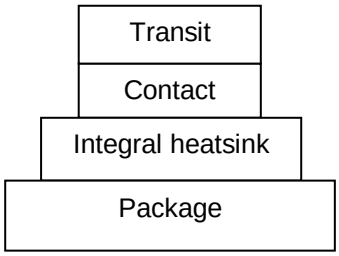

Table 4-1: Thermal resistance values for the structural elements forming the conventional Gunn diode. Values calculated with device biased at 5 V, 0.9 A (4.5 W), T_{amb} = 80 °C.

4.5.4 Model validation using IR thermal microscopy

The modelled temperature results for the conventional Gunn diode sample were experimentally validated using IR thermal microscopy. The Quantum Focus IR microscope was used to make temperature measurements on the top metal contact of the device over a range of power levels (0.5 – 5.0 W). A graph showing the measured peak operating temperature rise plotted against dissipated power is shown in Figure 4.16. Temperatures can be seen to increase almost linearly with dissipated power and reach 130 °C, at 5 W.

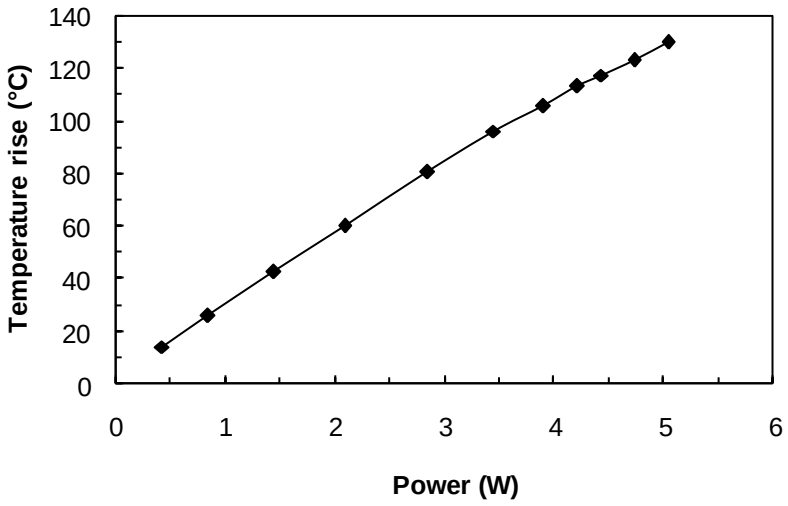

Figure 4.16: Temperature rise measured on the top contact of the modelled conventional Gunn diode using IR thermal microscopy. T_{amb} = 80 °C.

A comparison between the thermal resistance values obtained from the model and experimental temperature measurements, over a range of operating power levels, is shown in Figure 4.17. The results are in good agreement. The thermal resistance of the Gunn diode is shown to be fairly flat over the range of operating power levels, around 27 °C/W.

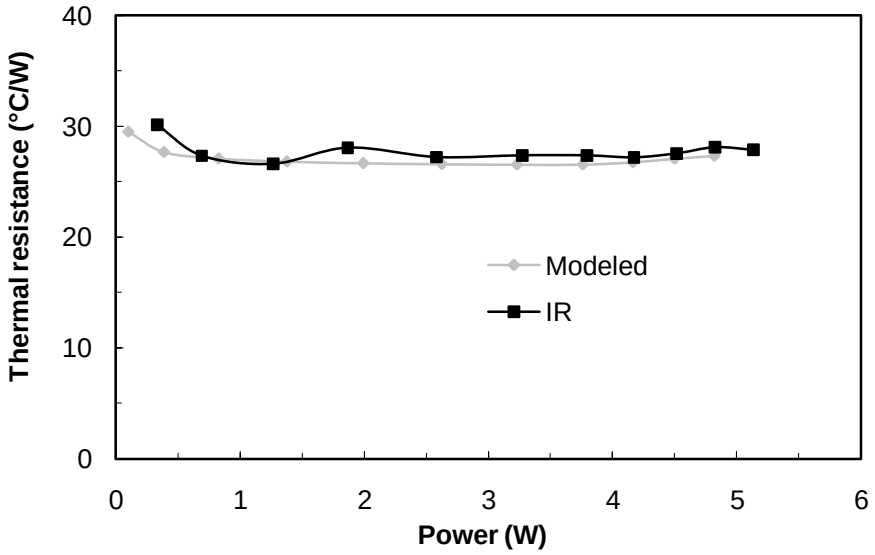

Figure 4.17: Comparison between modelled and measured thermal resistance values of the conventional Gunn diode plotted as a function of dissipated power. T_{amb} = 80 °C.

4.6 Conclusions

The thermal performance of the conventional GaAs Gunn diode was studied. Micro-Raman spectroscopy was used, for the first time, to make high resolution temperature measurements along the mesa side of the device. The measured micro-Raman temperature profile was found to agree well with established thermal models, with temperatures reaching a maximum in the transit layer. Measurements along the substrate layer suggested that ohmic heating has a negligible effect on the device operating temperature. Compared to IR thermal microscopy, micro-Raman spectroscopy offers increased spatial resolution (~ 1 μm) and does not suffer from the emissivity related errors identified both in this chapter and also in Chapter 3 (see

Section 3.8). A disadvantage with the technique is its slow recording time and inability to make measurements on metalised areas.

Combined electro/thermal modelling of the conventional Gunn diode was also undertaken. Modelled operating temperatures were used to calculate the thermal resistance of the individual structural elements. The thermal resistance values of the contact layer and metallised package were shown to have a significant bearing on the total thermal resistance of the device. Design modifications to reduce the thermal resistance of the package and the GaAs contact layer have been suggested. The modelled temperature results were successfully validated using IR measurements made on the top contact of the device.

CHAPTER 5. SOURCES OF ERROR IN CONVENTIONAL IR TEMPERATURE MEASUREMENTS

5.1 Introduction

Infrared thermal microscopy is often used to obtain 2D temperature maps on larger sized types of semiconductor device, for example, high power transistor structures [28]. These devices are generally coated with a high emissivity layer to improve the measurement accuracy. As shown by this and other work [94], accurate IR measurements can often be obtained. However, increased temperature errors occur when direct temperature measurements are made on certain uncoated materials. One example is when IR measurements are made on metallised surfaces, for example, contact pads. These surfaces generally have a low emissivity and can reflect significant amounts of background radiation [2]. Some temperature errors are also thought to occur when optically transparent semiconductor layers are studied [89].

The accuracy of IR temperature measurements made on two types of semiconductor device was investigated. The first device was an AlGaN/GaN transmission line method (TLM) heterostructure grown on a Si substrate. Wide band-gap III-V nitrides are increasingly used in the fabrication of microwave HEMTs, for radar and communication applications [95]. The accurate measurement of operating temperature on these structures is important to optimise device performance, improve packing capacity and reliability. The second device was a metallised heated test structure which consisted of a thin, highly reflective, Au metallised element, fabricated on an undoped GaAs substrate.

5.2 Infrared Temperature Measurements on an AlGaN/GaN TLM Structure

5.2.1 Device construction

The AlGaN/GaN heterojunction TLM structure used in this study was fabricated by Aachen University, Germany, using metal organic vapour phase epitaxy (MOVPE) [96]. A cross sectional diagram, showing the construction of the TLM structure is shown in Figure 5.1. The structure is analogous to a gateless HEMT and consists of a conducting channel between two ohmic contacts. The TLM structures were grown on a 400 µm thick Si substrate with a 1.2 µm GaN layer, followed by a 30 nm n-doped AlGaN layer. Low resistance Ti/Al/Mo/Au based ohmic contacts were used with thick Au metallisation. The channel had a length of 50 µm and a width of 100 µm. The average measured 2D electron sheet carrier concentration (n_s) was 8×10^{12} electrons/cm^2. The structure was passivated with silicon nitride (SiN).[3]

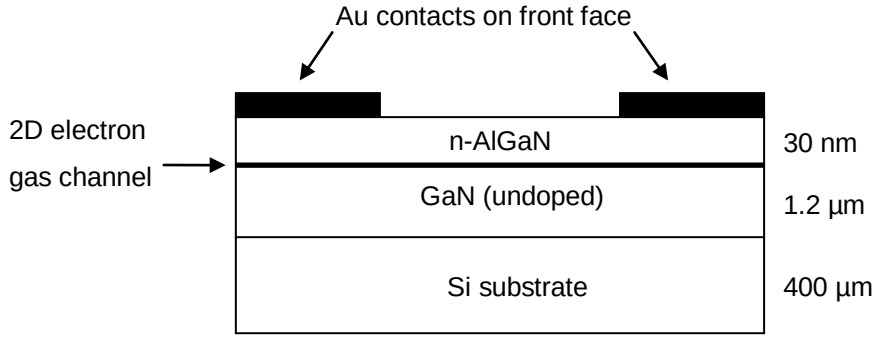

Figure 5.1: Construction of the AlGaN/GaN TLM structure.

When the TLM structure is electrically powered, heat is generated in the 2D electron gas layer, at the heterojunction interface (indicated in Figure 5.1). The heat source is effectively on the surface of the structure, as the AlGaN and passivation layers are only 40 nm thick. Surface temperature measurements made in the channel region

[3] Passivation enhances the electrical performance by reducing surface trapping effects and also provides protection to the surface during processing.

should, therefore, give a good estimate of the maximum channel operating temperature.

5.2.2 Measurement procedure

The experimental arrangement used to make the conventional IR temperature measurements on the AlGaN/GaN TLM structure is shown in Figure 5.2. The wafer structure was thermally bonded onto an aluminium baseplate, which in turn was mounted onto the Peltier heated-stage of the IR microscope. A thermocouple was mounted in the baseplate, directly below the sample to give an indication of the ambient temperature. To electrically power the TLM structure, Wentworth DC probes were used to make contact with the ohmic metal contacts. A four probe arrangement was used to eliminate the effect of contact resistance on the measured channel voltage. One pair of probes provided the DC bias, while the other pair were used to accurately monitor the voltage across the channel. During electrical biasing, the baseplate temperature was stabilised at 80 °C and IR temperature measurements made. A two temperature emissivity measurement procedure was used, with radiance measurements captured at 50 and 80 °C, respectively (see Section 2.3.1 of Chapter 2).

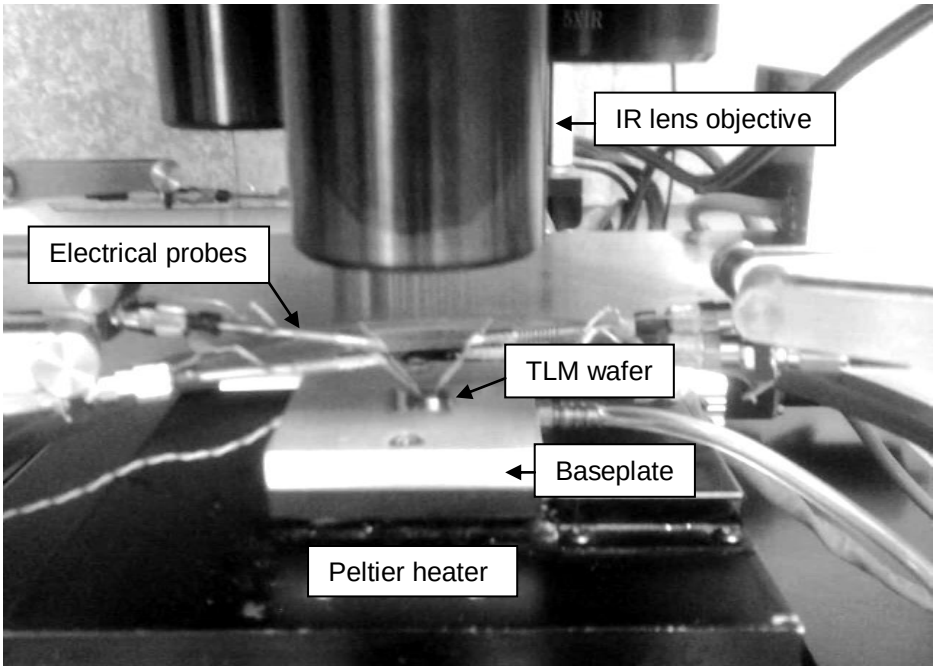

Figure 5.2: Experimental arrangement used to make the conventional IR temperature measurements on the AlGaN/GaN TLM structure.

During the emissivity measurement procedure, it was noted that thermal expansion of the heated baseplate caused the sample to shift position. To assess the effect of thermal expansion, a radiance image of the TLM structure was initially captured at a baseplate temperature of 50 °C. At this temperature, the position of the channel region was marked for reference in the capture window of the IR microscope, see Figure 5.3. The baseplate temperature was then raised and a second radiance image captured at 80 °C (the position of the microscope lens objective was kept constant during the temperature change). At the higher baseplate temperature, the marked reference point indicated that thermal expansion caused the sample to shift position by ~ 9 μm , a distance equivalent to 18 % of the channel length.

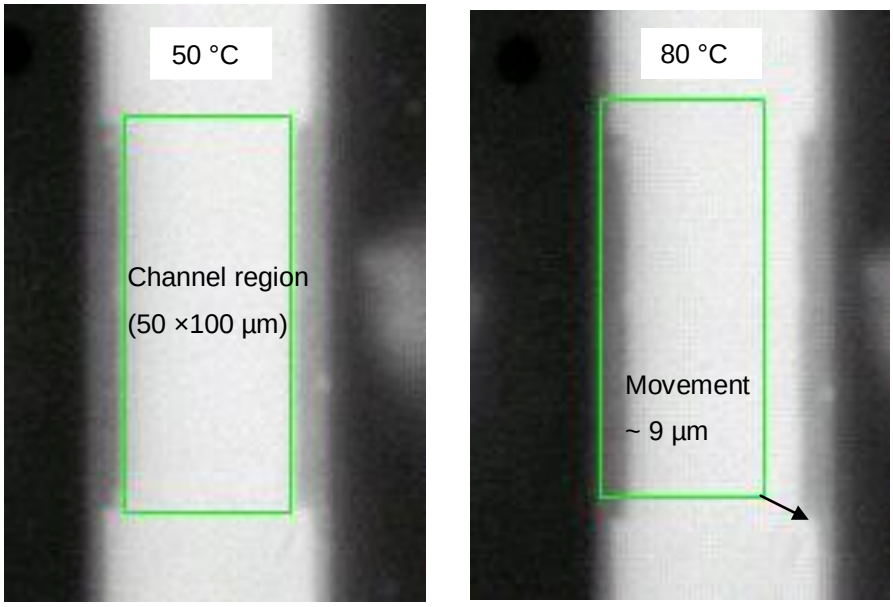

Figure 5.3: Radiance images of the TLM structure captured at separate baseplate temperatures. Thermal expansion of the baseplate caused a shift in sample location.

If uncorrected, sample movement due to thermal expansion will cause errors in the emissivity map, as the two sets of radiance data used to compute it will be misaligned. An example of a distorted emissivity map is shown in Figure 5.4. In the image, emissivity distortions are apparent, especially at the interface between the low emissivity metal and higher emissivity semiconductor regions. To correct for the effects of thermal expansion, the lens objective of the IR microscope was realigned, so the same area of the TLM structure was scanned at both emissivity measurement

temperatures. Using the lens positioning system of the IR microscope, an alignment accuracy of 1μm was achievable.

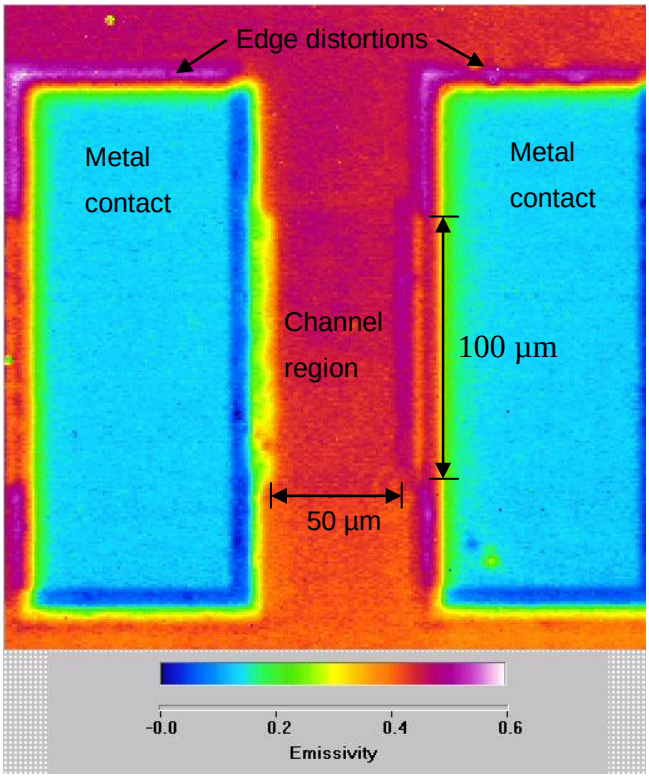

Figure 5.4: An emissivity map of the AlGaN/GaN TLM structure showing the distortions caused by misalignment of the radiance data.

5.2.3 Temperature results

An accurate emissivity map of the TLM structure is shown in Figure 5.5. On either side of the image are the metal contacts (shown in blue), which have a low emissivity (< 0.1). Between the metal contacts is the semiconductor channel region, where the measured emissivity is considerably higher (~ 0.7) than that of the metal. It is important to realise that the semiconductor layers will be at least partially transparent to IR radiation. Some radiation contributions are, therefore, likely to originate from subsurface layers, for example, from the underlying thermal paste, which has a relatively high emissivity (~ 0.6). Indeed, when the radiance images were acquired, the distribution of the thermal paste could easily be observed through the transparent semiconductor layers.

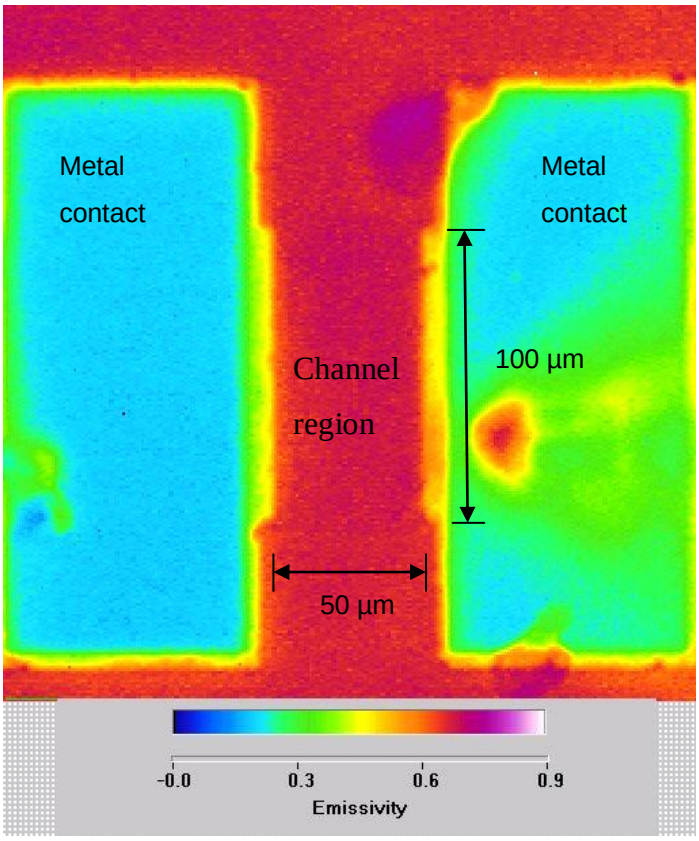

Figure 5.5: Emissivity map of the AlGaN/GaN TLM structure. Electrical probes touching the metal contacts are partially visible.

A conventional IR temperature image of the electrically biased TLM structure is shown in Figure 5.6. The structure was biased at 18 V, 40 mA (0.72 W). The measurements show areas of high temperature on the edge of the metal contacts, adjacent to the channel region. In contrast, the channel region appears to be cooler at a temperature of around 80 °C (close to the ambient baseplate temperature). The measured temperature profile contradicts the electrical operation of the device, as peak temperatures should occur in the channel region, close to where heat is generated. Additionally, the measured temperature profile is not in agreement with published thermal models of similar structures [97].

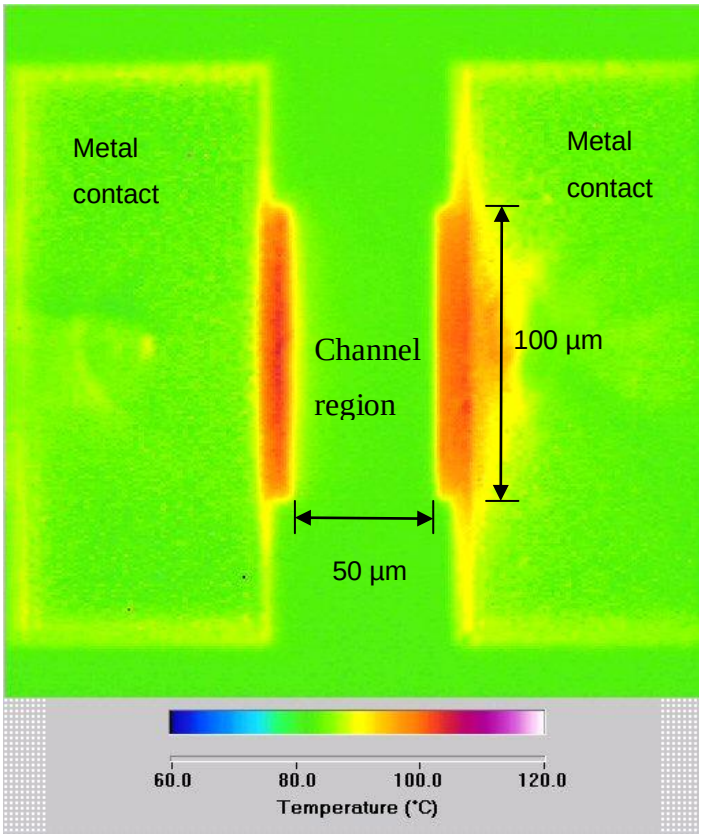

Figure 5.6: Infrared temperature image of the electrically powered AlGaN/GaN TLM structure. P_{dis} = 0.72 W, T_{amb} = 80 °C.

Anomalies in the measured IR temperature profile on the TLM structure are a consequence of the transparency of the semiconductor layers to IR radiation. Consider the simplified view of the TLM structure shown in Figure 5.7. The temperature at surface position 'X' is to be measured using the IR microscope. The emitted infrared radiation reaching the lens objective from this focal point will not just originate from the semiconductor surface but will also include additional transmitted subsurface contributions, for example, from the underlying semiconductor layers and the baseplate. When the emissivity measurements are made, the entire structure will be uniformly heated and no thermal gradient will exist between the channel and baseplate (heatsink) $\delta T / \delta z$ =0. On electrically powering the structure, a thermal gradient will exist between the heterostructure channel (heat source) and baseplate. However, due to the transparency of the semiconductor, only a small fraction of the radiation detected at 'X' will originate from the higher temperature surface layer. Conventional IR temperature measurements will, therefore, underestimate the actual

surface temperature, as significant amounts of radiation will be collected from cooler subsurface layers. Indeed, IR temperature measurements made on the channel region of the electrically powered TLM structure, give temperatures close to the ambient baseplate temperature, suggesting considerable subsurface radiation contributions.

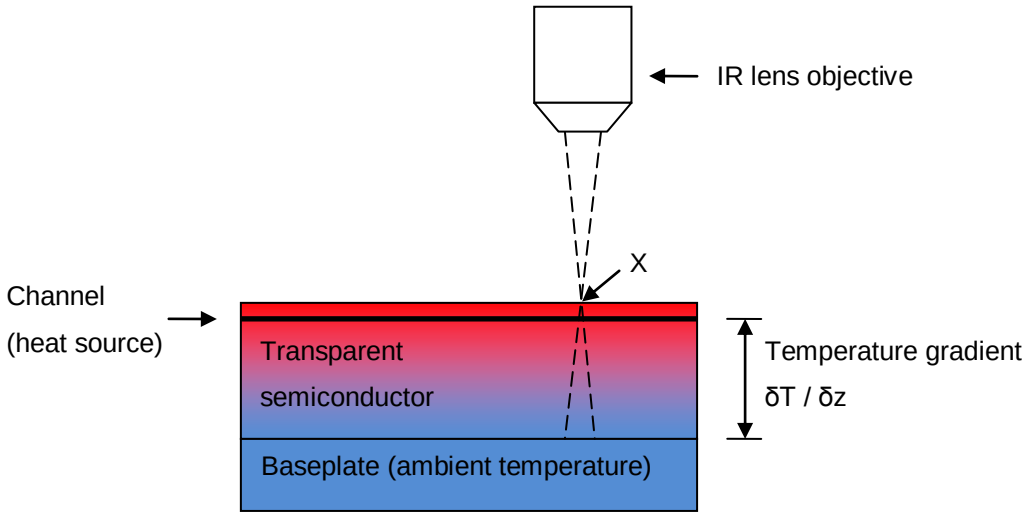

Figure 5.7: Simplified diagram of the IR transparent AlGaN/GaN TLM semiconductor structure, indicating the intended IR temperature measurement location at the focal point 'X'. The vertical temperature gradient $\partial T / \partial z$ is also indicated.

5.2.4 Effect of coating

To see if improved measurement accuracy could be obtained on the TLM structure, it was initially coated with an ink based solution to enhance its surface emissivity and the IR temperature measurement repeated. Figure 5.8 shows a comparison between the temperature rise measured along the length of the uncoated and ink coated channel region and the adjacent metal contacts at a bias level of 22.5 V, 47.7 mA (1.07 W). With ink coating, the average temperature rise measured along the length of the channel region is significantly higher (> 30 °C) than of the uncoated structure. However, temperatures are still around 10 °C higher on the edge of the opaque metal contacts, close to the channel region, which suggests that the coating is not fully opaque. To try and give a more opaque coating, a thick layer of black paint was

applied to the TLM structure and the IR temperature measurement repeated, see Figure 5.8. With the paint coating applied, the measured temperature profile is more realistic; no temperature discrepancy occurs at the metal/channel region interface and temperatures reach a peak (58 °C) in the center of the channel region, as would be expected.

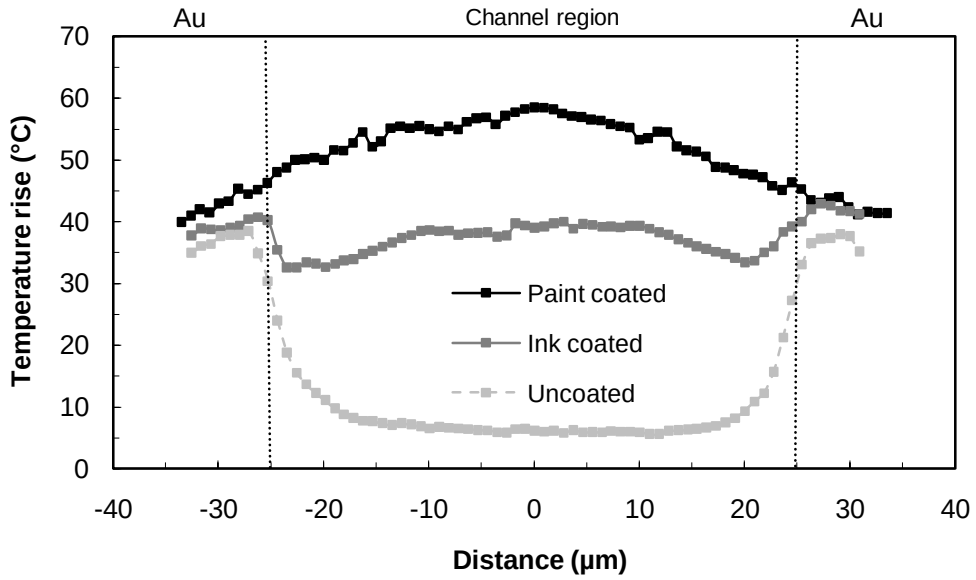

Figure 5.8: Infrared temperatures profile measured along the length of the channel region of the TLM structure between the contact pads. Uncoated and coated results are shown. Both ink based and paint coatings were used. P_{dis} = 1.07 W, T_{amb} = 80 °C.

5.3 Infrared Temperature Measurements on a Metallised Heated Structure

5.3.1 Heater construction

A schematic diagram showing the construction of the metallised heater structure is shown in Figure 5.9. The heater structure consisted of a thin Au element bridged between two metal contacts. The Au metallisation was deposited by evaporation on a 320 µm thick, semi-insulating, GaAs substrate. The width of the heater element was approximately 3 µm. It had a total length of 100 µm and a thickness of 1 µm. The

unbiased resistance of the heater element was ~ 5 Ω. Current flow through the element resulted in ohmic heating. With a supply voltage of 1 V, the heater dissipated a power of 120 mW.

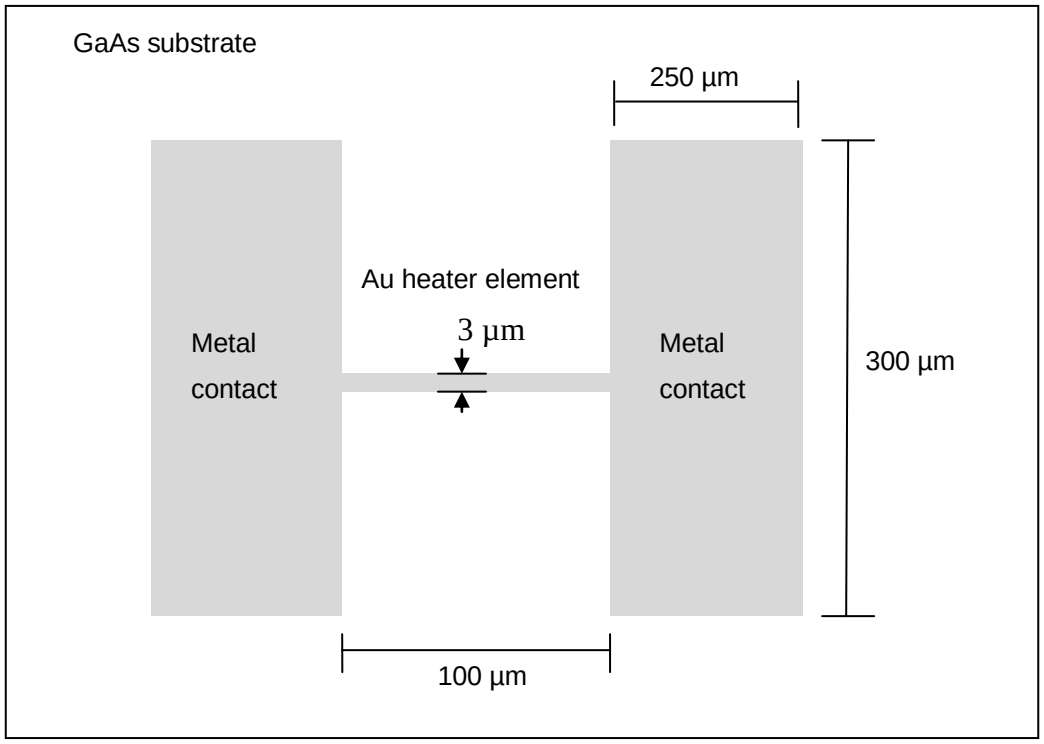

Figure 5.9: A diagram showing the construction of the metallised heater structure. The area of the substrate was 2 × 3 mm.

5.3.2 Measurement procedure

The experimental arrangement used to make the conventional IR temperature measurements on the heater structure was similar to that adopted to thermally characterise the AlGaN/GaN TLM structure described in Section 5.3.2 of this chapter.

5.3.3 Temperature results

An emissivity map of the heater structure is shown in Figure 5.10. The average emissivity measured on the GaAs semiconductor layer (0.5) was higher than that measured on the metal contacts (< 0.2). Due to the optical IR transparency of the semiconductor layer, subsurface radiation contributions from the baseplate and thermal paste were found to artificially increase its measured emissivity. The metal

heater element is just visible in the centre of the image. Interestingly, the emissivity of the heater element appears to be higher than that of the metal contact pads. It is thought that some IR radiation is reflected from the edge of the metal which causes this apparent emissivity enhancement.

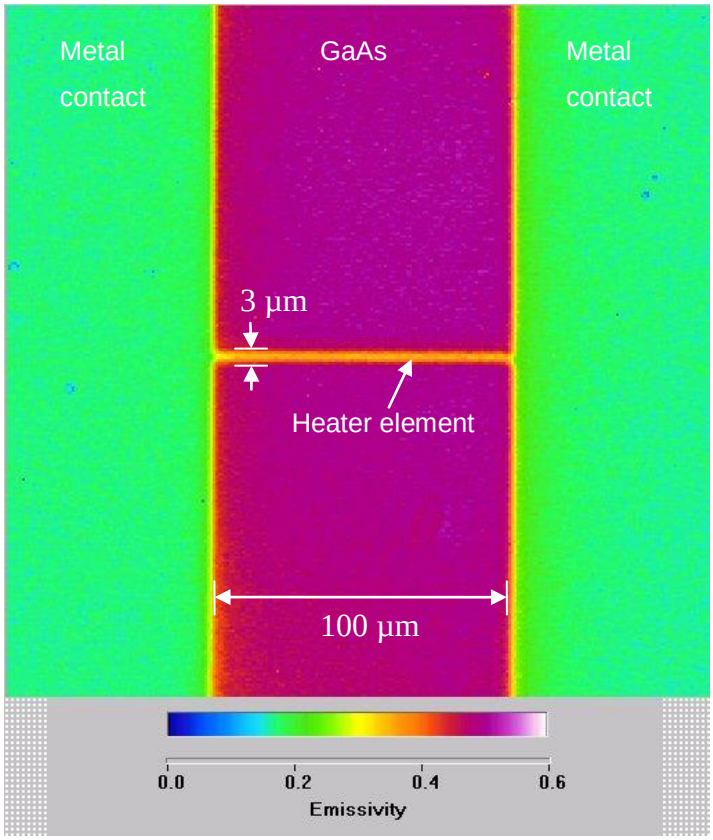

Figure 5.10: Emissivity map of the metallised heater structure.

A conventional IR temperature image measured on the electrically powered heater structure is shown in Figure 5.11. The heater element was biased at 1 V, 116 mA (0.12 W). These conventional IR measurements suggest that operating temperatures are relatively constant over the entire surface.

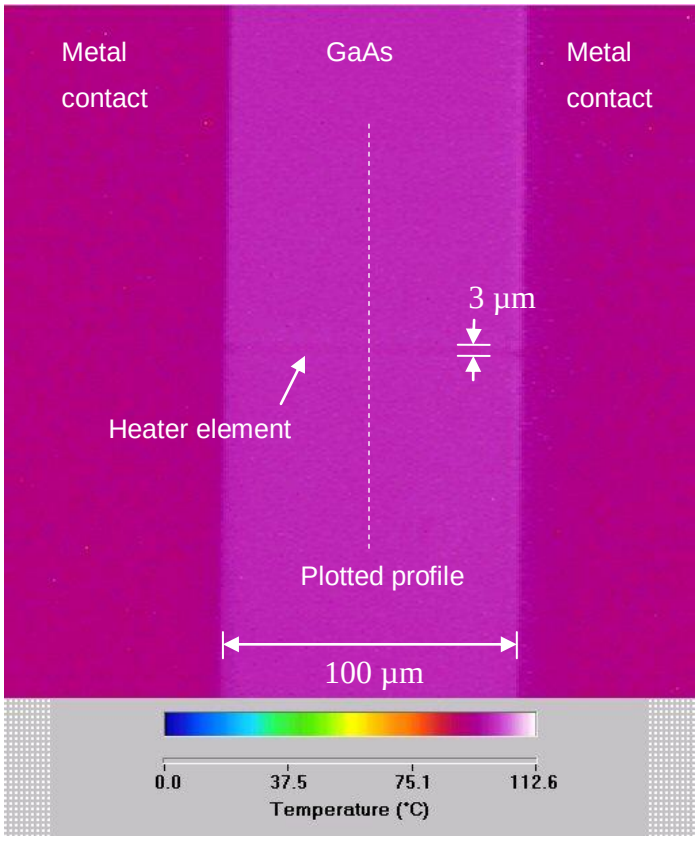

Figure 5.11: Conventional IR temperature image of the electrically powered metallised heater structure. P_{dis} = 0.12 W, T_{amb} = 80 °C.

A graph showing the conventional IR temperature profile measured across the electrically biased heater element and adjacent GaAs semiconductor regions is shown in Figure 5.12 (the location of the plotted thermal profile is indicated in Figure 5.11). Temperatures are elevated and peak slightly around the heater element and show a maximum rise of 39 °C. To try and improve the measurement accuracy, a thick layer of black paint was applied to increase the surface emissivity of the structure and the IR measurements repeated. The results of the coated measurements are also shown in Figure 5.12. Compared to the uncoated results, the coated measurements show a significantly higher average temperature rise and a more pronounced temperature peak on the heater element (66 °C). This temperature discrepancy strongly indicates sources of error in the uncoated measurement.

There are a number of sources of error with the conventional IR temperature measurements made on the uncoated heater structure. As with the TLM structure

considered in Section 5.2, measurements made on the optically transparent GaAs semiconductor layer will not give an indication of the true surface temperature, as radiation contributions will reach the detector from cooler subsurface layers, including the back-face. Even on the opaque metallised element, radiance measurements will be corrupted by a combination of noise and reflected background radiation, as it has a low emissivity and is highly reflective.

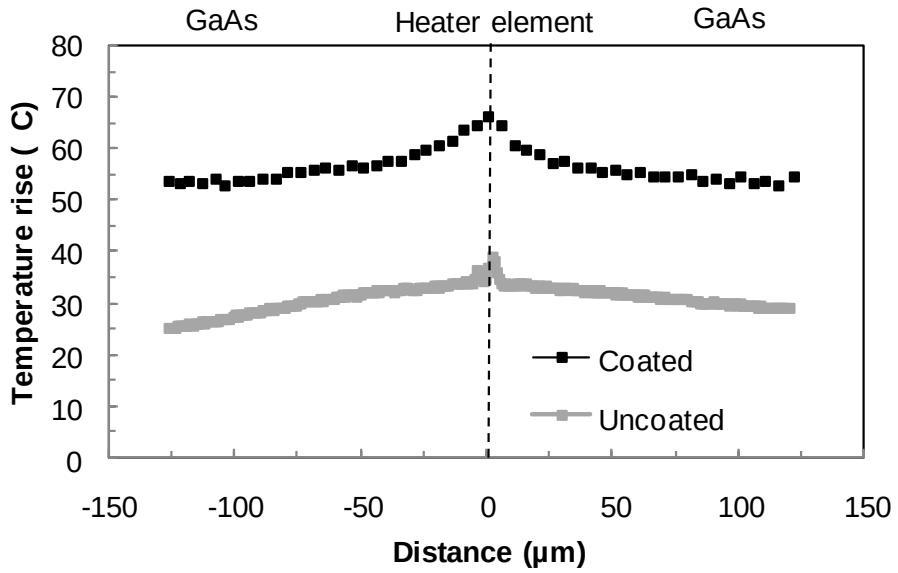

Figure 5.12: Infrared temperature profile measured on the uncoated and coated heater structure. Distance shown from heater element. P_{dis} = 0.12 W, T_{amb} = 80 °C.

5.4 Conclusions

The work highlights the difficulty in using conventional IR thermal microscopy to obtain accurate surface temperature measurements on electrically powered semiconductor devices. The radiative properties of the materials under study were shown to have a large effect on the measurement accuracy. On IR transparent semiconductor layers, a significant underestimation of the surface temperature can occur, as radiation contributions are collected from cooler subsurface regions. Indeed, IR measurements made on the channel region of the AlGaN/GaN TLM structure gave temperatures close to the ambient baseplate temperature, suggesting significant subsurface radiation contributions. Some underestimation of the surface temperature

also occurred when measurements were made on the metallised heater structure. Metals generally have a low emissivity and are highly reflective of background radiation.

The accuracy of IR temperature measurements can be improved if a high emissivity coating is applied to transparent and low emissivity surfaces. However, when applied to transparent surfaces, the coating must be fully opaque to block subsurface radiation contributions. Coating also has some disadvantages: it can cause heat spreading, reducing the effective spatial resolution. It may also damage the device. Chapter 6 introduces a new IR measurement technique which overcomes some of the disadvantages associated with coating.

CHAPTER 6. USE OF CARBON MICROPARTICLES FOR IMPROVED IR TEMPERATURE MEASUREMENTS

6.1 Introduction

As shown in Chapter 5, significant errors can occur when IR temperature measurements are made on the low emissivity/highly reflective metal surfaces and IR transparent semiconductor layers of electronic devices. Although a high emissivity coating can be applied to try and improve the measurement accuracy, coating has a number of disadvantages. Coating can cause heat spreading, distorting the measured temperature profile and effectively reducing the spatial resolution of the instrument. Additionally, the coating can also damage the device and obscure areas for inspection.

As part of this work, a new measurement technique was developed to significantly improve the accuracy of IR temperature measurements made on uncoated semiconductor devices. The new technique employs spherical, carbon microparticles, placed in temporary isothermal contact with the surface under study. Infrared measurements made on the microparticles can be used to obtain an accurate estimate of the surface temperature, even on IR transparent semiconductor layers and metals. A patent application has been submitted (United Kingdom Patent Application 0821112.0). A paper has also been submitted for consideration of publication in IEEE Transactions on Electron Devices (see Section 1.4, Publication no. 7).

6.2 Current Work

The chapter provides a description of the new IR microparticle temperature measurement technique, together with the work undertaken to assess its accuracy. Initial tests were made to determine the feasibility of the technique. Temperature measurements were then carried out on two electrically heated test structures: an AlGaN/GaN TLM structure and a thin metallised heater fabricated on GaAs (both fully described in Chapter 5). Temperatures measured on the test structures were compared to those obtained from micro-Raman temperature probing (Bristol

University) and thermal electrical measurements. Finally, the IR microparticle technique was applied to thermally characterise the GaAs Gunn diode.

6.3 Description of the Technique

The experimental arrangement used to make the IR microparticle temperature measurements is shown in Figure 6.1. The diagram shows an opaque, high emissivity microparticle, on the surface of the material under study. It is assumed that isothermal conditions exist between the surface under study and the microparticle, as the microparticle is thermally isolated from other structures. The dimensions of the microparticle are sufficiently large to enable emitted radiation from its surface to be detected by an IR microscope. Its temperature can, therefore, be measured using the standard IR temperature measurement procedure, enabling an indirect estimate of the surface temperature of the material under study. The method can be considered pseudo contact-less, compared to scanning thermal probing (AFM) [61].

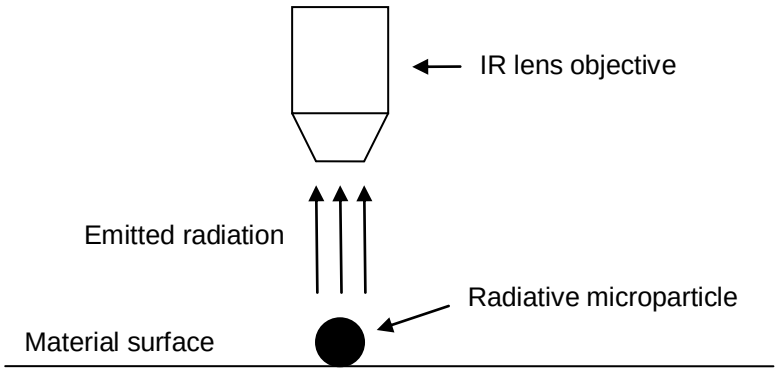

Figure 6.1: Experimental arrangement used for the new IR microparticle measurement technique. Not to scale.

When compared to the conventional IR temperature measurement procedure, the IR microparticle technique was expected to provide two main advantages:-

- The temperature accuracy should be independent of the radiative surface properties of the material under study, therefore, potentially offering

significant benefits when transparent semiconductor materials or low emissivity metals are studied.

- A higher spatial resolution should be obtainable compared to coating, as individual microparticles will have a small contact area with the surface under study, thereby, limiting heat spreading.

6.4 Initial tests

6.4.1 Choice of microparticles

Spherical, amorphous, carbon particles (Sigma Aldrich 484164), having diameters between 2 - 12 μm, were purchased for use in this work. Carbon was chosen because in bulk form it is known to have a high emissivity (0.95) and is opaque to IR radiation [98]. Additionally, it has a high ignition temperature (450 °C). A disadvantage with using carbon is that it is electrically conductive; a possible problem when microparticles are applied to a biased semiconductor device. However, it has to be borne in mind that the contact area between the microparticle and device will be very small. Additionally, the semiconductor surfaces of most electronic devices are normally electrically passivated[4].

6.4.2 Radiance measurements

The level of infrared radiation emitted by the carbon microparticles was initially measured. A collection of carbon microparticles were brushed onto a 320 μm thick Si wafer. Naturally occurring electrostatic and van der Waal forces act to stick the particles to the wafer [99]. Figure 6.2 shows optical and IR radiance images of the deposited microparticles.

[4] A non-conducting film of silicon dioxide (SiO_2) is often used to passivate HEMTs.

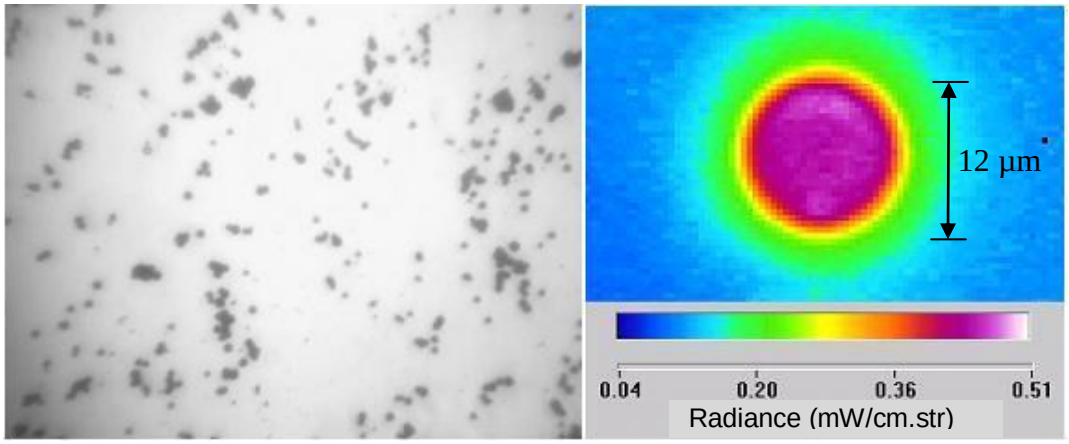

a b

Figure 6.2: (a) Optical image (20 × magnification) showing the carbon microparticles scattered on the surface of the Si wafer. (b) Infrared radiance image of a single microparticle 12 µm in diameter.

The Si wafer was heated and the radiance level from the deposited microparticles measured using the QFI IR microscope. Figure 6.3 shows the radiance level from a microparticle (12 µm in diameter) with increasing Si wafer temperature. As the wafer temperature is increased from 30 to 110 °C, the emitted radiance level rises from 0.11 to 1.2 mW/cm.str. The radiance measurements indicate that the temperature of the microparticle is strongly dependent on the Si wafer temperature.

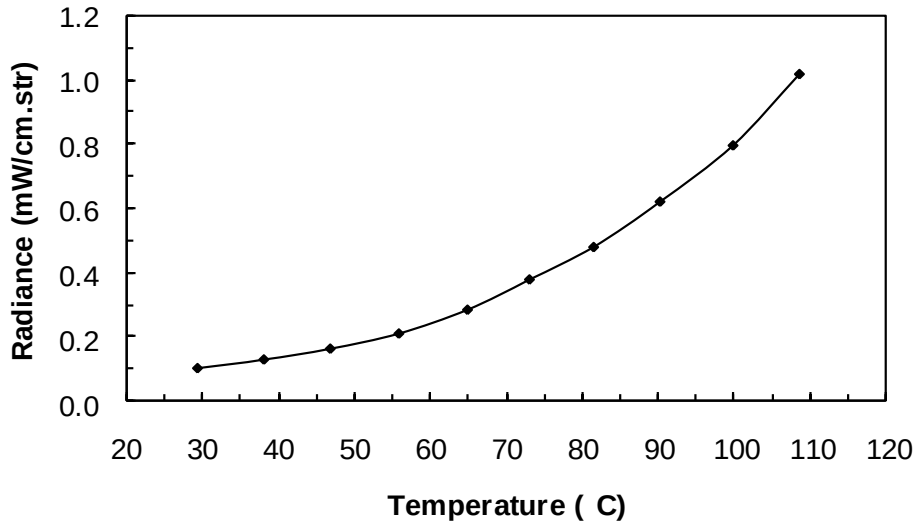

Figure 6.3: Infrared radiance level measured from the carbon microparticle (12 µm in diameter) heated on the Si wafer.

6.4.3 Effect of thermal contact resistance

It was initially thought that the temperature of the microparticles would be highly dependent on their thermal contact resistance with the surface under study. The thermal contact resistance was thought to be high, as scanning electron microscope imaging (see Figure 6.4) indicated that the carbon microparticles were nearly perfect spheres and had only a very small contact area with the surface of a Si wafer (< 1 μm in diameter). The thermal contact resistance was expected to be exacerbated when the microparticles were placed on low thermal conductivity surfaces which have a greater resistance to heat flow.

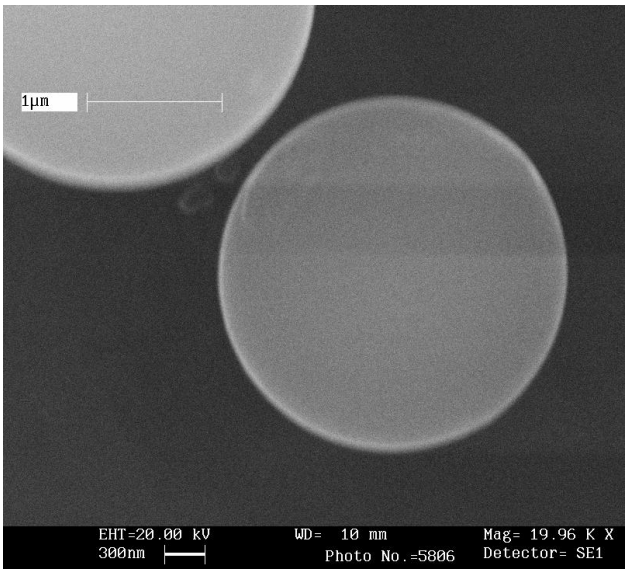

Figure 6.4: Scanning electron microscope image showing a carbon microparticle (3 μm in diameter) on a Si wafer.

To determine whether the thermal contact resistance has an effect on the microparticle temperature, IR radiance measurements were made on carbon microparticles placed on low and high thermal conductivity heated surfaces. The surfaces were a 320 μm thick Si wafer and a 3 mm thick Cu block, having nominal thermal conductivities of 149 and 401 $W.m^{-1}.K^{-1}$, respectively. The emitted radiation level from ten microparticles (12 μm in diameter) scattered at different locations on the heated

surfaces (80 °C) is shown in Figure 6.5. The average emitted radiation level from microparticles deposited on both types of surface was almost identical: GaAs = 0.476 mW/cm.str and Cu = 0.477 mW/cm.str, a difference of < 0.5 %. This suggests that changes in thermal contact resistance have a negligible effect on the microparticle temperature.

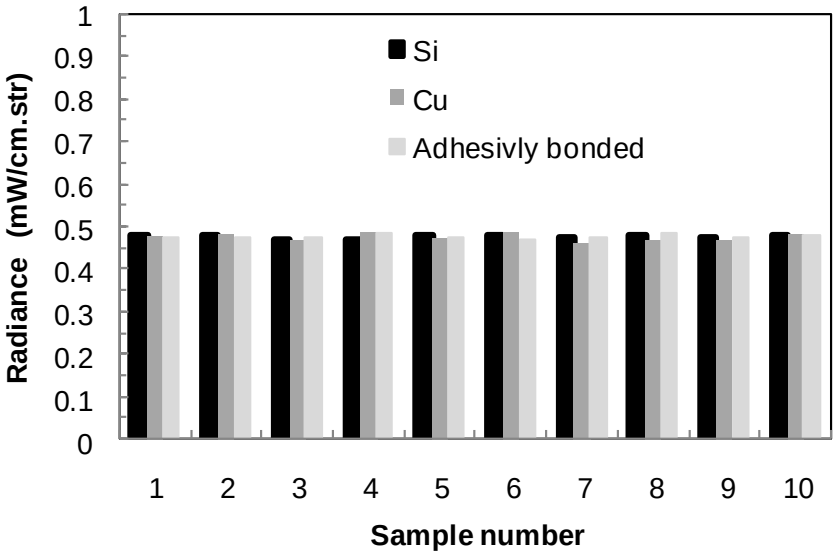

Figure 6.5: Emitted radiance level from the carbon microparticles (12 µm in diameter) deposited on the copper block and gallium arsenide wafers. Results are also shown for the microparticles adhesively bonded to the Si wafer. The surfaces were heated to 80 °C.

To fully confirm that the temperature of the microparticle matched that of the contacting surface, further radiance measurements were made on a collection of carbon microparticles adhesively bonded to a Si wafer. To bond the particles, a thin layer of cyanoacrylate adhesive was coated onto the wafer. The microparticles were then dropped onto the adhesive and left to set. The adhesive ensured an increased heat path between the microparticle and wafer surface. The wafer was heated to 80 °C and radiance measurements made. An IR radiance image showing the microparticles embedded in the adhesive is shown in Figure 6.6. A comparison between the radiance level measured from the adhesively and naturally bonded microparticles is shown in Figure 6.5 (a table of results is also given in Appendix D). The radiance level

measured from all three sets of samples is in good agreement. The results suggest that the naturally occurring thermal bond between the microparticles and contacting surface is sufficient to ensure isothermal conditions.

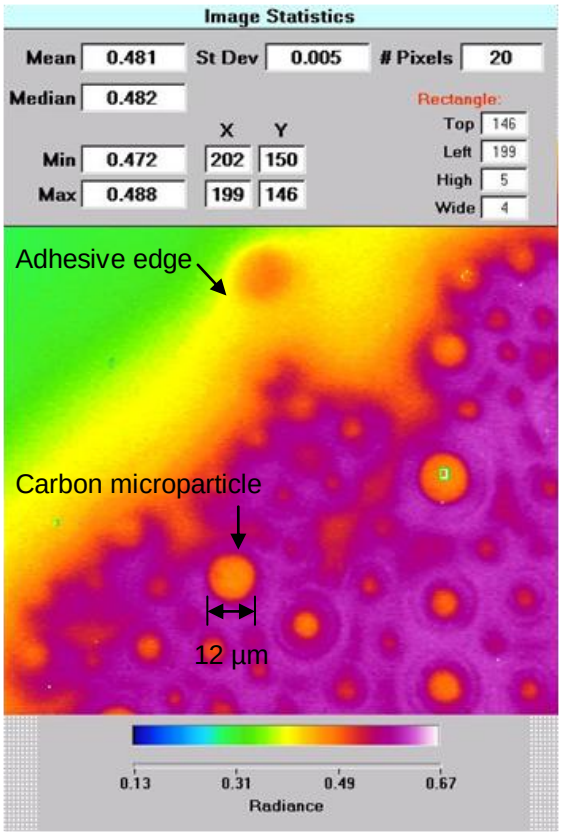

Figure 6.6: Infrared radiance image showing the carbon microparticles embedded in the cyanoacrylate adhesive which thermally bonds them to the Si wafer.

6.4.4 Temperature measurements on a uniformly heated semiconductor wafer

Initial tests were undertaken to determine whether the IR microparticle technique could be used to give an indirect estimate of the surface temperature of a uniformly heated semiconductor wafer. A schematic diagram showing the experimental arrangement is shown in Figure 6.7.

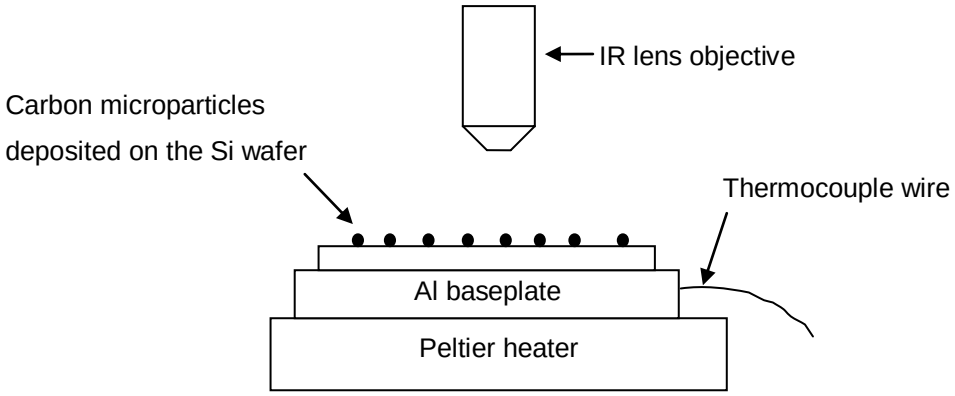

Figure 6.7: Experimental arrangement used for the IR microparticle temperature measurements on the uniformly heated Si wafer. Not to scale.

For measurement purposes, a fine coating of carbon microparticles was deposited onto a Si wafer. The Si wafer was then placed on an aluminium baseplate mounted onto the Peltier heated stage of the IR microscope. A recessed thermocouple in the baseplate provided an indication of the wafer temperature.[5] Infrared temperature measurements were made on the carbon microparticles using the QFI IR microscope. The emissivity of the microparticles was determined using the two temperature technique (described in Section 2.3.1 of Chapter 2), with radiance measurements captured at temperatures of 50 and 80 °C, respectively. An emissivity image of a carbon microparticle (12 µm in diameter) is shown in Figure 6.8. The emissivity was found to be relatively high (~ 0.7).

[5] It is assumed that the wafer temperature matched that of the baseplate, as the small amount of radiated heat loss from the wafer will be compensated for by conducted heat flow from the Peltier heater.

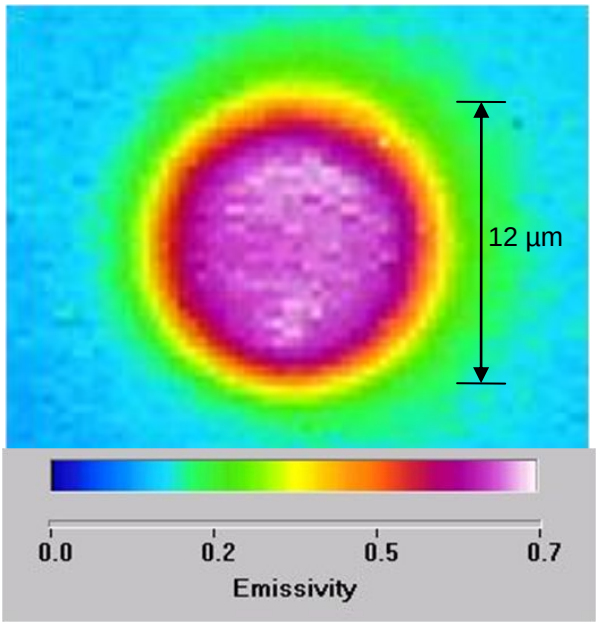

Figure 6.8: Emissivity map of single carbon microparticles (12 µm in diameter).

Tests were undertaken to determine whether IR measurements made on the carbon microparticles could be used to track the temperature of the Si wafer. The Peltier heater was used to vary the wafer temperature in 10 °C steps from 50 to 130 °C. At each temperature point, the IR microscope system was used to record the temperature of the carbon microparticles. A bar graph showing a comparison between the measured microparticle and wafer temperatures is shown in Figure 6.9 (a table of results is given in Appendix D). As can be seen from the graph, measurements made on the microparticle accurately track the wafer temperature to within ± 0.5 °C. These initial results indicated that the IR microparticle technique was capable of providing accurate surface temperature measurements on isothermally heated structures.

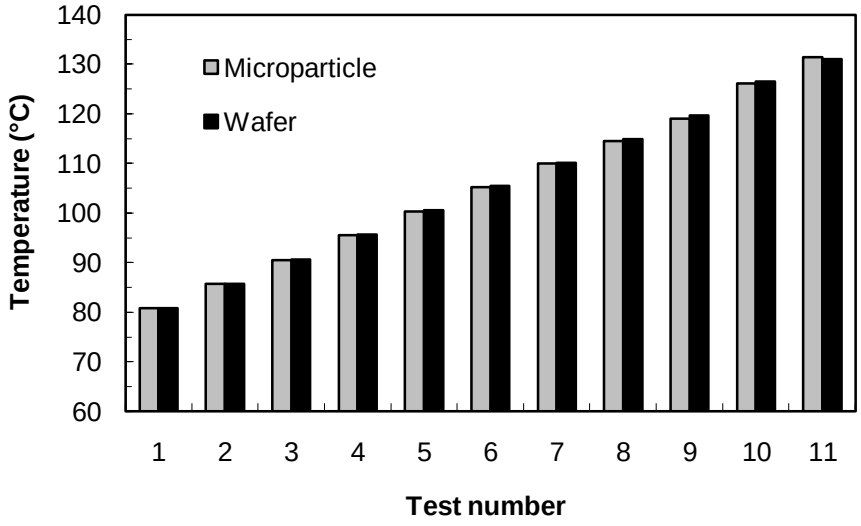

Figure 6.9: Comparison between the wafer temperature (thermocouple measurement) and microparticle temperatures measured using IR. A number of comparisons were made at different wafer temperatures.

6.5 Temperature Measurements on an Optically Transparent AlGaN/GaN TLM Structure

In Section 5.2 of Chapter 5, conventional IR temperature measurements were made on an electrically powered AlGaN/GaN TLM structure. Significant surface temperature errors were shown to occur on the IR transparent semiconductor layers, as the small amount of radiation collected from the structure's surface cannot be isolated from larger subsurface radiation contributions.

Use of the microparticle technique was expected to significantly improve the accuracy of IR measurements made on optically transparent semiconductor layers. Carbon microparticles placed in isothermal contact with the structure will provide an opaque, radiative area, on which indirect surface temperature measurements can be made. To confirm the advantage of using the approach, the IR microparticle technique was used to thermally characterise the AlGaN/GaN TLM structure. The IR microparticle measurements were compared to those obtained from micro-Raman thermal spectroscopy (University of Bristol), an established technique for making non-contact

high spatial resolution (< 1 µm) temperature measurements on AlGaN/GaN devices [100].

6.5.1 Microparticle placement and manipulation procedure

The experimental arrangement used to make the IR microparticle temperature measurements on the AlGaN/GaN TLM structure is shown in Figure 6.10. The wafer structure was placed on an aluminium baseplate, which was mounted onto the Peltier heated stage of the IR microscope.

A 3 µm diameter carbon microparticle was initially deposited onto the TLM structure. A micromanipulator probe (Wentworth PVX400), having a 5 µm diameter tungsten tip, was used to pick up the microparticle from a Si wafer positioned next to the sample (the Si wafer having been coated with the microparticles). Naturally occurring electrostatic and van der Waal forces were sufficient to weakly stick the microparticle to the probe tip. Once attached, the probe tip was moved over the desired position on the TLM structure and the microparticle released at by a sudden movement of the probe tip or contacting the microparticle with the surface. A similar procedure for depositing microparticles has been used by other authors [101]. In this work, a single microparticle was deposited, however, a fine coating of microparticles could be brushed over the general area of interest, if exact positioning is not required.

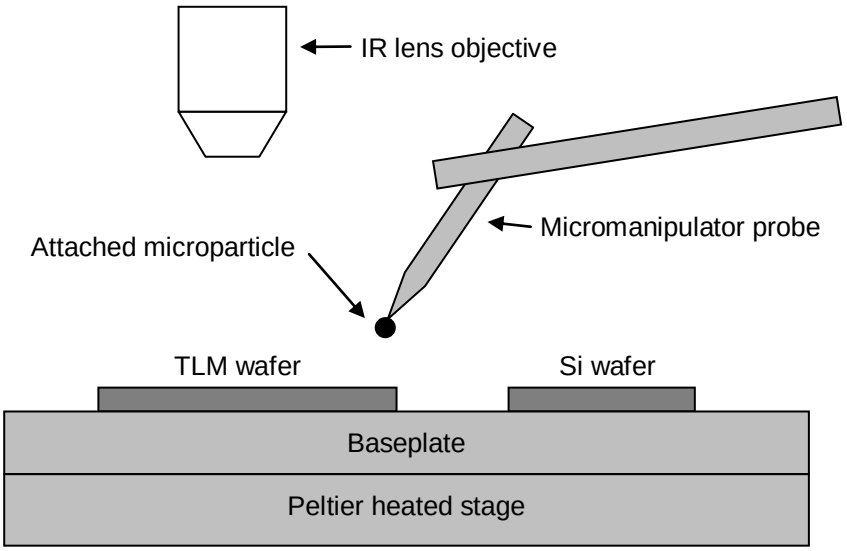

Figure 6.10: Experimental arrangement showing the procedure used to deposit the carbon microparticle onto the AlGaN/GaN TLM structure. Not to scale.

The deposited microparticle was fine positioned using a second micromanipulator probe. A finer, 0.5 μm diameter, probe tip was used to physically push the microparticle across the TLM structure. The microparticle was pushed into position using the side of the probe tip (the probe angle was approximately 45° to the vertical). The thin tip reduced intermolecular electrostatic and van der Waal forces, thereby, minimising adhesion. An optical image showing this manipulation procedure is shown in Figure 6.11.

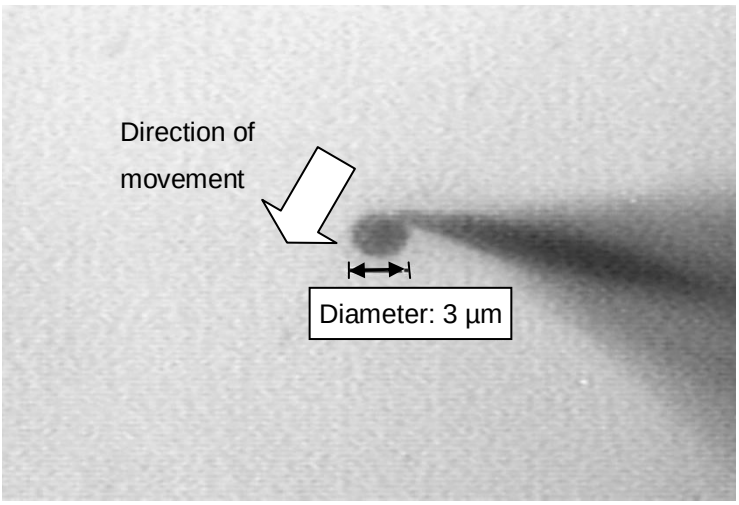

Figure 6.11: Optical image showing a spherical carbon particle being pushed into position on the surface of the AlGaN/GaN TLM structure. A fine, 0.5 μm diameter, tungsten tipped micromanipulator probe was used for fine positioning.

The exact location of the carbon microparticle on the surface of the TLM structure was monitored using an optical camera system integrated into the IR microscope. A 20 × lens objective was used for imaging. Figure 6.12 shows an optical image of the microparticle in the channel region.

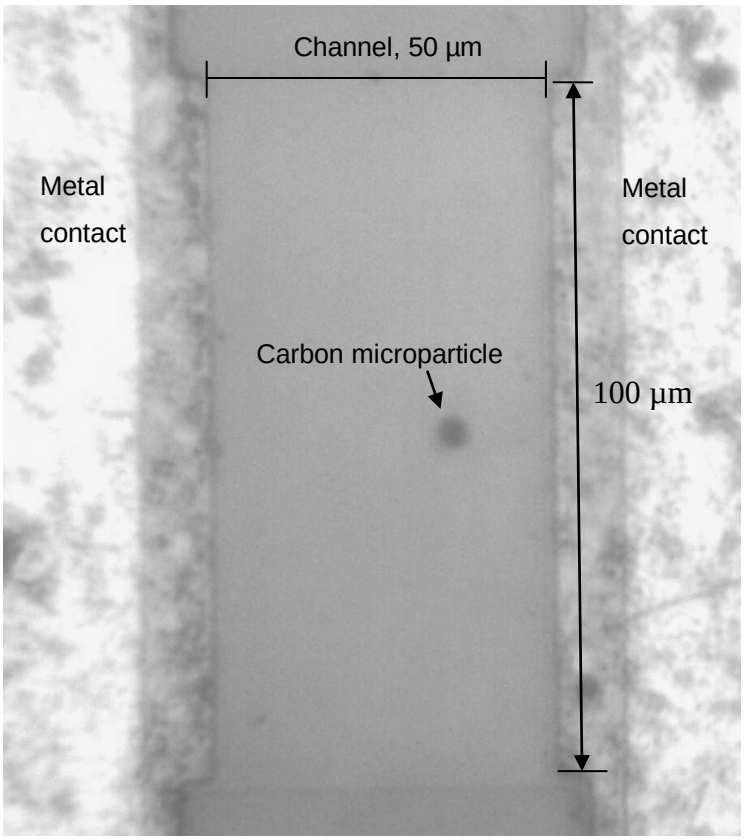

Figure 6.12: Optical images showing the carbon microparticle in the channel region of the AlGaN/GaN TLM structure.

6.5.2 Temperature measurements

Infrared temperature measurements were made on the deposited carbon microparticle using the QFI IR microscope. A 25 × lens objective was used for imaging, giving a field of view of 232 × 232 µm and a spatial resolution of ~ 2.5 µm. To make accurate temperature measurements, the emissivity of the microparticle was measured and found to be 0.5. The fact that this emissivity value is somewhat lower than the value measured for the larger sized microparticle in Section 6-3 is thought to be a consequence of the optical diffraction limit. Only short wavelength IR radiation will be detected from the 3 µm sized microparticle (the IR microscope integrates radiation over a wide 2 - 5 µm wavelength band).

6.5.3 Temperature results

An IR temperature image showing the carbon microparticle placed in the channel region of the electrically biased AlGaN/GaN TLM structure is shown in Figure 6.13. The bias level was 20 V, 42.8 mA (0.86 W). High temperatures (~ 90 °C) can be seen to occur on the edge of the metal contacts. However, temperatures in the channel region, on the IR transparent semiconductor layers, are abnormally cool and close to the ambient base plate temperature of 80 °C (see Section 5.2 of Chapter 5). Infrared measurements made on the microparticle appear to give a more realistic indication of the temperature in the channel region (133 °C).

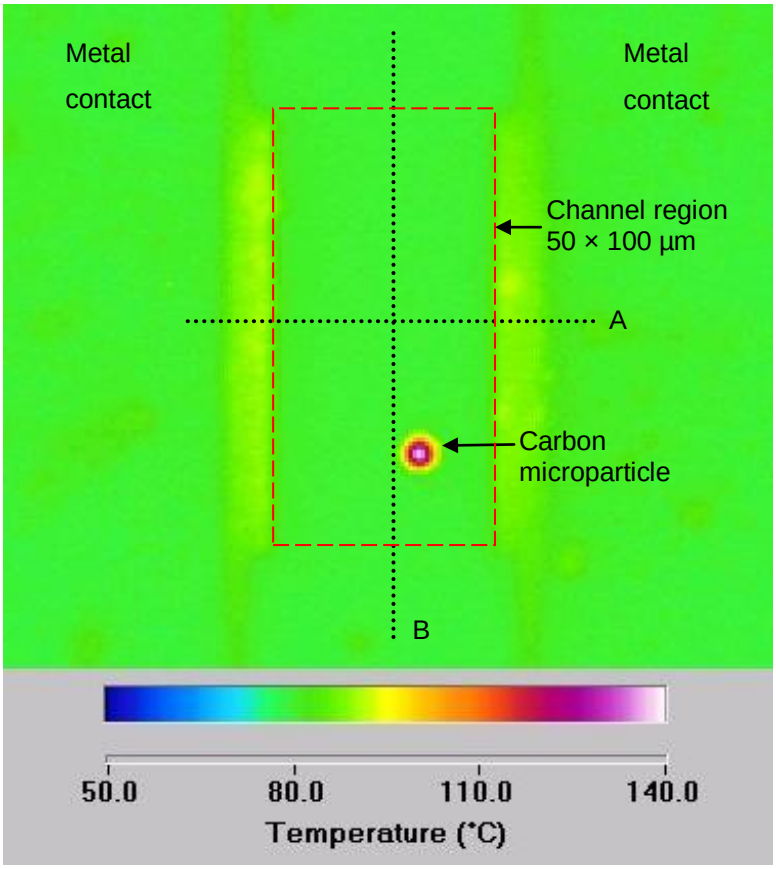

Figure 6.13: Infrared temperature image showing the carbon microparticle in the channel region of the electrically powered AlGaN/GaN TLM structure. Two lines showing the measured temperature profiles are also marked.

P_{dis} = 0.86 W, T_{amb} = 80 °C

Using the manipulation procedure described in Section 6.5.1 of this chapter, the carbon microparticle was moved between the two metal contacts of the TLM structure to enable a temperature profile to be built up (profile location marked as line 'A' in Figure 6.13). The step size was under 20 µm. The measured temperature profile is shown in Figure 6.14. For comparison, the conventional IR profile measured on the uncoated structure is also plotted. In the channel region, temperatures measured using the microparticle technique are significantly higher (~ 400 %) than those measured using the conventional IR approach. The conventional uncoated IR measurements underestimate the actual surface temperature on the optically transparent semiconductor layers. In contrast, the microparticle technique gives a realistic temperature profile across the channel region, with the temperature rise peaking between the two metal contacts (53 °C). The thermal profile also shows no temperature discontinuity between the transparent semiconductor and opaque metal surfaces. The comparison clearly shows the advantage of using the IR microparticle technique to obtain a realistic temperature profile across both semiconductor and metallised regions of a structure.

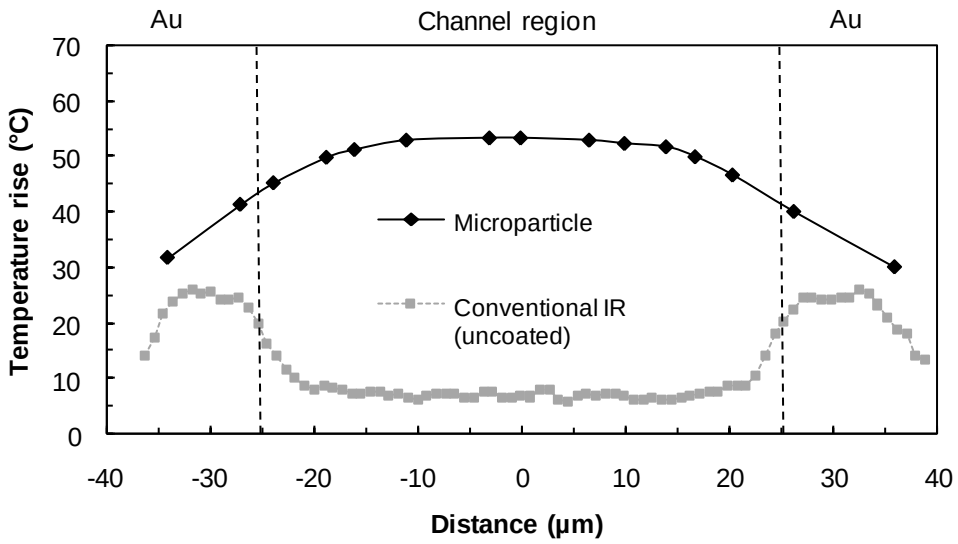

Figure 6.14: Temperature profiles measured across the channel region and adjacent metal contacts of the AlGaN/GaN TLM structure using the microparticle and conventional IR techniques. P_{dis} = 0.86 W, T_{amb} = 80 °C.

A microparticle temperature profile was also built up along the width of the channel region and periphery (profile location marked as line 'B' in Figure 6.13). The thermal profile is shown in Figure 6.15. Over the central portion of the channel region (i.e. on the heat source) the temperature rise is very uniform (~ 53 °C). However, towards the edge of the channel region, temperatures rapidly decay in an almost inverse exponential manner, consistent with other work [102]. At a distance of 40 μm away from the channel region (heat source), the temperature rise is approximately half its peak value.

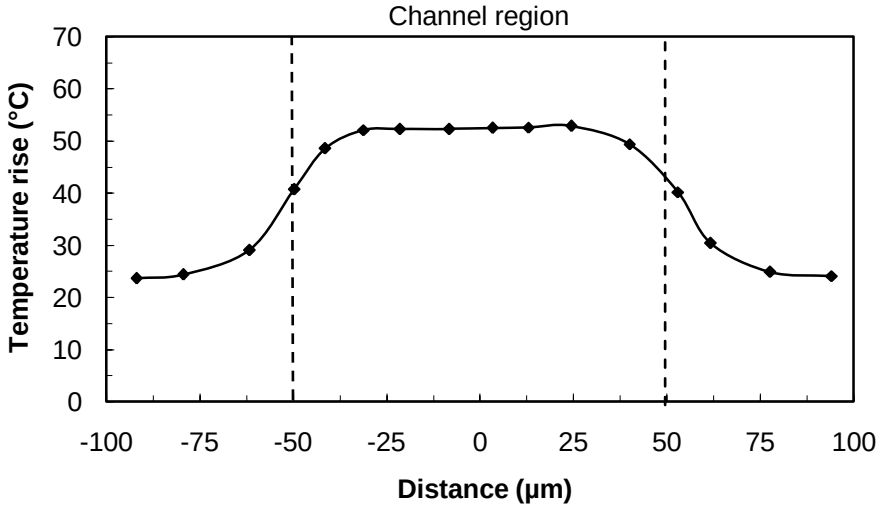

Figure 6.15: Temperature profile measured along the width of the channel region and periphery of the AlGaN/GaN TLM structure using the IR microparticle technique. P_{dis} = 0.86 W, T_{amb} = 80 °C.

The peak device operating temperature was extracted from the IR microparticle measurements and is plotted as a function of dissipated power in Figure 6.16. The temperature rises linearly with increasing power level. A temperature rise of 62 °C was recorded at 1 W. The linearity of the temperature rise is also reflected in the thermal resistance results (plotted as a function of dissipated power in Figure 6.17). The thermal resistance is shown to be very flat over all power levels (~ 62 °C/W); indicating negligible change in the overall thermal conductivity of the semiconductor structure within the measured temperature range.

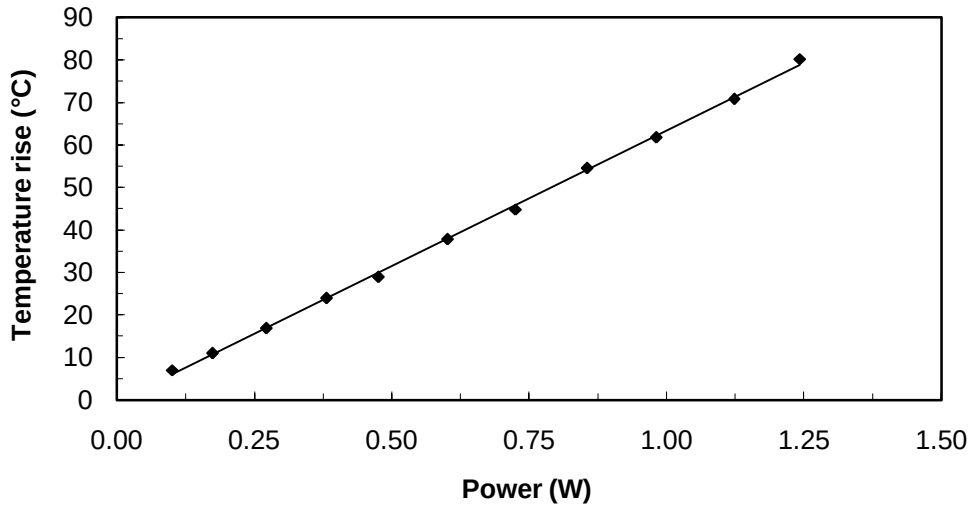

Figure 6.16: Peak temperature rise measured on the AlGaN/GaN TLM structure plotted as a function of dissipated power.

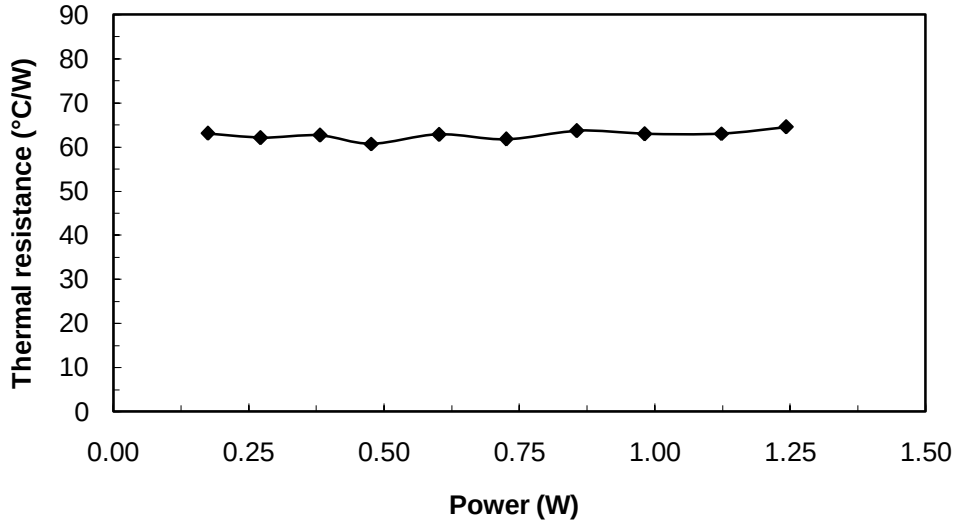

Figure 6.17: Thermal resistance of the AlGaN/GaN TLM structure plotted as a function of dissipated power.

6.5.4 Temperature validation using micro-Raman spectroscopy

A micro-Raman spectroscopy system at Bristol University was used to validate the accuracy of the IR microparticle temperature measurements made on the AlGaN/GaN

TLM structure. Micro-Raman spectroscopy measures scattered laser light from the semiconductor to detect temperature induced shifts in phonon frequency. The technique is described in Section 2.3.2 of Chapter 2.

A diagram showing the experimental arrangement used for the micro-Raman measurements is shown in Figure 6.18. For measurement purposes, the wafer of the TLM structure was mounted onto a Peltier heated stage to allow its temperature to be controlled during electrical powering. A 488 nm Ar^{+} ion laser was used as an excitation source. An XY table was used to position the sample under the optical path of the laser beam.

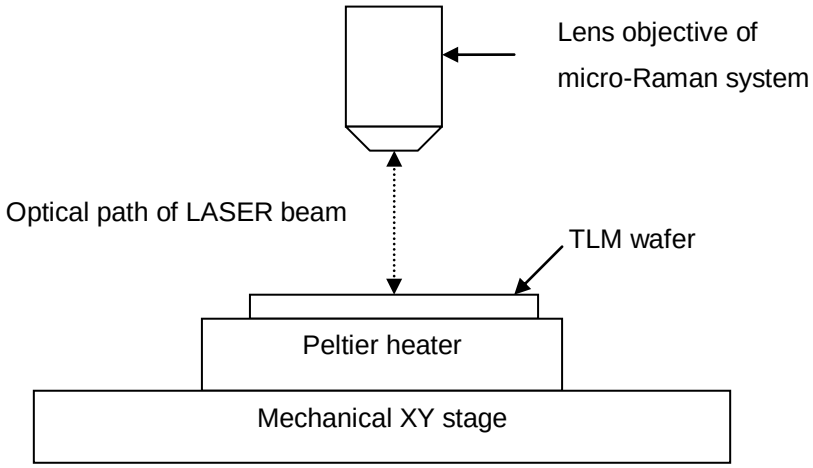

Figure 6.18: Experimental arrangement used for the micro-Raman temperature measurements on the AlGaN/GaN TLM structure.

A schematic diagram showing the location of the measured micro-Raman temperature profile is shown in Figure 6.19. A 50 × lens objective was used to focus the laser beam onto the Si substrate, a few micrometers below the GaN layer, giving a spot size of around 1 μm in diameter. The Si phonon peaks are much stronger than the GaN, so better temperature accuracy is achievable in this sub-layer. Temperatures in this area of the Si substrate are expected to closely match the maximum channel temperature, as the distance to the channel (~ 3 μm) is small compared to the total thickness of the substrate (400 μm). A scanning mode was used to obtain a temperature profile between the two metal contacts. In the scanning mode, the probing laser beam

acquires the Raman phonon spectrum at each spot and is then moved to the next position using the motorised XY stage. The step size was 1 µm. During recording, the laser photon energy was limited to less than 3 mW to minimise laser-induced heating and carrier generation within the semiconductor.

Temperatures were determined by measuring the phonon frequency shift of the strong A1 (LO) mode with the device in un-powered and powered conditions. This, together with the phonon shift temperature dependence, was used to calculate the operating temperature. With the system, a temperature accuracy of ± 6 °C is achievable [38].

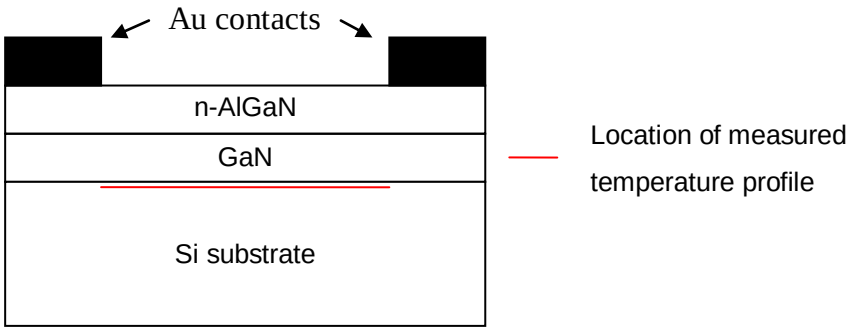

Figure 6.19: Diagram of the AlGaN/GaN TLM structure showing the location of the micro-Raman temperature profile.

A comparison between the micro-Raman and IR microparticle temperature profiles measured across the length of the channel region under identical bias conditions (0.86 W) is shown in Figure 6.20. Good agreement was obtained between the peak temperature rise measured using both techniques (~ 53 °C). However, the micro-Raman profile is slightly noisier, particularly towards the metal contacts. Longer integration time of the recovered micro-Raman signal may have helped reduce noise but at the expense of increased measurement time.

A conventional IR temperature profile, measured on the paint coated TLM structure, is also shown in Figure 6.20. The coated IR results appear to show a slight underestimation of the peak surface temperature (~ 7 °C). Heat spreading, caused by the thick coating, is likely to lead to a slight temperature reduction. The results clearly

show the advantage of using the improved IR microparticle technique which gives a temperature accuracy in the centre of the channel region comparable to micro-Raman spectroscopy.

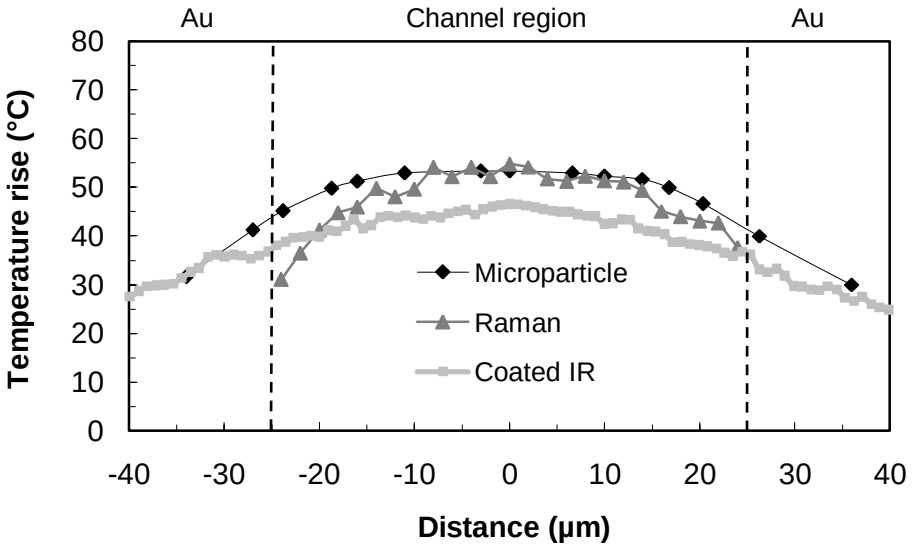

Figure 6.20: Comparison between the micro-Raman, microparticle and conventional IR (coated) temperature profiles measured along the channel region of the TLM structure, between the metals contact pads. P_{dis} = 0.86 W, T_{amb} = 80 °C.

6.6 Temperature Measurements on a Metallised Heater Structure

The IR microparticle technique was used to make temperature measurements on the metallised heater structure described in Section 5.3 of Chapter 5. The structure was difficult to measure using conventional IR, as it consisted of a highly reflective, thin Au heater element, fabricated on an optically transparent, undoped, GaAs substrate. To validate the accuracy of the microparticle measurements, the temperature results were compared to those obtained from an electrical technique.

6.6.1 Microparticle temperature measurement procedure

An optical image showing the heater structure is shown in Figure 6.21. In the image, the thin, 3 µm wide, heater element can be seen bridged between two Au metal contacts, spaced 100 µm apart. A spherical carbon microparticle (~ 3 µm in diameter) was deposited onto the structure using a micromanipulator probe and moved across its

surface to enable temperature profiles to be built up along the axis marked in Figure 6.21. During positioning, care was taken to prevent the sharp probe tip from damaging the delicate metal element.

The heater was powered and voltage monitored using a four probe arrangement. During powering, temperature measurements were made on the deposited carbon microparticle using the QFI IR microscope. The ambient temperature of the baseplate, on which the structure was placed, was stabilised at 80 °C.

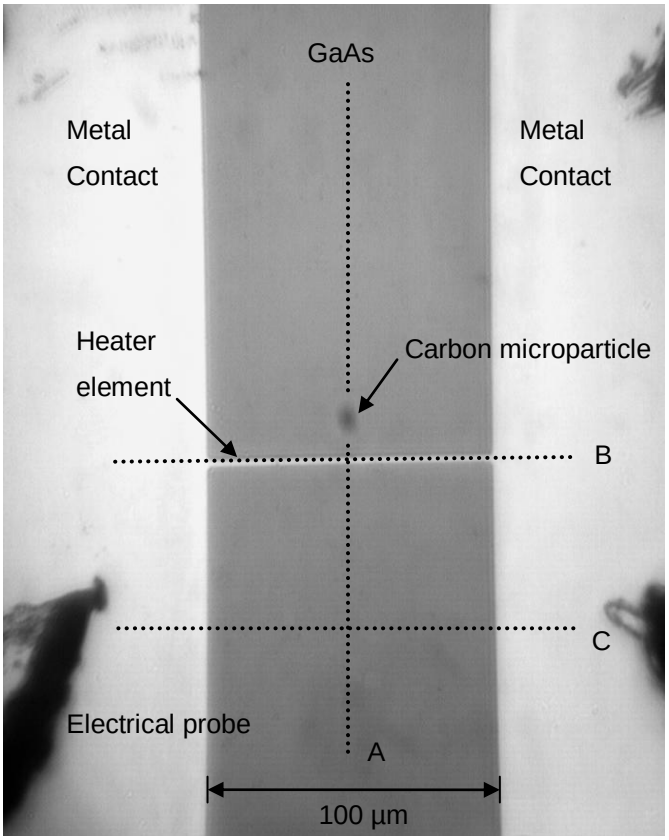

Figure 6.21: Optical image showing the carbon microparticle deposited on the surface of the metallised heater structure. Lines showing the location of the measured temperature profiles are marked.

6.6.2 Temperature results

An IR temperature image, showing the microparticle placed on the electrically biased heater element is shown in Figure 6.22. The dissipated power was 66 mW.

Measurements on the microparticle indicate that the maximum temperature of the Au heater element is 131.6 °C. On the surrounding metal and GaAs areas, the measured temperatures are depressed (~ 100 °C).

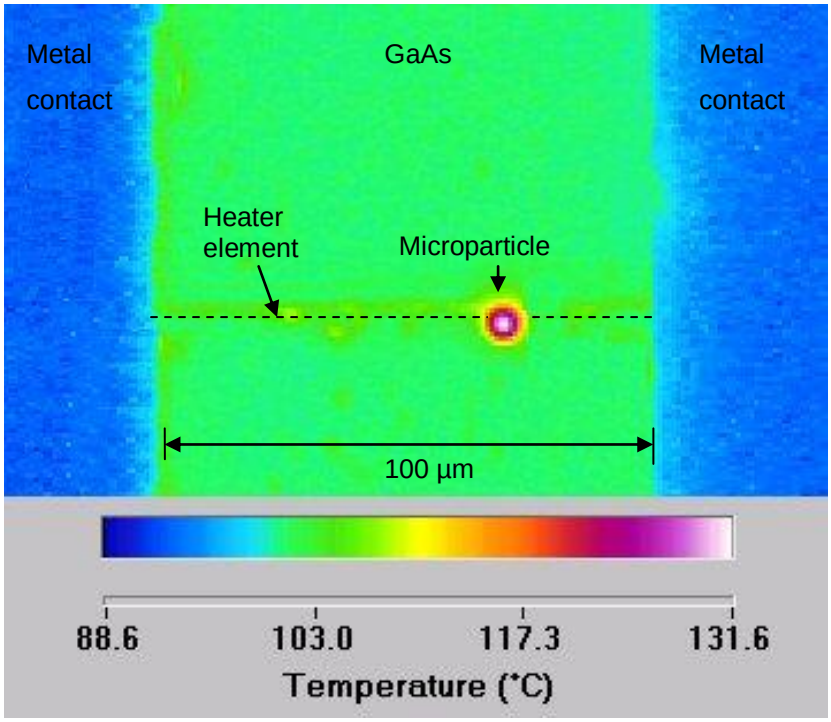

Figure 6.22: Infrared temperature image showing the microparticle on the electrically powered heater structure. P_{dis} = 66 mW, T_{amb} = 80 °C.

The IR microparticle temperature profile measured across the electrically powered heater element is shown in Figure 6.23 (location marked as line 'A' in Figure 6.21). The bias power was 39 mW. The IR microparticle measurements show a realistic surface temperature profile across the structure, with a temperature peak of 44 °C on the heater element. Temperatures rapidly decay away from the heat source. Figure 6.23 also shows the temperatures profile obtained from conventional IR measurements made on the paint coated structure. Although showing elevated temperatures, the coated results underestimate the peak temperature rise on the heater element by 23 °C. Heat spreading caused by the thick paint coating is thought to cause a severe reduction in surface temperature. The effect of heat spreading is likely to be exacerbated, as the thermal resistance of the heater structure is extremely high (estimated > 1000 °C/W). The results show the advantage of using the IR

microparticle technique to obtain realistic, high spatial resolution, surface temperature measurements on and around the narrow (3 μm) heater element.

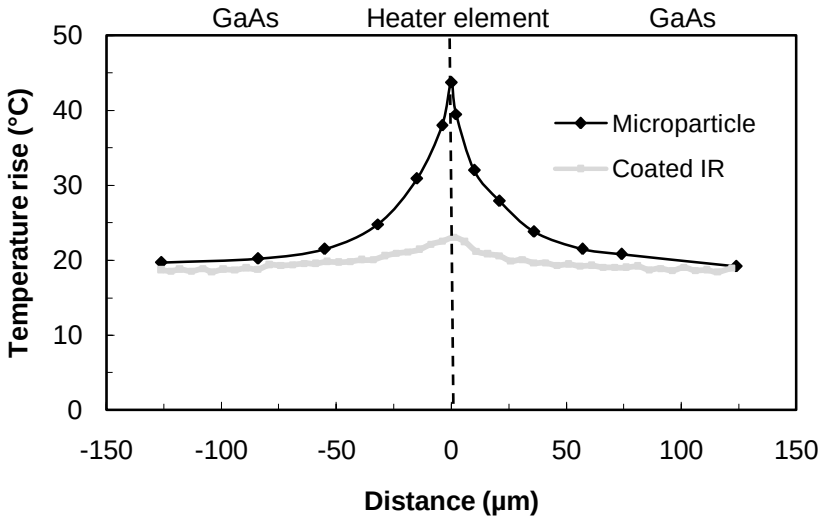

Figure 6.23: Microparticle and conventional IR (coated) temperature profiles measured across the heater element (location marked as line 'A' in Figure 6.21). P_{dis} = 39 mW, T_{amb} = 80 °C.

Figure 6.24 shows an IR microparticle temperature profile measured along the length of the heater element and metal contacts under identical bias conditions (location marked as line 'B' in Figure 6.21). The IR microparticle measurements show a near uniform temperature rise (~ 45 °C) on all areas of the heater element. On the contact pads, at a distance of 50 μm from the heater edge, the temperature rise decays to around 27 °C.

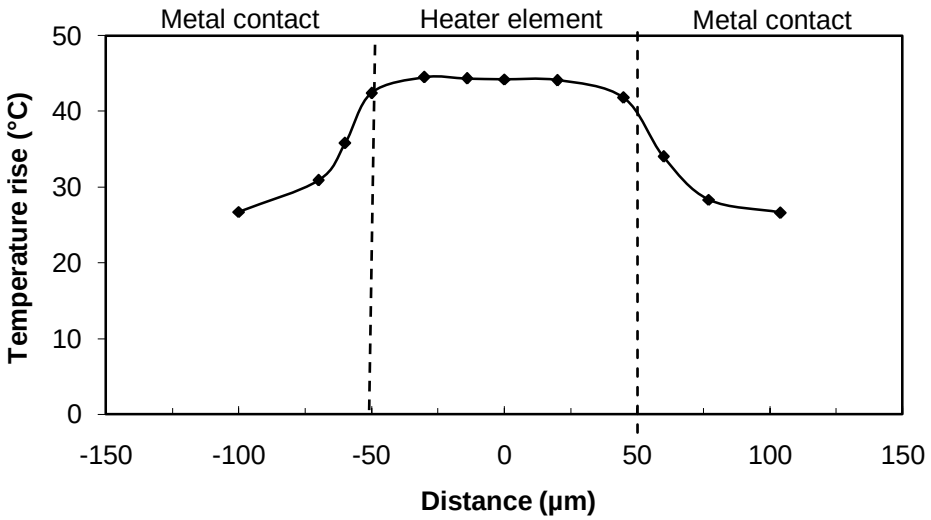

Figure 6.24: Temperature profile measured along the length of the heater element and on the adjacent contact pads using the IR microparticle technique (location marked as line 'B' in Figure 6.21). P_{dis} = 39 mW, T_{amb} = 80 °C.

Figure 6.25 shows a temperature profile measured at a distance of 50 µm away from the heater element, between the contact pads (location marked as line 'C' in Figure 6.21). At this distance, a near uniform temperature rise occurs across the structure. This is not unexpected, as heat flux will be very diffuse in this region.

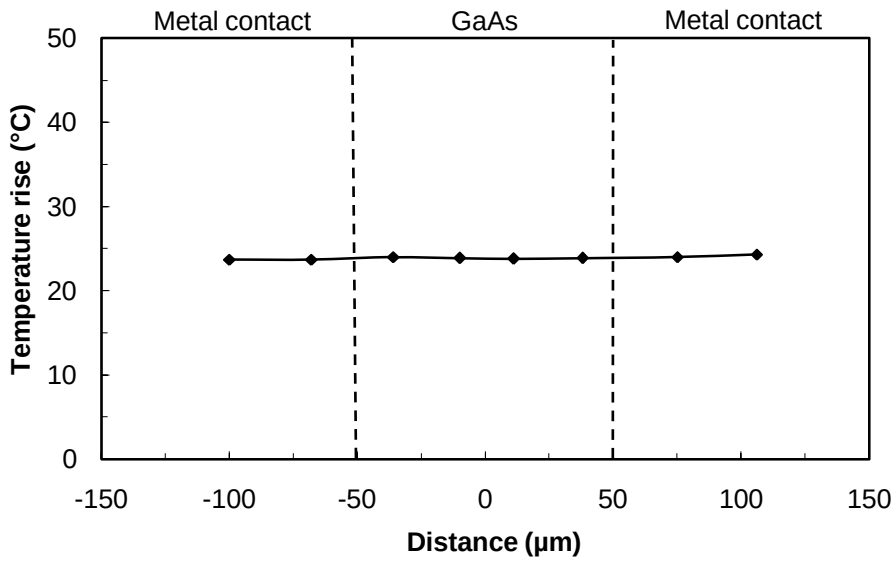

Figure 6.25: Temperature profile measured between the metal contacts at a distance of 50 µm from the heater element using the IR microparticle technique (location marked as line 'C' in Figure 6.21). P_{dis} = 39 mW, T_{amb} = 80 °C.

6.6.3 Comparison with electrical temperature measurements

The peak heater temperature rise measured using the IR microparticle technique was compared to results obtained from electrical temperature measurements. The electrical technique exploits the near linear temperature dependent resistance of the metal heater element. For calibration purposes, the temperature coefficient of resistance was initially established. A very small constant current of ~ 2 mA (insufficient to cause significant self-heating) was passed through the heater element. The voltage across the heater element V_{he} was then monitored under DC conditions and the IV results used to determine its electrical resistance R_{he}. During monitoring of R_{he}, the temperature of the heater element was changed by varying the stage temperature from 50 to 120 °C. As expected, R_{he} increased linearly with temperature, with a coefficient α = 0.018 Ω/°C, see Figure 6.26.

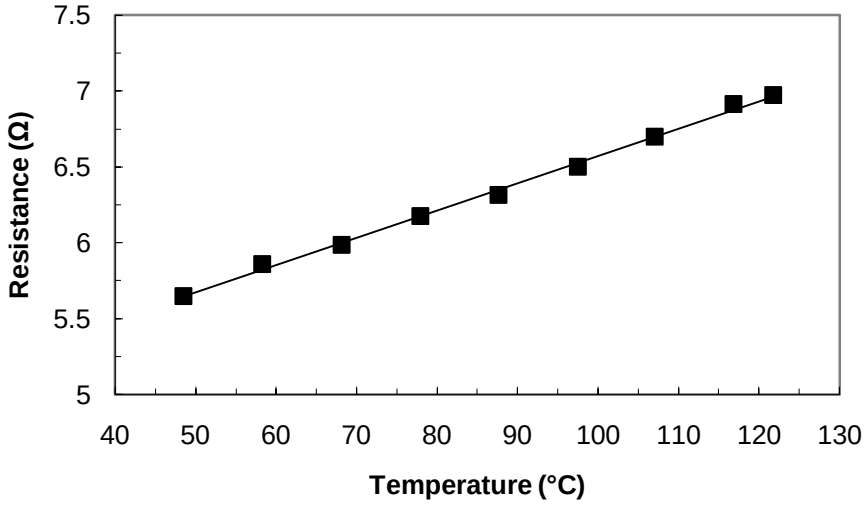

Figure 6.26: Electrical resistance of the heater element plotted as a function of temperature.

The average temperature rise T_{rise} of the electrically powered heater element was calculated using the following expression, where ΔR_{he} is the change in heater resistance from unpowered to powered conditions and α is its temperature coefficient.

$$T_{rise} = \frac{\Delta R_{he}}{\alpha} \tag{6-1}$$

A comparison between the temperature rise measured on heater element using the IR microparticle and electrical techniques is shown in Figure 6.27. Both sets of results are in good agreement to within ± 5 °C. The results help to validate the accuracy of the IR microparticle measurements made on the metallised heater structure.

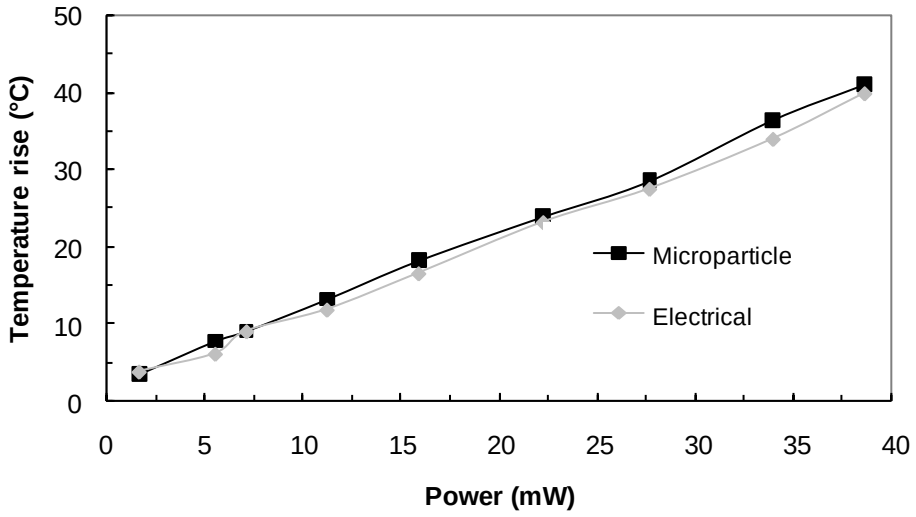

Figure 6.27: Comparison between the temperature rise measured using the electrical and IR microparticle techniques plotted as a function of power.

6.7 Application to the Gallium Arsenide Gunn Diode

Significant errors can occur when conventional IR temperature measurements are made on uncoated metal surfaces. In previous work on the Gunn diode (see Chapter 3 and Chapter 4), the metal top contact was coated with a high emissivity layer to improve the measurement accuracy. Although accurate temperature measurements can be obtained by using this approach, coating damages the device and is difficult to fully remove. Also, a thick coating will result in a certain amount of heat spreading.

Work was undertaken to assess the feasibility of using the microparticle technique to make improved IR temperature measurements on the top metal contact of the Gunn diode. Unlike coating, the technique is non-destructive, as it requires the deposition of only a single microparticle on the metal. To help validate the accuracy of the microparticle measurements, electrical and conventional IR temperature profiling was undertaken.

6.7.1 Microparticle measurement procedure

A standard 77 GHz graded-gap Gunn diode, fabricated by e2v (Lincoln) Ltd, was studied. For temperature measurement purposes, the Gunn diode was mounted in a purpose built aluminium jig which was in turn mounted onto the Peltier heated stage of the IR microscope. Figure 6.28 shows the experimental arrangement.

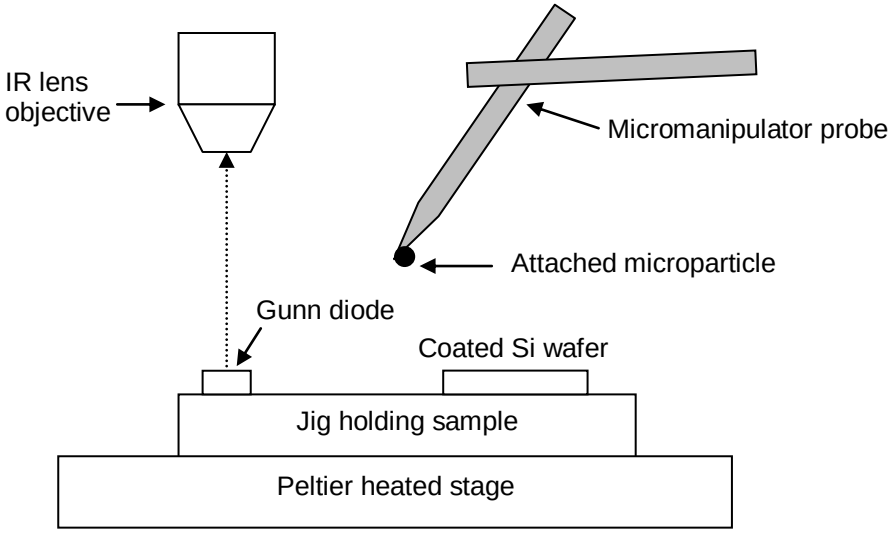

Figure 6.28: Experimental arrangement used to male the microparticle temperature measurements on the top contact of the Gunn diode. Not to scale.

A manipulation procedure, similar to that described in Section 6.5.1 of this chapter, was used to place a spherical carbon microparticle (3 μm in diameter) onto the metal top contact of the Gunn diode. A micromanipulator probe, having a 5 μm diameter tungsten tip, was used to electrostatically pick up the microparticle from an adjacent Si wafer. The attached microparticle was then slowly lifted and positioned over the metal top contact, which was 80 μm in diameter. Careful lowering of the microparticle onto the metal surface was found to be sufficient to release it onto the center of the top contact. An optical image of the deposited microparticle is shown in Figure 6.29. In the image, it appears centrally as a small black dot against the highly reflective metal.

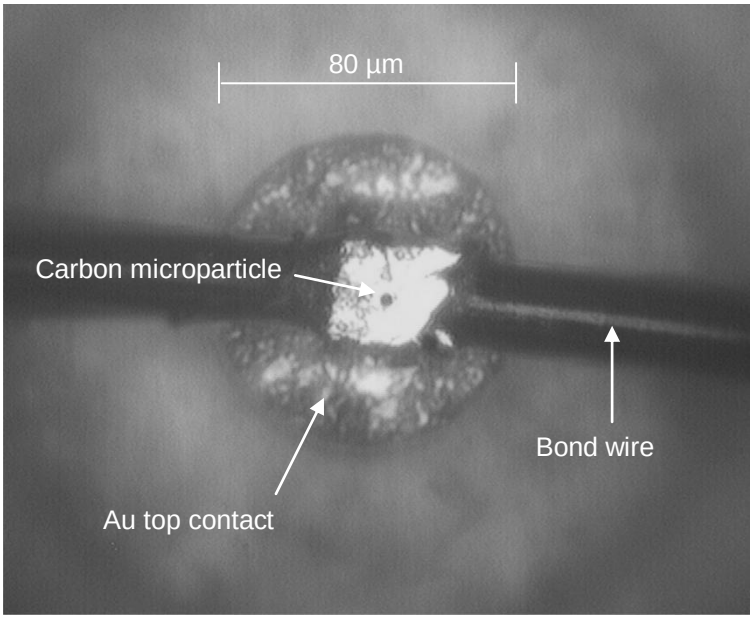

Figure 6.29: Optical image showing the carbon microparticle on the metal top contact of the Gunn diode.

Temperature measurements were made on the deposited microparticle using the QFI IR microscope and a 25 × lens objective. To obtain accurate temperatures, the microparticle emissivity (determined to be 0.5 from previous measurements) was entered into the IR measurement system. During device powering and temperature measurements, the ambient jig temperature was stabilised at 50 °C.

6.7.2 Temperature results

An IR temperature image showing the carbon microparticle on the top contact of the electrically powered Gunn diode is shown in Figure 6.30. The device was biased at 6 V, 990 mA (5.94 W). The peak temperatures on the microparticle is 225 °C, indicating a rise in top contact temperature of 175 °C above ambient. In contrast, temperatures measured directly on the low emissivity metal surface are significant depressed (~ 115 °C). In the image, a high temperature area appears to occur around the periphery of the metal contact. This is an artefact caused by radiation from the mesa being reflected by the surrounding metal surface (no heat source exists in this region).

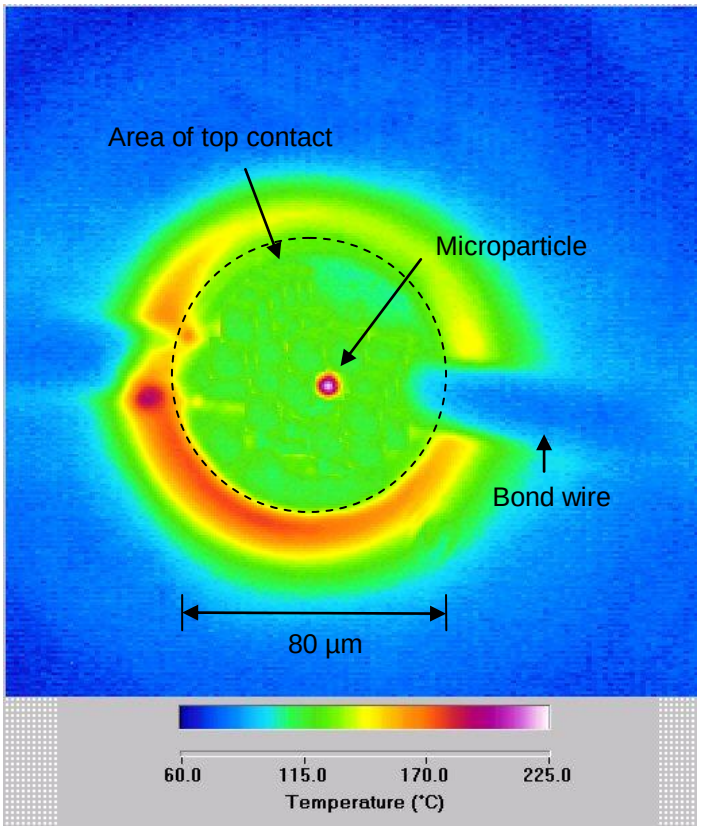

Figure 6.30: Infrared temperature image showing the carbon microparticle on the metal top contact of the electrically powered Gunn diode.

P_{dis} = 5.94 W, T_{amb} = 50 °C.

The microparticle technique was used to obtain the peak operating temperature of the Gunn diode over a range of power levels. A graph showing the measured temperature rise is shown in Figure 6.31. For comparison, the results of conventional IR measurements made on the uncoated top contact are also plotted. The microparticle measurements show far higher operating temperatures. The microparticle measurements show a temperature rise of 200 °C at 4.2 W, compared to 133 °C using the conventional uncoated IR approach. On the uncoated metal, the emitted radiation level will be low and noise and reflected background radiation will seriously corrupt the measurement. The thermal resistance of the Gunn diode was calculated from the microparticle temperature measurements and is plotted as a function of dissipated power in Figure 6.32. The thermal resistance is relatively constant (~ 50 °C/W) for this device.

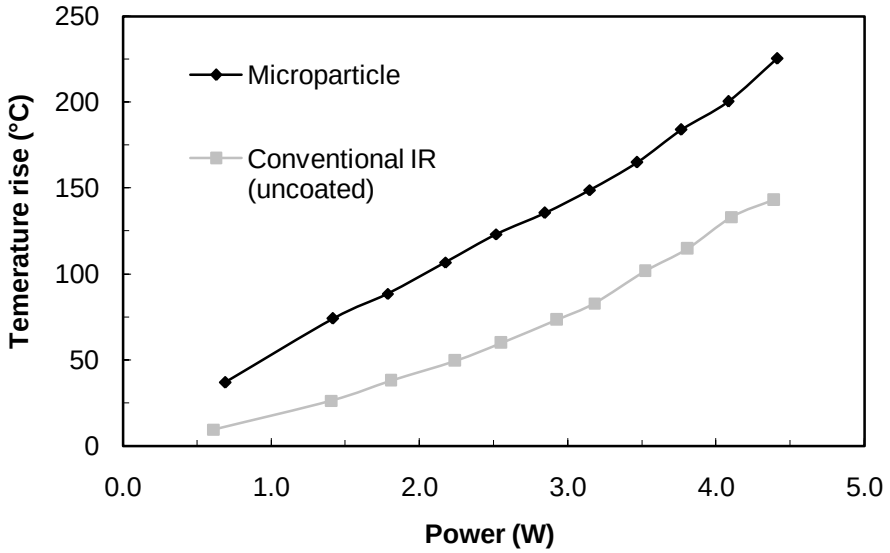

Figure 6.31: Comparison showing the peak temperature rise measured on the top metal contact of the Gunn diode using the microparticle and conventional IR techniques. T_{amb} = 50 °C.

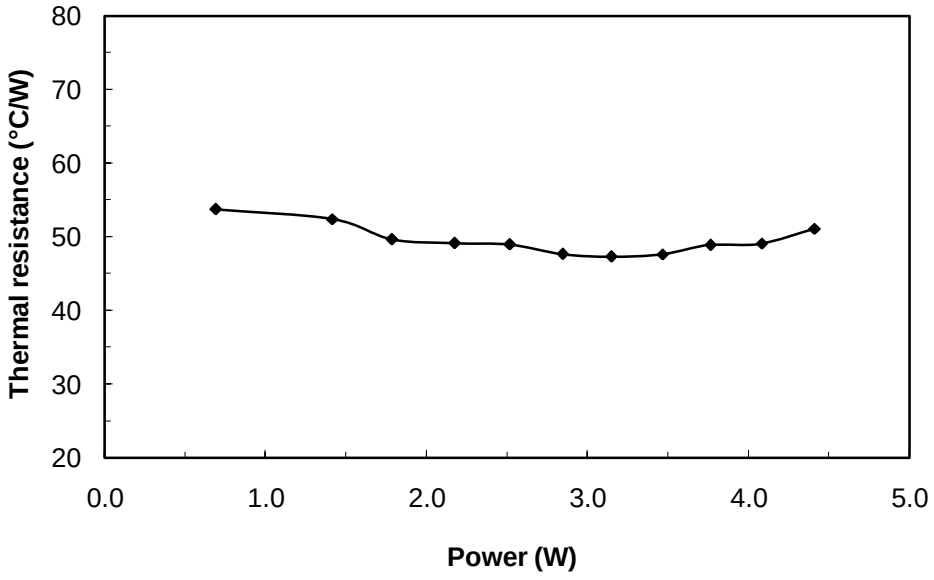

Figure 6.32: Thermal resistance of the Gunn diode plotted as a function of dissipated power. Results calculated from the IR microparticle temperature measurements made on the metal top contact. T_{amb} = 50 °C.

6.7.3 Comparisons with electrical temperature measurements

A pulsed electrical system has been developed by e2v (Lincoln) Ltd. for measuring the average operating temperature of the Gunn diode. The system is similar to that adopted by Fentem and Neg [103] and exploits the temperature dependent resistivity of the GaAs transit layer.

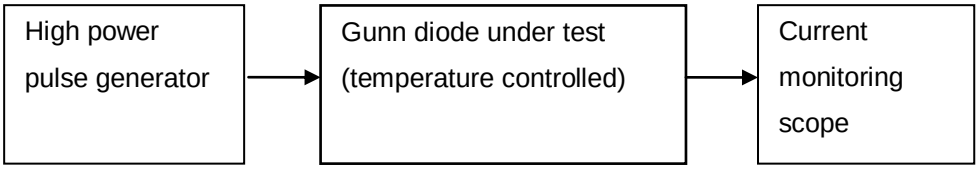

Figure 6.33: Experimental arrangement used to make the electrical temperature measurements on the Gunn diode.

A diagram of the electrical temperature measurement system is shown in Figure 6.33. To calibrate the system, the variation in diode current I_d was measured as a function temperature. A purpose built pulse generator, developed by e2v (Lincoln) Ltd., was used to supply short pulses of current to the device at known bias voltages. To avoid self-heating, the pulse duration was limited to much less than the thermal time constant (estimated from the electric stabilisation time to be 5 µs). A pulse width of 100 ns was used, with a period of 10 ms. During current pulsing, the temperature of the diode was varied from 20 to 180 °C and I_d monitored using a current sensing oscilloscope. As temperature increased, I_d decreased linearly due to the reduction in GaAs mobility, with a coefficient β = - 1.3 mA/°C. Once the system was calibrated, the Gunn diode was conventionally powered. Knowing the change in current level due to self-heating ΔI_d and the temperature coefficient β, the average transit layer temperature rise T_{rise} can be calculated using

$$T_{rise} = \frac{\Delta I_d}{\beta} \qquad (6\text{-}2)$$

It was only possible to make a limited number of electrical temperature measurements on the Gunn diode because the system oscillated at low bias voltages. A comparison between the electrical and IR microparticle temperature results is shown in Figure 6.34. Results from both techniques appear to be in reasonable agreement. For example, at 4 W, the electrical and microparticle temperatures are 181 and 199 °C, respectively. The fact that the electrical technique gives a slightly lower temperature is probably because it records an average transit layer temperature, rather than a peak value.

The results of conventional IR temperature measurements made on the paint coated top contact are also shown in Figure 6.34. Good agreement (± 5 °C) exists between the coated and IR microparticle results. In this case, the coated results are thought to be accurate, as temperature errors due to heat spreading are minimised (the top contact is large and is thermally isolated from other structures).

The work shows how the IR microparticle technique can be used to make accurate non-destructive temperature measurements on metallised devices such as the Gunn diode.

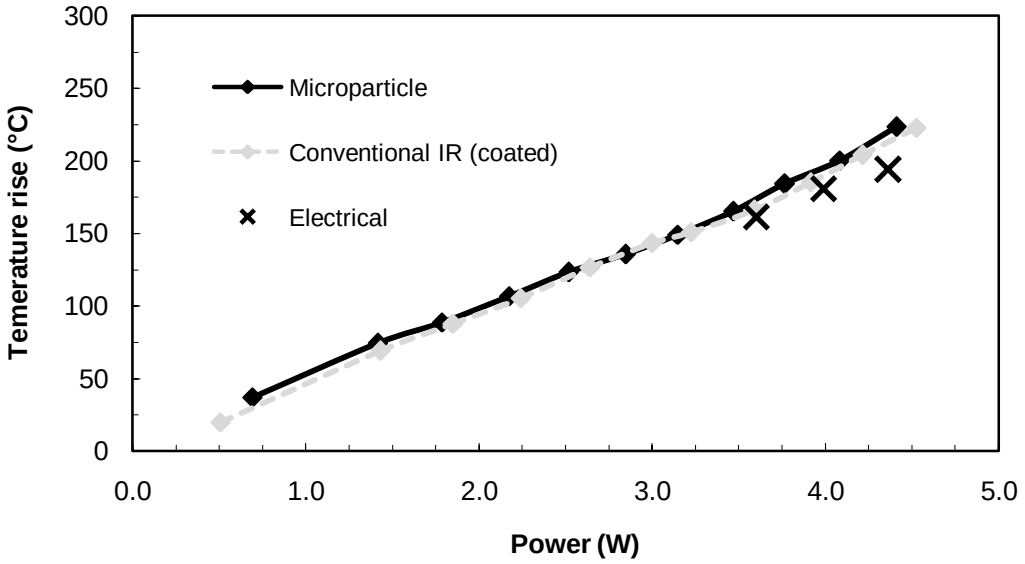

Figure 6.34: Temperature rise measured on the metal top contact of the Gunn diode using the microparticle and convention IR (coated) measurements. Electrical results are also shown at a limited number of bias levels.

6.8 Conclusions

The use of carbon microparticles for improved IR surface temperature measurements on semiconductor devices has been demonstrated. The technique can be used with existing IR microscopes to significantly enhance their measurement capability, especially when transparent semiconductor layers and low emissivity metals are studied. Measurements made on an AlGaN/GaN TLM structure show the potential of the new technique to give a temperature accuracy comparable to micro-Raman spectroscopy. The IR microparticle technique can remove the need to coat a device, which can cause damage and significant heat spreading, especially when studying localised heat sources.

Micromanipulator probes were shown to be a convenient tool for individual microparticle manipulation. Probes can be used to deposit and also remove individual particles after the measurement, leaving the device intact (unlike coating). When the placement of individual microparticles is not required, a fine coating of microparticles can be brushed onto a surface.

CHAPTER 7. CONCLUSIONS

7.1 Current work

7.1.1 Gunn diode

In Chapter 3, IR thermal microscopy was shown to be a useful tool for thermal characterisation of the Gunn diode. The technique can be used to obtain 2D temperature measurements on the exposed metal top contact of the device, enabling the extraction of its peak operating temperature - this type of temperature measurement provides invaluable information to the manufacturer regarding the safe operating power limits. A slight disadvantage with making temperature measurements on the top contact is the need to coat the device with a high emissivity layer, which can damage the device. An improved IR measurement technique, which removes the need to coat the Gunn diode, is discussed in Chapter 6.

Although conventional IR microscopy is a useful tool for obtaining temperature measurements on the metal top contact of the Gunn diode, temperature errors were found to occur when the IR transparent GaAs semiconductor layers were studied. As shown in Chapter 4, micro-Raman spectroscopy can be used as an alternative technique to obtained high resolution temperature measurements on the GaAs semiconductor layers. Micro-Raman temperature profiling along the mesa side of the electrically powered device showed a characteristic temperature rise from the interface with the integral heatsink towards the transit layer, where heat is generated. Temperatures were uniform along the length of the substrate, indicating negligible ohmic heating and heat loss through this layer.

7.1.2 IR measurement technique

The radiative properties of the materials under study were shown to have a large effect on the accuracy of conventional IR temperature measurements made on semiconductor devices. Measurements made on optically transparent semiconductor layers and low emissivity metals can result in a significant underestimation of the true

surface temperature. Application of a high emissivity coating can be used to improve measurement accuracy, however, it permanently damages the device. On some structures, especially localised heat sources, coating can also cause significant heat spreading which distorts the temperature profile.

The use of spherical carbon microparticles for improved IR surface temperature measurements has been demonstrated. A major advantage of using the IR microparticle technique is that the temperature accuracy is independent of the radiative properties of the surface under study. Accurate surface temperature measurements can, therefore, be made on transparent semiconductor layers and low emissivity/reflective metals, significantly enhancing the measurement capability of existing IR instruments.

A procedure for depositing individual microparticles onto devices was demonstrated. Naturally occurring electrostatic and van der Waal forces were found to be sufficient to attach individual microparticles to a micromanipulator probe for deposition onto a structure. Unlike coating, individual microparticles cause insignificant heat spreading and can be removed after the measurement, leaving the device intact.

7.2 Future work

7.2.1 Gunn diode

The next generation of Gunn diode devices is being developed for terahertz applications, for example, body scanning [104].Thermal design will be particularly challenging due to the high power dissipation densities involved; novel cooling schemes will have to be adopted. Detailed thermal characterization of teraherz devices and their active cooling systems will be essential for development purposes. It is expected that both IR thermal microscopy and micro-Raman thermal spectroscopy will be used as complementary measurement techniques - IR for making measurements on metalised surfaces and micro-Raman for investigating semiconductor layers.

.

7.2.2 Microparticle technique

In this work, an electrostatic ‘pick and place’ procedure, employing a micromanipulator probe, was used to deposit individual carbon microparticles onto surfaces. A further refinement of the technique would be to control the electrostatic attractive force between the microparticle and probe tip [105]. It would then be possible to release microparticles from the probe tip, without the risk of the probe touching delicate devices. Another approach would be to deposit and manipulate individual microparticles using atomic force microscopy (AFM) [106].

When individual carbon microparticles are deposited onto a device, they are unlikely to short circuit any metal contacts. However, if a large number are brushed onto a device, such a risk could exist. To mitigate this risk, the carbon microparticles could be coated with a thin, transparent, insulating layer. GEA Niro Ltd. have developed a process which could be used to coat microparticles with an insulating layer [107].

In the future, other temperature dependent particulate properties could be studied. For example, micro-Raman spectroscopy could be used to measure phonon scattering in semiconductor particles. As micro-Raman uses shorter wavelengths of optical radiation, sub-micrometer sized particles could be used to achieve temperature measurements with a very high spatial resolution (< 500 nm). The technique could be used to make high resolution temperature measurements on metals, which are currently impossible to obtain using the conventional micro-Raman measurement procedure.

APPENDIX A. GRADED GAP GUNN DIODE DIMENSIONS

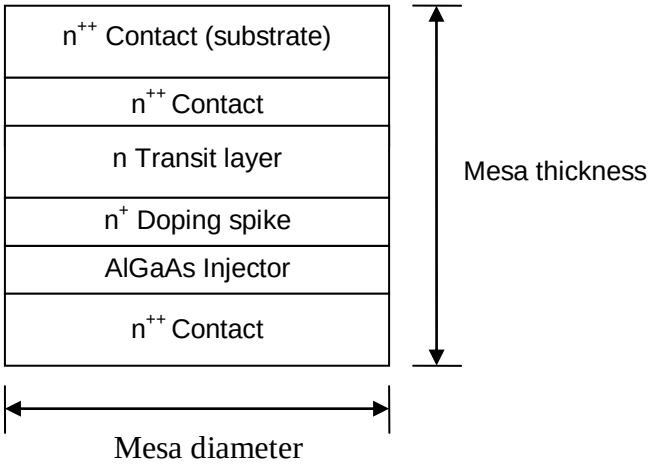

Figure A-1: Diagram showing the named dimensions of the graded-gap Gunn diode.

	Sample No.		
Dimension Type	**1**	**2**	**3**
Mesa diameter	70 µm	80 µm	60 µm
GaAs layer thicknesses:-			
Substrate	10 µm		
Transit	1.6 µm		
Doping spike	10 nm		
Injector	100 nm		
n^{++} Contacts	500 nm		
Total mesa thickness	12.7 µm		

Table A-2: Table showing the dimensions of the graded-gap Gunn diode samples.

APPENDIX B. MATLAB THERMAL MODEL

```
% DEFINE PARAMETERS
Mr=35e-6;              % Mesa radius (m)
A=2*pi*(Mr)^2;         % Mesa area (m^2)

Lt=1.6e-6;     % Transit layer length (m)
Li=0.1e-6;     % Injector layer length
Lc=0.5e-6;     % Semiconductor contact length

Rihs=21.7;     % Thermal resistance of integral heatsink and package (C/W)

Tamb=353;      % Ambient unpowered temperature of device (K)

Tt=Tamb;       % Ambient transit layer temperature (K)
Ti=Tamb;       % Ambient injector layer temperature
Tc=Tamb;       % Ambient ambient contact layer temperature

Pdis=0.5       % Dissipated power (W)


% ITERATIVE CALULATION ROUTINE
for P=0.001:0.01:Pdis          %Start of loop

Kt=62000*Tt^-1.25;  % Calculate transit layer thermal conductivity (W/m.K)
Ki=28120*Ti^-1.25;  % Calculate injector layer thermal conductivity
Kc=44550*Tc^-1.25;  % Calculate contact layer thermal conductivity

Rt=Lt(A*Kt);  % Calculate transit layer thermal resistance (C/W)
Ri=Li(A*Ki);           % Calculate injector layer thermal resistance
Rc=Lc(A*Kc);           % Calculate contact layer thermal resistance

Tt=P*(Rihs+Rc+Ri+0.5*Rt)+Tamb; % Calculate average transit layer temp. (C)
Ti=P*(Rihs+Rc+0.5*Ri)+Tamb;      % Calculate average injector layer temp.
Tc=P*(Rihs+0.5*Rc)+Tamb;         % Calculate average contact layer temp.

end

% CALCULATE FINAL VALUES
Rth=Rt+Ri+Rc+Rihs          % Total thermal resistance (C/W)
Trise=Rth*Pdis             % Peak temperature rise (C)
```

APPENDIX C. CONVENTIONAL GUNN DIODE DIMENSIONS

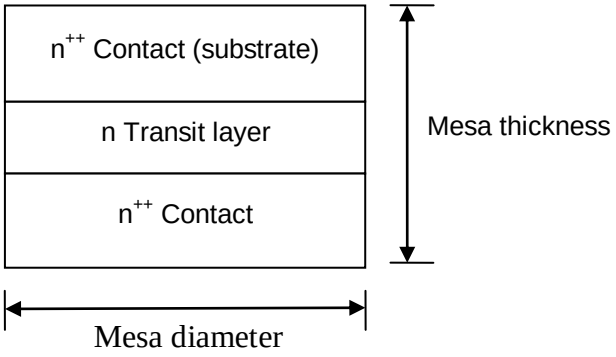

Figure C-1: Diagram showing the named dimensions of the conventional Gunn diode.

	Sample No.	
Dimension Type	**1**	**2**
Mesa diameter	160 µm	200 µm
GaAs layer thicknesses:-		
Substrate	80 µm	72 µm
Transit	10 µm	13 µm
n++ Contact	10 µm	15 µm
Total mesa thickness	100 µm	100 µm

Table C-1: Table showing the dimensions of the conventional Gunn diode samples.

APPENDIX D. MICROPARTICLE IR MEASUREMENTS

Temperature (°C)	
Wafer	**Microparticle**
80.9	80.9
85.7	85.7
90.5	90.5
95.4	95.5
100.2	100.4
105.1	105.2
109.9	110
114.7	114.5
119.6	119.1
126.7	126.1
131.5	131.4

Table D-1: Comparison between the wafer temperature (thermocouple measurement) and the temperatures measured on the carbon microparticle using IR.

	Radiance (mW/cm.str)		
Sample no.	**Si**	**Cu**	**Bonded**
1	0.479	0.478	0.474
2	0.478	0.484	0.475
3	0.47	0.469	0.473
4	0.471	0.488	0.483
5	0.48	0.471	0.477
6	0.482	0.487	0.468
7	0.474	0.462	0.473
8	0.478	0.469	0.485
9	0.473	0.469	0.475
10	0.481	0.484	0.481
Average	0.4766	0.4761	0.4764

Table D-2: Comparison between the IR radiance level measured from the carbon microparticles deposited on the Si and Cu surfaces. Figures for the carbon microparticles which were adhesively bonded to the Si wafer are also shown. The surface temperatures were 80 °C.

REFERENCES

[1] Förster, A.; Stock, J.; Montanari, S.; Lepsa.; M.I.; Lüth, H., “Fabrication and Characterisation of GaAs Gunn Diode Chips for Applications at 77 GHz in Automotive Industry,” Sensors Journal, vol. 6, pp.350-360, 2006

[2] Webb, P.W., "Thermal imaging of electronic devices with low surface emissivity ," IEE Proceedings G on Circuits, Devices and Systems, vol.138, no.3, pp.390-400, Jun 1991

[3] Akita, M.; Kishimoto, S.; Mizutani, T., "High-frequency measurements of AlGaN/GaN HEMTs at high temperatures ," IEEE Electron Device Letters, vol.22, no.8, pp.376-377, Aug 2001

[4] Gaska, R.; Chen, Q.; Yang, J.; Osinsky, A.; Asif Khan, M.; Shur, M.S., "High-temperature performance of AlGaN/GaN HFETs on SiC substrates ," IEEE Electron Device Letters, vol.18, no.10, pp.492-494, Oct 1997

[5] Pierce, D.G.; P.G, Brusius., “Electromigration: A review, Microelectronics and Reliability,” Reliability Physics of Advanced Electron Devices, vol.37, no.7, pp.1053-1072, July 1997

[6] Torregrosa-Penalva, G.; Asensio-Lopez, A.; Blanco-del-Campo, A., "Electro-thermal model extraction for MMIC power amplifiers," European Gallium Arsenide and Other Semiconductor Application Symposium (EGAAS), pp.397-400, Oct. 2005

[7] Batty, W.; Christoffersen, C.E.; Yakovlev, A.B.; Whitaker, J.F.; Mortazawi, A.; Al-Zayed, A.; Ozkar, M.; Ortiz, S.C.; Reano, R.M.; Yang, K.; Katehi, L.P.B.; Snowden, C.M.; Steer, M.B., "Global coupled EM-electrical-thermal simulation and experimental validation for a spatial power combining MMIC array," IEEE Transactions on Microwave Theory and Techniques, vol.50, no.12, pp.2820-2833, Dec 2002

[8] Mouthaan, K.; Tinti, R.; Arno, A.; de Graaff, H.C.; Tauritz, J.L.; Slotboom, J., "Thermal resistance modelling of RF high power bipolar transistors," Proceedings 27th European Solid-State Device Research Conference (ESSDERC), pp. 184-187, Sept. 1997

[9] Johnson, R.G.; Snowden, C.M.; Pollard, R.D., "A physics-based electro-thermal model for microwave and millimetre wave HEMTs," IEEE Microwave Symposium Digest, vol.3, pp.1485-1488, Jun 1997

[10] Johnson, R.G.; Batty, W.; Panks, A.J.; Snowden, C.M., "Fully physical coupled electro-thermal simulations and measurements of power FETs," IEEE Microwave Symposium Digest, vol.1, pp.461-464, 2000

[11] Sarua, A.; Hangfeng Ji; Hilton, K.P.; Wallis, D.J.; Uren, M.J.; Martin, T.; Kuball, M., "Thermal Boundary Resistance Between GaN and Substrate in AlGaN/GaN Electronic Devices," IEEE Transactions on Electron Devices, vol.54, no.12, pp.3152-3158, Dec. 2007

[12] Sze, S. M.. “Physics of Semiconductor Devices,” John Wiley and Sons, 1982

[13] Cain, B.M.; Goud, P.A.; Englefield, C.G., "Electrical measurement of the junction temperature of an RF power transistor," IEEE Transactions on Instrumentation and Measurement, vol.41, no.5, pp.663-665, Oct 1992

[14] Adlerstein, M.G.; Zaitlin, M.P., "Thermal resistance measurements for AlGaAs/GaAs heterojunction bipolar transistors," IEEE Transactions on Electron Devices, vol.38, no.6, pp.1553-1554, Jun 1991

[15] Yang-Hua Chang; Ying-Yih Wu, "Measurement of junction temperature in heterojunction bipolar transistors," Proceedings of the Third IEEE International Caracas Conference on Devices, Circuits and Systems, pp.D59/1-D59/4, 2000

[16] Yang-Hua Chang; Ying-Yih Wu; Lu, J.-M., "Calculation of junction temperature in heterojunction bipolar transistors," IEEE Proceedings of Electron Devices Meeting, pp.110-112, 1999

[17] Liu, W.; Yuksel, A., "Measurement of junction temperature of an AlGaAs/GaAs heterojunction bipolar transistor operating at large power densities," IEEE Transactions on Electron Devices, vol.42, no.2, pp.358-360, Feb. 1995

[18] Xi, Y.; Schubert, E.F., "Junction-temperature measurements in GaN UV light-emitting diodes using the diode forward voltage," Proceedings IEEE Lester Eastman Conference on High Performance Devices, pp. 84-89, Aug. 2004

[19] Donarski, R.J.; Jastrzebski, A.K.; Barnaby, J.E., "Pulsed I-V and temperature measurement system for characterisation of microwave FETs," IEEE MTT-S International Microwave Symposium Digest, vol.3, pp.1523-1526, May 1995

[20] Mehrotra, Vivek; Boutros, Karim; Brar, Berinder, "Electric-Field Dependence of Junction Temperature in GaN HEMTs," 65th Annual Device Research Conference, pp.143-144, June 2007

[21] Kuzmik, J.; Javorka, P.; Alam, A.; Marso, M.; Heuken, M.; Kordos, P., "Investigation of self-heating effects in AlGaN-GaN HEMTs," International Symposium on Electron Devices for Microwave and Optoelectronic Applications (EDMO), pp.21-26, 2001

[22] Hamann, H.F.; Lacey, J.; Weger, A.; Wakil, J., "Spatially-resolved imaging of microprocessor power (SIMP): hotspots in microprocessors," The Tenth Intersociety Conference on Thermal and Thermomechanical Phenomena in Electronics Systems (ITHERM), pp.5-125, June 2006

[23] Mc Donald, J.; Albright,G., "Microthermal Imaging in the infrared," Electronics Cooling, vol. 3, no.1, 1997

[24] Dai, P.; Canfield, P., “Location of defective cells in HBT power amplifier arrays using IR emission microscopy,” Microelectronics Reliability, vol.41, pp.1137-1141, 2001

[25] Hefner, A.; Berning, D.; Blackburn, D.; Chapuy, C.; Bouche, S., "A high-speed thermal imaging system for semiconductor device analysis," Seventeenth Annual IEEE Symposium on Semiconductor Thermal Measurement and Management (SEMI-THERM), pp.43-49, 2001

[26] Webb, P.W.; Russell, I.A.D., "Thermal resistance of gallium-arsenide field-effect transistors," IEE Proceedings G Circuits, Devices and Systems, vol.136, no.5, pp. 229-234, Oct 1989

[27] Oxley, C.H.; Coaker, B.M.; Priestley, N.E., "Measured thermal images of a gallium arsenide power MMIC with and without RF applied to the input," Solid State Electronics, vol.47, pp.755-758, 2003

[28] Radivojevic, Z.; Andersson, K.; Bogod, L.; Mahalingam, M.; Rantala, J.; Wright, J., "Novel materials for improved quality of RF-PA in base-station applications," IEEE Transactions on Components and Packaging Technologies, vol.28, no.4, pp. 644-649, Dec. 2005

[29] Mahalingam, M.; Mares, E., "Infrared temperature characterization of high power RF devices," IEEE MTT-S International Microwave Symposium Digest, vol.3, pp.2199-2202, 2001

[30] Wilson, J.; Decker, K., "GaAs MMIC thermal modeling for channel temperatures in accelerated life test fixtures and microwave modules," IEEE/CPMT Proceedings of the Semiconductor Thermal Measurement and Management Symposium (SEMI-THERM), pp.121-128, Feb 1994

[31] Hunter, A.; Adams, B.; Ramanujam, R., "Traceable emissivity measurements in RTP using room temperature reflectometry," 11th IEEE International Conference on Advanced Thermal Processing of Semiconductors (RTP), pp. 85-88, Sept. 2003

[32] Wada, S.; Iuchi, T., "Simultaneous measurement of emissivity and temperature for glossy metals near room temperatures," Proceedings of the 41st SICE Annual Conference, vol.4, pp. 2065-2069, Aug, 2002

[33] Chen, Z-H.; Uchida, T.; Minami, S., “Real-time emissivity corrected infrared microthermography based on a double modulation technique,” Measured Sciences Technology, vol.4, pp.288-292, 1993

[34] Kuball, M.; Hayes, J.M.; Uren, M.J.; Martin, I.; Birbeck, J.C.H.; Balmer, R.S.; Hughes, B.T., "Measurement of temperature in active high-power AlGaN/GaN HFETs using Raman spectroscopy," IEEE Electron Device Letters, vol.23, no.1, pp.7-9, Jan 2002

[35] Sarua, A.; Bullen, A.; Haynes, M..; Kuball, M.., "High-Resolution Raman Temperature Measurements in GaAs p-HEMT Multifinger Devices," IEEE Transactions on Electron Devices, vol.54, no.8, pp.1838-1842, Aug. 2007

[36] Hangfeng, Ji.; Kuball, M.; Sarua, A.; Jo Das; Ruythooren, W.; Germain, M.; Borghs, G., "Three-dimensional thermal analysis of a flip-chip mounted AlGaN/GaN HFET using confocal micro-Raman spectroscopy," IEEE Transactions on Electron Devices, vol.53, no.10, pp.2658-2661, Oct. 2006

[37] Kuball, M.; Riedel, G. J.; Pomeroy, J. W.; Sarua, A.; Uren, M. J.; Martin, T.; Hilton, K. P.; Maclean, J. O.; Wallis, D. J., "Time-Resolved Temperature Measurement of AlGaN/GaN Electronic Devices Using Micro-Raman Spectroscopy," IEEE Electron Device Letters, vol.28, no.2, pp.86-89, Feb. 2007

[38] Rajasingam, S.; Pomeroy, J.W.; Kuball, M.; Uren, M.J.; Martin, T.; Herbert, D.C.; Hilton, K.P.; Balmer, R.S., "Micro-Raman temperature measurements for electric field assessment in active AlGaN-GaN HFETs," IEEE Electron Device Letters, vol.25, no.7, pp. 456-458, July 2004

[39] Timans, P. J., “The experimental determination of the temperature dependence of the total emissivity of GaAs using a new temperature technique,” Journal of Applied Physics, vol.72, no.2, July 1992

[40] Steins, R.; Kaluza, N.; Hardtdegen, H.; Zorn, M.; Haberland, K.; Zettler, J.-T., "Use of SiC band gap temperature dependence for absolute calibration of emissivity corrected pyrometers in III-nitride MOVPE," Journal of Crystal Growth, vol. 272, pp.81-86, 2004

[41] Regoliosi, P.; Reale, A.; Di Carlo, A.; Romanini, P.; Peroni, M.; Lanzieri, C.; Angelini, A.; Pirola, M.; Ghione, G., "Experimental validation of GaN HEMTs thermal management by using photocurrent measurements," IEEE Transactions on Electron Devices, vol.53, no.2, pp.182-188, Feb. 2006

[42] Konuma, K.; Asano, Y.; Masubuchi, K.; Utsumi, H.; Tohyama, S.; Endo, T.; Azuma, H.; Teranishi, N., "An infrared-bi-color Schottky-barrier CCD image sensor for precise thermal images," IEEE Transactions on Electron Devices, vol.43, no.2, pp.282-286, Feb 1996

[43] Tago, Y.; Akimoto, F.; Kitagawa, K.; Arai, N., "Measurements of surface temperature and emissivity by two-dimensional four-color thermometry with narrow bandwidth," Energy, vol.30, pp.485-495, 2005

[44] Kaplinsky, M.B.; Kosonocky, W.F.; McCaffrey, N.J.; Jun Li; Hou, E.S.F.; Manikopoulos, C.N.; Ravindra, N.M., "Multi-wavelength imaging pyrometer for noncontact temperature sensing," Proceedings of the IEEE International Symposium on Industrial Electronics (ISIE), vol.1, pp.199-204, Jul 1995

[45] Garfinkel, M.; Tiemann, J.J.; Engeler, W. E., "Piezoreflectivity of the Noble Metals," Physics Review, vol.148, no.2, pp.695-706, 1966

[46] Christofferson, J.; Vashaee, D.; Shakouri, A., "Real time sub-micron thermal imaging using thermoreflectance," International Mechanical Engineering Congress and Exhibition, New York, Nov. 2001

[47] Christofferson, J.; Shakouri, A., "Camera for thermal imaging of semiconductor devices based on thermoreflectance," Twentieth Annual IEEE Semiconductor Thermal Measurement and Management Symposium (SEMI-THERM), pp.87-91, Mar 2004

[48] Christofferson, J.; Vashaee, D.; Shakouri, A.; Melese. P.; “High resolution non-contact thermal characterization of semiconductor devices,” Proceedings of SPIE, vol.4275, pp.119–125, 2001

[49] Grauby, S.; Tessier, G.; Rachet, V.; Hole S.; Fourier, D., “Quantitative thermal imaging with CCD array coupled to an heterodyne multichannel lock in detection,” Analytical Sciences, vol.17, pp.67-69, April 2001

[50] Komarov, P.-L.; Burzo, M. G.; Raad, P.E., “CCD thermoreflectance thermography system: methodology and experimental validation,” Proceedings of 12th International Workshop on Thermal investigations of ICs (THERMINIC), Nice, France, 2006

[51] Tessier, G.; Hole, S.; Fourier, D.; “Quantitative thermal imaging by synchronous thermoreflectance with optimised illumination wavelengths," Applied Physics Letters, vol.78, no.16, April 2001

[52] England, J. M. C.; Zissis, N.; Timans, P. J.; Ahmed, H., “Time-resolved reflectivity measurements of temperature distributions during swept-line electron-beam heating of silicon,” Journal of Applied Physics, vol.70, no.1, pp.389-397, July 1991

[53] Arai, F.; Ng, C.; Pou Liu; Lixin Dong; Imaizumi, Y.; Maeda, K.; Maruyama, H.; Ichikawa, A.; Fukuda, T., "Ultra-small site temperature sensing by carbon nanotube thermal probes," 4th IEEE Conference on Nanotechnology, pp.146-148, Aug. 2004

[54] Shaukatullah, H.; Claassen, A., "Effect of thermocouple wire size and attachment method on measurement of thermal characteristics of electronic packages," 19th Annual IEEE Semiconductor Thermal Measurement and Management Symposium (SEMI-THERM), pp.97-105, March 2003

[55] Salem, T.E.; Ibitayo, D.; Geil, B.R., "Validation of Infrared Camera Thermal Measurements on High-Voltage Power Electronic Components," IEEE Transactions on Instrumentation and Measurement, vol.56, no.5, pp.1973-1978, Oct. 2007

[56] Shi, L.; Kwon, O.; Miner, A.C.; Majumdar, A., "Design and batch fabrication of probes for sub-100 nm scanning thermal microscopy," Journal of Microelectromechanical Systems, vol.10, no.3, pp.370-378, 2001

[57] Ho, H.P.; Lo, K.C.; Wu, S.Y., "A scanning thermocouple probe for temperature mapping," IEEE Transactions on Instrumentation and Measurement, vol.50, no.5, pp.1167-1170, Oct 2001

[58] Arai, F.; Ng, C.; Pou Liu; Lixin Dong; Imaizumi, Y.; Maeda, K.; Maruyama, H.; Ichikawa, A.; Fukuda, T., "Ultra-small site temperature sensing by carbon nanotube thermal probes," 4th IEEE Conference on Nanotechnology, pp.146-148, Aug. 2004

[59] Borca-Tasciuc, T.; Chen, G.; Wang, D.; Wang, K. L., "Thermal Conductivity Measurement and Microscopy of Thin Film Structures," 16th Conference on Thermoelectrics, pp.726-729, 1997

[60] Mittereder, J.A.; Roussos, J.A.; Anderson, W.T.; Ioannou, D.E., "Quantitative measurement of channel temperature of GaAs devices for reliable life-time prediction," IEEE Transactions on Reliability, vol.51, no.4, pp.482-485, Dec 2002

[61] Raphal Aubry; Jean-Claude Jacquet; J. Weaver; Olivier Durand; P. Dobson; G. Mills; Marie-Antoinette di Forte-Poisson; Simone Cassette; Sylvain-Laurent Delage, "SThM Temperature Mapping and Nonlinear Thermal Resistance Evolution With Bias on AlGaN/GaN HEMT Devices," IEEE Transactions on Electron Devices, vol.54, no.3, pp.385-390, March 2007

[62] Heridarto, E.; Altes, A.; Heiderhoff, R.; Phang, J.C.H.; Balk, L.J., "Investigation on the thermal distribution of nmosfets under different operation modes by scanning thermal microscopy," IEEE Proceedings 43rd Annual International Reliability Physics Symposium (IRPS), pp.294-299, April 2005

[63] Park, J.H.; Lee, C.C., "A new configuration of nematic liquid crystal thermography with applications to GaN-based devices," IEEE Transactions on Instrumentation and Measurement, vol.55, no.1, pp. 273-279, Feb. 2006

[64] Azar, K.; Farina, D., "Measuring Chip Temperatures with Thermochromic Liquid Crystals," Electronics Cooling, vol.3, no.1, 1997

[65] Roesch, W.J., "Thermo-reliability relationships of GaAs ICs," IEEE 10th Annual Gallium Arsenide Integrated Circuit (GaAs IC) Symposium, pp.61-64, Nov 1988

[66] Park, J.; Shin, M.W.; Lee, C.C., "Thermal modeling and measurement of AlGaN-GaN HFETs built on sapphire and SiC substrates," IEEE Transactions on Electron Devices, vol.51, no.11, pp.1753-1759, Nov. 2004

[67] Park, J.; Lee, C.C., "A new thermal measurement technique using nematic liquid crystals with IR laser illumination for visible light emitting devices," Proceedings 55th Electronic Components and Technology Conference (ECTC), vol.2, pp.1607-1610, May-June 2005

[68] Altmann, F.; Riediger, T.; Breitenstein, O.; Rakotoniaina, J.P., ”Fault Localisation of ICs by Lock-in Fluorescent Microthermal Imaging,” Proceedings 7th International Quantitative Infrared Thermography Conference (QIRT), 2004

[69] Goedeke, S.M., “Determination of surface temperature on micrometer scaled objects,” Proceedings 48th International Instrumentation Symposium of the ISA, San Diego, CA, May 2002

[70] Aigouy, L.; Tessier, G.; Mortier, M.; Charlot, B.; “Scanning thermal imaging of microelectronic circuits with a fluorescent nanoprobe,” Applied Physics Letters. vol.87, no.18, pp.184105, 2005

[71] Priestley, N.; Newsome, K.; Dale, I.; Norton, P., "A Gunn diode based surface mount 77 GHz oscillator for automotive applications," IEEE MTT-S International Microwave Symposium Digest, vol.3, pp.1863-1866, 2002

[72] Zaklikiewicz, A.M., "LF noise and reliability of Gunn diodes," Proceedings 12th International Conference on Microwaves and Radar (MIKON), pp.79-83 vol.1, May 1998

[73] Batcheior, V.; Postoyalko, J., “Thermal analysis for improved performance of transferred-electron oscillators,” Journal of Appt. Phys. vol.70, no.2, pp.1028-1030, July 1991

[74] Kazubski, W.; Modelski, J., "Two-dimensional modelling of the thermal properties of Gunn diodes ," 12th International Conference on Microwaves and Radar (MIKON), vol.3, pp.728-731, May 1998

[75] Meyer, M., "A simple method for the measurement of Gunn diode thermal resistance," IEEE Transactions on Electron Devices, vol.21, no.2, pp. 175-176, Feb 1974

[76] Gunn, J.B., “Microwave oscillations of current in III/V semiconductors,” Solid State Communications, vol.1, no.88, 1963

[77] Blakemore, J.S., “Semiconducting and other major properties of Gallium Arsenide,” Journal of Applied Physics, vol.53, no.10, pp.123-181, 1982

[78] Dyadchenko, A.V.; Mishnyov, A.A.; Polyanski, N.E., "Broadband GaAs-oscillators of mm-range [utilizing Gunn diodes]," The Fifth International Kharkov Symposium on Physics and Engineering of Microwaves, Millimeter, and Submillimeter Waves (MSMW), vol.2, pp.543-545, June 2004

[79] “E2V Technologies Gunn Diodes Application Notes,” Issue 4, September 2002

[80] Couch, N.R.; Spooner, H.; Beton, P.H.; Kelly, M.J.; Lee, M.E.; Rees, P.K.; Kerr, T.M., "High-performance, graded AlGaAs injector, GaAs Gunn diodes at 94 GHz," IEEE Electron Device Letters, vol.10, no.7, pp.288-290, Jul 1989

[81] Carlstrom, J.E.; Plambeck, R.L.; Thornton, D.D., "A Continuously Tunable 65--15-GHz Gunn Oscillator," IEEE Transactions on Microwave Theory and Techniques, vol.33, no.7, pp.610-619, Jul 1985

[82] Takeuchi, M.; Higashisaka, A.; Sekido, K., "GaAs planar Gunn diodes for DC-biased operation," IEEE Transactions on Electron Devices, vol.19, no.1, pp.125-127, Jan 1972

[83] Beton, P.H.; Long, A.P.; Couch, N.R.; Kelly, M.J., "Use of n+ spike doping regions as nonequilibrium connectors," Electronics Letters , vol.24, no.7, pp.434-435, 31 Mar 1988

[84] Teoh King Long; Goh Mei Li; Seetharamu, K.N.; Hassan, A.Y., "A fresh look at thermal resistance in electronic packages," Proceedings 3rd Electronics Packaging Technology Conference (EPTC), pp.124-130, 2000

[85] Afromowitz, M.A., J. Appl. Phys., vol.44, no.3, pp.1292-1294, 1973

[86] Bravman, J.S.; Eastman, L.F., "Thermal effects of the operation of high average power Gunn devices," IEEE Transactions on Electron Devices, vol.17, no.9, pp.744-750, Sep 1970

[87] Förster, A.; Stock, J.; Montanari, S.; Lepsa, M.I.; Hans Lüth., "Fabrication and characterisation of GaAs Gunn diode chips for applications at 77 GHz in automotive industry," Sensors, no.6, pp.350-360, 2006

[88] Shaukatullah, H.; Claassen, A., "Effect of thermocouple wire size and attachment method on measurement of thermal characteristics of electronic packages," 19th Annual IEEE Semiconductor Thermal Measurement and Management Symposium (SEMI-THERM), pp.97-105, March 2003

[89] van der Wel, P.J.; Bielen, J.A.; Henderson, T.; Middleton, J., "State of the art thermal analysis of GaAs/InGaP HBT," IEEE Compound Semiconductor Integrated Circuit Symposium (CSICS), pp.79-82, Oct. 2004

[90] Judaschke, R.; Schunemann, K., "InP transferred electron devices for power generation at frequencies above 130 GHz," Proceedings Third International Kharkov Symposium of Physics and Engineering of Millimeter and Submillimeter Waves (MSMW), vol.1, pp.24-29, 1998

[91] Sarua, A.; Hangfeng Ji; Kuball, M.; Uren, M.J.; Martin, T.; Hilton, K.P.; Balmer, R.S., "Integrated micro-Raman/infrared thermography probe for monitoring of self-heating in AlGaN/GaN transistor structures," IEEE Transactions on Electron Devices, vol.53, no.10, pp.2438-2447, Oct. 2006

[92] Jimenez, J.; Martin, E.; Torres, A.; Landesman, J. P., “Temperature dependence of the Raman spectrum of AlxGa1-xAs ternary alloys,” Phys. Rev. B, Condens. Matter, vol.58, no.16, pp.10 463–10 469, Oct. 1998.

[93] Millar, P.; Birch, R.B.; Kemp, A.J.; Burns, D., "Synthetic Diamond for Intracavity Thermal Management in Compact Solid-State Lasers," IEEE Journal of Quantum Electronics, vol.44, no.8, pp.709-717, Aug. 2008

[94] Salem, T.E.; Ibitayo, D.; Geil, B.R., "Validation of Infrared Camera Thermal Measurements on High-Voltage Power Electronic Components," IEEE Transactions on Instrumentation and Measurement, vol.56, no.5, pp.1973-1978, Oct. 2007

[95] Nagy, W.; Singhal, S.; Borges, R.; Johnson, J.W.; Brown, J.D.; Therrien, R.; Chaudhari, A.; Hanson, A.W.; Riddle, J.; Booth, S.; Rajagopal, P.; Piner, E.L.; Linthicum, K.J., "150 W GaN-on-Si RF power transistor," IEEE MTT-S International Microwave Symposium Digest, p.4, June 2005

[96] Fieger, M.; Eickelkamp, M.; Rahimzadeh K.L.; Dikme, Y.; Noculak, A.; Kalisch, H.; Heuken, M.; Jansen, R.H.; Vescan, A., “ MOVPE, processing and characterization of AlGaN/GaN HEMTs with different Al concentrations on silicon substrates,” Journal of Crystal Growth, 13th International Conference on Metal Organic Vapor Phase Epitaxy (ICMOVPE), vol.298, pp.843-84, Jan. 2007

[97] Benbakhti, B.; Rousseau, M.; Soltani, A.; De Jaeger, J.-C., "Analysis of Thermal Effect Influence in Gallium-Nitride-Based TLM Structures by Means of a Transport–Thermal Modeling," IEEE Transactions on Electron Devices, vol.53, no.9, pp.2237-2242, Sept. 2006

[98] Stenzel, O.; Rau, B.; Schaarschmidt, G.; “Optical properties of amorphous carbon, deposited by an ion-plating technique,” Solid State Physics, vol.115, no.2, pp.247-250, 1989

[99] Zhou, Yu.; Nelson, B.J., "The effect of material properties and gripping force on micrograsping," Proceedings IEEE International Conference on Robotics and Automation, vol.2, pp.1115-1120, 2000

[100] Das, J.; Oprins, H.; Ji, H.; Sarua, A.; Ruythooren, W.; Derluyn, J.; Kuball, M.; Germain, M.; Borghs, G., "Improved Thermal Performance of AlGaN/GaN HEMTs by an Optimized Flip-Chip Design," IEEE Transactions on Electron Devices, vol.53, no.11, pp.2696-2702, Nov. 2006

[101] Miyazaki, H.; Sato, T., "Pick and place shape forming of three-dimensional micro structures from fine particles," Proceedings IEEE International Conference on Robotics and Automation (ICRA), vol.3, pp.2535-2540, Apr. 1996

[102] Darwish, A.M.; Bayba, A.J.; Hung, H.A., "Utilizing infrared for improved FET channel temperature prediction," 2008 IEEE MTT-S International Microwave Symposium Digest, pp.1301-1303, June 2008

[103] Fentem, P.J.; Nag, B.R., "Short pulse techniques for estimating the temperature and impurity concentration of the active layer of a Gunn diode," Solid-State Electronics, vol. 16, pp.1297-1299, 1973

[104] Khalid, A.; Pilgrim, N.J.; Dunn, G.M.; Holland, M.C.; Stanley, C.R.; Thayne, I.G.; Cumming, D.R.S., "A Planar Gunn Diode Operating Above 100 GHz ," IEEE Electron Device Letters, vol.28, no.10, pp.849 – 851, Oct. 2007

[105] Shigeki, S.; Hideo, H.; Kunio, T., "Electrostatic detachment of an adhering particle from a micromanipulated probe," Journal of Applied Physics, vol.93, no.4, pp.2219-2224, 2003

[106] Tafazzoli, A.; Pawashe, C.; Sitti, M., "Atomic Force Microscope based Two-Dimensional Assembly of Micro/Nanoparticles," IEEE International Symposium on Nano to Macro Assembly and Manufacturing (ISATP), pp.230-235, July 2005

[107] Lee, L.; Wyatt, F.; Ganske, H.; Sander, E.H., "Apparatus and process for coating particles." U.S. Patent 6 312 521, Nov. 6, 2001